Filling the holes

Katsouras, Ilias

Filling the Holes

Ilias Katsouras

Filling the holes
Ilias Katsouras
Ph.D. Thesis

university of groningen / faculty of mathematics and natural sciences / zernike institute for advanced materials

Zernike Institute PhD Thesis Series 2013 – 06
ISSN: 1570 – 1530
ISBN: 978-90-367-6131-4 (print)
ISBN: 978-90-367-6130-7 (digital)

The work described in this thesis was financially supported by the Zernike Institute for Advanced Materials and the European Community's Seventh Framework Programme (FP7/20072013) under the Grant agreements ONE-P No. 212311 and MOMA No. 248092.

RIJKSUNIVERSITEIT GRONINGEN

Filling the holes

Proefschrift

ter verkrijging van het doctoraat in de
Wiskunde en Natuurwetenschappen
aan de Rijksuniversiteit Groningen
op gezag van de
Rector Magnificus, dr. E. Sterken,
in het openbaar te verdedigen op
vrijdag 26 april 2013
om 16.15 uur

door

Ilias Katsouras

geboren op 3 januari 1985
te Ioannina, Griekenland

Promotores:	Prof. dr. ir. P.W.M. Blom
	Prof. dr. D.M. de Leeuw
Beoordelingscommissie:	Prof. dr. G. Hadziioannou
	Prof. dr. B. Noheda
	Prof. dr. ir. H.J.W. Zandvliet

To everyone who made it possible

In memory of

Bert de Boer (1973-2009)

Contents

CHAPTER 1

Introduction

Nanotechnology is envisioned to create new materials and devices with a vast range of applications. It entails the application of fields of science as diverse as surface science, organic chemistry, molecular biology, semiconductor physics and microfabrication. Due to the variety of potential applications, nanotechnology is a key technology for the future and governments have invested billions of euros in its research. Phenomena at the nanometer scale are likely to constitute a completely new world. Properties of matter at nanoscale may not be as predictable as those observed at larger scales. With an eye on molecular electronics, it is important to investigate the electrical transport properties of materials as a function of length scale. Interesting phenomena occur when one of the dimensions of the investigated system is in the order of a few nanometers. The investigation of the scaling with the lateral dimensions requires a technology that can reproducibly address the electrical transport of layers varying from single molecules self-assembled in ultra-thin films to bulk films.

1.1 Nanotechnology and scaling

The term nanotechnology, in its traditional sense, is the engineering of functional systems at the molecular scale. The fabrication is from the bottom up, with atomic precision. This theoretical capability was envisioned as early as 1959 by the renowned physicist Richard Feynman.

> "*I want to build a billion tiny factories, models of each other, which are manufacturing simultaneously... The principles of physics, as far as I can see, do not speak against the possibility of maneuvering things atom by atom. It is not an attempt to violate any laws; it is something, in principle, that can be done; but in practice, it has not been done because we are too big*"- Richard Feynman, Nobel Prize winner in physics

The length scale of nanotechnology is elucidated in Figure 1.1. One nanometer (nm) is one billionth, or 10^{-9}, of a meter. By comparison, the spacing between atoms in a molecule is in the range 0.12 - 0.15 nm, and a DNA double-helix has a diameter around 2 nm. On the other hand, the smallest cellular life-forms, the bacteria of the genus Mycoplasma, are around 200 nm in length. By convention, nanotechnology is taken as the scale range between 1 and 100 nm. The lower limit is set by the size of atoms since nanotechnology must build its devices from atoms and molecules. The upper limit is more or less arbitrary but is around the size that phenomena not observed in larger structures start to become apparent.

Nanotechnology is envisioned to create new materials and devices with a vast range of applications, such as in medicine, electronics, biomaterials and energy production. It entails the application of fields of science as diverse as surface science, organic chemistry, molecular biology, semiconductor physics and microfabrication. Due to the variety of potential applications, nanotechnology is a key technology for the future and governments have invested billions of euros in its research.

Several phenomena become pronounced as the size of the system decreases. These include statistical mechanical effects, as well as quantum mechanical effects, for example the "quantum size effect" where the electronic properties of solids are altered with great reductions in particle size. This effect does not come into play by going from macro to micro dimensions. However, quantum effects become dominant when the nanometer size range is reached, typically at dimensions of 100 nanometers or less, the so-called quantum realm.

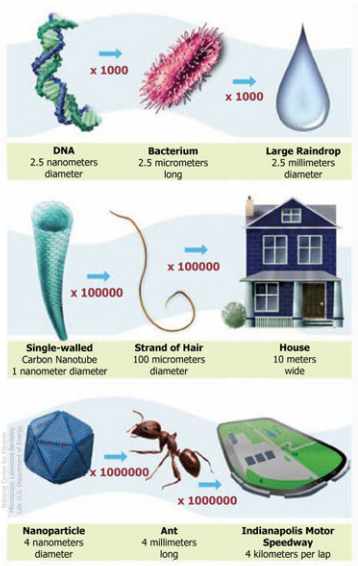

Figure 1.1: The scale of nanotechnology. Adapted from reference [1].

Figure 1.2: Size dependent fluorescence. Photograph of solutions of 2 to 7 nm CdSe nanocrystals, with increasing diameter from left to right. The semiconductor band gap increases with decreasing nanocrystal size, leading to a color shift from red to blue. [2]

Phenomena at the nanometer scale are likely to constitute a completely new world. Properties of matter at nanoscale may not be as predictable as those observed at larger scales. Designed and controlled fabrication and integration of nanomaterials and nanodevices is likely to be revolutionary for science and technology. Important changes in behavior are caused not only by continuous modification of characteristics

with diminishing size, but also by the emergence of totally new phenomena such as quantum confinement. A typical example is presented in Figure 1.2, where the color of light emission from semiconducting nanoparticles is shown to depend on their size. The change in color is due to quantum confinement and can be described as the classical particle in a box problem. In classical systems, for example a ball trapped inside a box, the particle can move at any speed within the box. However, when the well becomes very small, on the scale of a few nanometers, quantum effects become important. The particle may only occupy certain energy levels. Since the electron energy levels of the nanoparticle are discrete rather than continuous, variation of the nanoparticle's size alters its bandgap, hence its color of emission.

Additionally, a number of physical (mechanical, electrical or optical) properties change when compared to macroscopic systems. Materials reduced to the nanoscale can show different properties compared to what they exhibit on a macroscale, enabling unique applications. For instance, opaque substances become transparent (copper); stable materials turn combustible (aluminum); insoluble materials become soluble (gold). Another example is the increase in surface area to volume ratio altering mechanical, thermal and catalytic properties of materials. Moreover, the classical notion of friction needs to be adapted at the nanoscale, where a deviation from Amontons' law - which states that the frictional force is proportional to the weight of the moving object - at the micro- to meso-scale has been observed.[3] These new phenomena make nano structures distinct from devices which are merely miniaturized versions of an equivalent macroscopic device.

With an eye on molecular electronics, it is important to investigate the electrical transport properties of materials as a function of length scale. For example, at the macroscopic level the conductance of a wire increases continuously with its diameter. However, at the nano scale, the wire's conductance is quantized - the increases occur in discrete steps.[4] Current research topics where scaling of electrical properties with the lateral dimensions is investigated are for instance ferroelectrics and spin-cross over materials for data storage applications and charge transport through single molecules for molecular electronics.

In a ferroelectric material the polarization can be switched between two stable states by an external electric field. The switching is accompanied by a hysteresis of the polarization versus the applied field. The hysteresis loop is characterized by the ferroelectric saturation polarization, the remanent polarization and the coercive field. It is well known that the switching kinetics for the so-called extrinsic switching is due to inhomogeneous nucleation of small domains with reversed polarization.[5,6]

The growth of these domains accompanied by domain wall motion leads to the switching of the whole material. Studies using ultra-thin vinylidene fluoridetrifluoroethylene (P(VDF-TrFE)) copolymer films led to the supposition that in these films the switching kinetics follow different rules, referred to as intrinsic switching.[7,8] The switching mechanism depends on the dimensions of the film and it is worthwhile to investigate the ferroelectric properties as a function of length scale. Furthermore, the charge transport properties depend on the length scale as well. Thick films are insulating and behave as ferroelectric capacitors. However, in ultra-thin films transport by tunneling is possible. The magnitude of the tunneling current is expected to depend on the ferroelectric polarization.[9] In order to realize ferroelectric tunnel junctions a technology is required that can overcome the obstacles of parasitic effects, such as local conductivity and transport via localized states.

Spin-crossover compounds, also named spin transition compounds, are functional switching materials able to change their spin state upon external stimuli. The phenomenon of spin-crossover (SCO) was discovered in 1931 by L. Cambi[10] and it has been observed in octahedral coordination complexes of transition metals.[11,12] Spin-crossover compounds were proposed for many applications, such as molecular memories, sensors, displays and more recently in hybrid electronics and optoelectronics.[13–17] The switching process involves a structural transition that produces an electron redistribution in the energy levels, as well as a change in other physical properties such as color, magnetic susceptibility, thermal and electric conductivity, dielectric constant and mechanical properties.[18–20] The transition is triggered by external stimuli, such as temperature, pressure, light, magnetic field or a combination of them, and it can occur gradually or abruptly depending on interactions among different molecules. The measured hysteresis implies that strong cooperative effects are present, which in turn suggests that the transition from one spin state to the other spin state depends on the length scale of the system under investigation. However, a testbed for the experimental verification of the scaling is missing.

The major target of molecular electronics is to combine functional molecules into integrated circuits of discrete junctions. The charge transport through single molecules self-assembled in a monolayer has been extensively investigated as a function of molecular length.[21–49] For small molecules, transport is by non-resonant tunneling. The conductance depends exponentially on the molecular length. However, for longer molecules, a transition from tunneling to hopping has been observed. The experiments were performed using conducting atomic force microscopy (c-AFM).[50] For practical applications it is desirable to upscale the technology to metal-molecule-metal

junctions.

In summary, the electrical properties of several classes of materials depend on the length scale. Interesting phenomena occur when one of the dimensions of the investigated system is in the order of a few nanometers. The investigation of the scaling with the lateral dimensions requires a technology that can reproducibly address the electrical transport of layers varying from single molecules self-assembled in ultra-thin films to micrometer-thick films.

1.2 Generic device technology

Well-defined molecular junctions can only be realized when the molecules are sandwiched between two electrodes. However, the limited reliability, stability and, especially, yield of conventional experimental testbeds are a bottleneck to the progress in the study of discrete devices and their integration into circuits. Electrical shorts in thin films are readily formed upon vapor deposition of the top electrode.[51] The formation of shorts has limited the diameter of the first reported molecular junctions to a few tens of nanometres.[39] A statistical analysis for manually measured molecular junctions with diameter of 2 μm, resulted in a yield of functional junctions of 1.2% (156 out of 13440).[38] Moreover, the stability and the parasitics of the junctions are major concerns when transport properties of films with thicknesses ranging from a few micrometers down to a few nanometers need to be investigated. To prevent cross-talk, the junctions should be completely electrically insulated from each other.

Technologies can be top-down or bottom-up, as schematically depicted in Figure 1.3. The traditional top-down approach to nanofabrication involves the creation of "nanostructures" from a large parent entity. The fabrication typically consists of three major steps: the deposition of thin films/coatings on a substrate, obtaining the desired shapes via photolithography and pattern transfer using either a lift-off process or selective etching. Top-down fabrication techniques are derived from the semiconductor industry for the fabrication of integrated circuits.

Bottom-up approaches, in contrast, use the chemical properties of single molecules to cause single-molecule components to self-organize into some useful conformation utilizing the concepts of molecular self-assembly and/or molecular recognition. The bottom-up approaches should be able to produce devices in parallel and much cheaper than top-down methods, but could potentially be overwhelmed as the size and complexity of the desired assembly increases. To study the scaling of charge transport it is desirable to have a complementary technology that combines the advantages of both

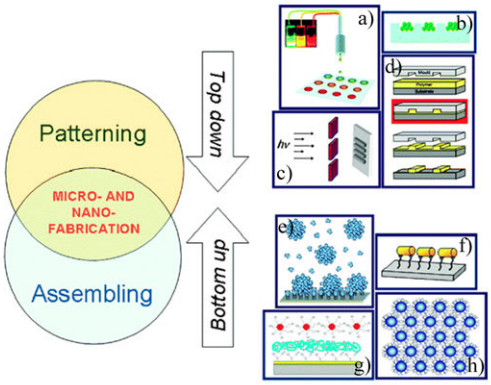

Figure 1.3: Scheme of complementary "top-down" and "bottom-up" approaches for fabrication of micro- and nano-structures. For the top-down strategies: (a) ink jet printing, (b) capillary assembly, (c) photolithography and (d) nanoimprinting lithography. For the bottom-up strategies: (e) host-guest chemistry, (f) covalent immobilization onto substrate, (g) electrostatic layer-by-layer deposition and (h) self-assembly. Adapted from reference [52].

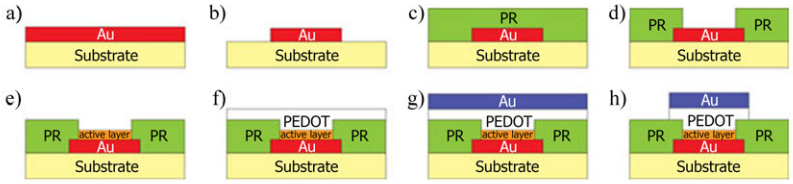

Figure 1.4: Schematic representation of the process flowchart for the fabrication of large-area molecular junctions. (a) deposition of Au bottom electrode, (b) patterning Au bottom electrode using photolithography, (c) spincoating of negative photoresist, (d) photolithographical definition of vertical interconnect, (e) active layer formation, (f) spincoating of PEDOT:PSS, (g) deposition of Au top electrode, (h) patterning top electrode using photolithography and self-aligned removal of PEDOT:PSS outside the junction area. Adapted from reference [22].

approaches.

In this thesis we combine both approaches by using a previously developed technology for molecular junctions.[21,22] As shown in Figure 1.4, the general structure of a large-area molecular junction consists of an active layer sandwiched between two electrodes, enclosed in an insulating matrix defined in photoresist. The junctions are formed on a thermally oxidized silicon wafer on top of which patterned bottom gold electrodes have been evaporated. Subsequently, a photoresist layer is spincoated and patterned by conventional I-line lithography, creating circular vertical interconnects

(vias, or holes) on top of the bottom electrodes. The active layer is deposited and the top layer of poly(3,4-ethylenedioxythiophene):poly(4-styrenesulfonic acid) (PEDOT:PSS) is spincoated. Ultra-thin films are prepared by self-assembly, while thicker films are made by spincoating. Finally, the junction is finished by evaporating the top gold electrodes and using them as a self-aligned mask to etch away the redundant PEDOT:PSS.

The key advantages of this technology are as follows. The use of the conducting polymer layer sandwiched between the active layer and the top electrode prevents electrical shorts, and processing within lithographically defined vertical interconnects (vias, or holes) prevents both parasitic currents and interaction between the environment and the active layer. The active layer can vary from a monolayer to bulk films. The length scale varies between a few nanometers and a micrometer. The technique is simple, compatible with standard integrated circuit fabrication processes and can be scaled up and extended to any molecule and any metal bottom electrode. The technology allows characterization over an unprecedented temperature and bias window.

In summary, a generic technology that allows the investigation of scaling of electrical transport with layer thickness is developed. The layer thickness can be varied between nanometers and micrometers. The molecules of interest are assembled in holes defined in photoresist, which, therefore, explains the title of this thesis, "Filling the holes".

1.3 Outline of the thesis

Large-area molecular junctions are two-terminal devices which allow the accurate and reproducible measurement of charge transport through layers ranging from self-assembled monolayers of molecules to bulk films. The properties can be measured systematically at unprecedented temperature and field ranges, offered by the stable and leakage-free junctions. An overview of the experimental procedure to fabricate and characterize large-area molecular junctions, the experimental testbed used throughout this thesis is presented in **Chapter 2**. The standard process flowchart is described, highlighting the features that make large-area molecular junctions a versatile testbed for the characterization of various materials.

In **Chapter 3** we investigate the electrical transport through mixed self-assembled monolayers (SAMs) of alkanemonothiols and alkanedithiols in large-area molecular junctions. To disentangle the role of the molecular length and the interfacial composition, monothiol -monothiol, dithiol-dithiol, and monothiol-dithiol binary combinations

are studied. In all cases, we find that the resistance of these mixed SAMs appears to depend exponentially on the average number of carbon atoms, thus resembling monocomponent SAMs, whose resistance is known to depend exponentially on molecular length. However, in monocomponent SAMs this behavior has a single-molecule tunneling origin, which is not directly relevant for mixtures. Furthermore, in certain mixed SAMs the resistance decreases with increasing average layer thickness. We suggest an explanation for the observed dependence of the resistance in the mixed SAMs on their composition within an equivalent circuit model, based on a simple assumption concerning their microdomain structure. The simulated dependence is non-exponential and leads to a good agreement between calculated and measured resistances with only two fit parameters.

Chapter 4 discusses the contact resistance of a transistor using self-assembled monolayer (SAM)-modified source and drain electrodes, which depends on the SAM tunnel resistance, the height of the injection barrier and the morphology at the contact. To disentangle the different contributions, we have combined transmission line measurements in transistors with transport measurements of SAMs in large-area molecular junctions. The tunnel resistance of the SAM has been independently extracted in two-terminal large-area molecular junctions. We show that the tunneling resistance of the SAM can be added linearly to the contact resistance of the transistor with bare metal electrodes, to account for the increased contact resistance in the SAM-modified transistor. The manifestation of the SAM in the contact resistance shows that transistors can potentially be used as an experimental testbed for molecular electronics.

In **Chapter 5** we achieve a large bias window and use it to discriminate between different transport models in large-area molecular junctions. Under continuous DC bias, the junctions irreversibly break down at fields over 9 MV/cm. We show that, by using pulse measurements, we can reach electrical fields of 35 MV/cm before degradation. The breakdown voltage is shown to depend logarithmically on both duty cycle and pulse width. A tentative interpretation is presented based on electrolysis in the polymeric top electrode. Expanding the bias window using pulse measurements unambiguously shows that the electrical transport exhibits not an exponential but a power-law dependence on bias.

In **Chapter 6** we investigate further the charge transport through alkanes and para-phenylene oligomers in large-area molecular junctions. The molecules are self-assembled in a monolayer and contacted with a top electrode consisting of poly(3, 4-ethylenedioxythiophene):poly(4-styrenesulfonic acid) (PEDOT:PSS). Using the technique described in **Chapter 5**, the complete set of $J(V, T)$ characteristics of both

saturated and π-conjugated molecules can be described quantitatively by a single equation with only two fit parameters. The derived parameters, in combination with a variation of the bulk conductivity of PEDOT:PSS, demonstrate that the absolute junction resistance is factorized with that of PEDOT:PSS.

In **Chapter 7** the charge transport in poly(2-methoxy, 5-(2' ethyl-hexyloxy)-p-phenylene vinylene) (MEH-PPV)-based hole-only diodes is investigated at high electric fields and low temperatures using a novel diode architecture. Charge carrier densities that are in the range of those in a field-effect transistor are achieved, bridging the gap in the mobility versus charge carrier density plot between polymer-based light-emitting diodes and field-effect transistors. The extended field range that is accessed allows us to discuss the applicability of current theoretical models of charge transport, using numerical simulations. Finally, within a simple approximation, we extract the hopping length for holes in MEH-PPV directly from the experimental data at high fields, and we derive a value of $1.0 \pm 0.1\ nm$.

Finally, in **Chapter 8** we have filled the holes with monolayers of DNA, spin-crossover compounds and the ferroelectric copolymer P(VDF-TrFE). The electrical transport has been measured and the preliminary data are presented. We show that dense monolayers of hybridized DNA molecules are obtained. However, the molecules are lying flat. The electrical data show that the charge transport is measured not along, but across the molecules. The conductance obtained indicates that the charge transport through DNA is due to non-resonant tunneling. Smooth thin films of a spin-crossover compound could be realized but the conductivity was too low to reliably identify a spin-crossover transition. The properties of ferroelectric capacitors with thick layers are in good agreement with literature data. Scaling down the thickness showed a gradual change in coercive field. Even ultra-thin films of about a few nanometers could be fabricated. The electrical transport data indicate the first ferroelectric tunnel junction, but more experiments are needed for verification. The examples presented unambiguously show that the technology is generic and versatile. The holes can be filled with unconventional semiconductors yielding scientifically interesting devices.

References

[1] http://tinyurl.com/a737pwv. National Center for Electron Microscopy, Lawrence Berkeley Lab, U.S. Department of Energy.

[2] http://tinyurl.com/bxb2gvc.

[3] M. P. de Boer, D. L. Luck, W. R. Ashurst, R. Maboudian, A. D. Corwin, J. A. Walraven, J. M. Redmont, J. Microelectromech. S. 13 (2004) 63.

[4] B. J. van Wees, H. van Houten, C. W. J. Beenakker, J. G. Williamson, L. P. Kouwenhoven, D. van der Marel, C. T. Foxon, Phys. Rev. Lett. 60 (1988) 1988.

[5] W. Merz, Phys. Rev. 95 (1954) 690.

[6] W. Merz, J. Appl. Phys. 27 (1956) 938.

[7] G. Vizdrik, S. Ducharme, V. M. Fridkin, S. G. Yudin, Phys. Rev. B. 68 (2003) 094113.

[8] A. V. Bune, V. M. Fridkin, S. Ducharme, L. M. Blinov, S. P. Palto, A. V. Sorokin, S. G. Yudin, A. Zlatkin, Nature 391 (1998) 874.

[9] E. Y. Tsymbal, H. Kohlstedt, Science 313 (2006) 181.

[10] L. Cambi, A. Cagnasso, Atti. Accad. Naz. Lincei, CI. Sci. Fis., Mat. Nut., Rend 13 (1931) 809.

[11] O. Sato, Acc. Chem. Res. 36 (2003) 692.

[12] A. Bousseksou, G. Molnár, P. Demont, J. Menegotto, J. Mater. Chem. 13 (2003) 2069.

[13] S. Bonhommeau, T. Guillon, L. M. L. Daku, P. Demont, J. S. Costa, J. F. Letard, G. Molnar, A. Bousseksou, Angew. Chem., Int. Ed. 45 (2006) 1625.

[14] M. Cavallini, I. Bergenti, S. Milita, G. Ruani, I. Salitros, Z. R. Qu, R. Chandrasekar, M. Ruben, Angew. Chem., Int. Ed. 47 (2008) 8236.

[15] O. Kahn, J. Krober, C. Jay, Adv. Mater. 4 (1992) 718.

[16] S. Shi, G. Schmerber, J. Arabski, J. B. Beaufrand, D. J. Kim, S. Boukari, M. Bowen, N. T. Kemp, N. Viart, G. Rogez, E. Beaurepaire, H. Aubriet, J. Petersen, C. Becker, D. Ruch, Appl. Phys. Lett. 95 (2009) 043303.

[17] M. Matsuda, H. Isozaki, H. Tajima, Chem. Lett. 37 (2008) 374.

[18] E. Breuning, M. Ruben, J. M. Lehn, F. Renz, Y. Garcia, V. Ksenofontov, P. Gutlich, E. Wegelius, K. Rissasen, Angew. Chem., Int. Ed. 39 (2000) 2504.

[19] P. Gutlich, Y. Garcia, H. A. Goodwin, Chem. Soc. Rev. 29 (2000) 419.

[20] F. Varret, K. Boukheddaden, E. Codjovi, A. Goujon, Hyperfine Interact. 165 (2005) 37.

[21] H. B. Akkerman, P. W. M. Blom, D. M. de Leeuw, B. de Boer, Nature 441 (2006) 69.

[22] P. A. van Hal, E. C. P. Smits, T. C. T. Geuns, H. B. Akkerman, B. C. De Brito, S. Perissinotto, G. Lanzani, A. J. Kronemeijer, V. Geskin, J. Cornil, P. W. M. Blom, B. de Boer, D. M. de Leeuw, Nat. Nanotechnol. 3 (2008) 749. (including supporting info).

[23] W. Wang, T. Lee, M. A. Reed, Phys. Rev. B 68 (2003) 035416.

[24] V. B. Engelkes, J. M. Beebe, C. D. Frisbie, J. Am. Chem. Soc. 126 (2004) 14287.

[25] B. Xu, N. J. Tao, Science 301 (2003) 1221.

[26] M. Suzuki, S. Fujii, M. Fujihira, Japan. J. Appl. Phys. 45 (2006) 2041.

[27] W. Haiss, R. J. Nichols, H. van Zalinge, S. J. Higgins, D. Bethell, D. J. Schiffrin, Phys. Chem. Chem. Phys. 6 (2004) 4330.

[28] F. Chen, X. Li, J. Hihath, Z. Huang, N. J. Tao, J. Am. Chem. Soc. 128 (2006) 15874.

[29] L. Venkataraman, J. E. Klare, I. W. Tam, C. Nuckolls, M. S. Hybertsen, M. L. Steigerwald, Nano Lett. 6 (2006) 458.

[30] J. M. Beebe, V. B. Engelkes, L. L. Miller, C. D. Frisbie, J. Am. Chem. Soc. 124 (2002) 11268.

[31] X. D. Cui, A. Primak, X. Zarate, J. Tomfohr, O. F. Sankey, A. L. Moore, T. A. Moore, D. A. Gust, L. A. Nagahara, S. M. Lindsay, J. Phys. Chem. B 106 (2002) 8609.

[32] T. Morita, S. Linsday, J. Am. Chem. Soc. 129 (2007) 7262.

[33] R. L. York, P. T. Nguyen, K. Slowinski, J. Am. Chem. Soc. 125 (2003) 5948.

[34] E. A. Weiss, R. C. Chiechi, G. K. Kaufman, J. K. Kriebel, Z. Li, M. Duati, M. A. Rampi, G. M. Whitesides, J. Am. Chem. Soc. 129 (2007) 4336.

[35] F. Milani, C. Grave, V. Ferr, P. Samori, M. A. Rampi, ChemPhysChem 8 (2007) 515.

[36] C. Chu, J. S. Na, G. N. Parsons, J. Am. Chem. Soc. 129 (2006) 2287.

[37] K. T. Shimizu, J. D. Fabbri, J. J. Jelincic, N. A. Melosh, Adv. Mater. 18 (2006) 1499.

[38] T. W. Kim, G. Wang, H. Lee, T. Lee, Nanotechnology 18 (2007) 315204.

[39] M. A. Reed, C. Zhou, C. J. Muller, T. Burgin, J. M. Tour, Science 278 (1997) 252.

[40] J. Reichert, R. Ochs, D. Beckmann, H. Weber, M. Mayor, H. v. Lohneysen, Phys. Rev. Lett. 88 (2002) 176804.

[41] C. A. Martin, D. Ding, H. S. J. van der Zant, J. M. van Ruitenbeek, New J. Phys. 10 (2008) 065008.

[42] E. H. Huisman, M. L. Trouwborst, F. L. Bakker, B. de Boer, B. J. van Wees, S. J. van der Molen, Nano Lett. 8 (2008) 3381.

[43] C. M. Guedon, J. Zonneveld, H. Valkenier, J. C. Hummelen, S. J. van der Molen, Nanotechnology 22 (2011) 125205.

[44] D. Fracasso, H. Valkenier, J. C. Hummelen, G. C. Solomon, R. C. Chiechi, J. Am. Chem. Soc. 133 (2011) 9556.

[45] G. Wang, Y. Kim, M. Choe, T.-W. Kim, T. Lee, Adv. Mater. 23 (2010) 755.

[46] H. J. Yan, A. J. Bergren, R. L. McCreery, J. Am. Chem. Soc. 133 (2011) 19168.

[47] Y. L. Loo, R. L. Willett, K. W. Baldwin, J. A. Rogers, Appl. Phys. Lett. 81 (2002) 562.

[48] J. Kushmerick, J. G. amd Naciri, J. C. Yang, R. Shashidhar, Nano Lett. 3 (2003) 897.

[49] L. T. Cai, H. Skulason, J. G. Kushmerick, S. K. Pollack, J. Naciri, R. Shashidhar, D. L. Allara, T. E. Mallouk, T. S. Mayer, J. Phys. Chem. B 108 (2004) 2827.

[50] S. H. Choi, B. Kim, C. D. Frisbie, Science 320 (2008) 1482.

[51] B. de Boer, M. M. Frank, Y. J. Chabal, W. Jiang, E. Garfunkel, B. Z., Langmuir 20 (2004) 1539.

[52] M. L. Curri, R. Comparelli, M. Striccoli, A. Agostiano, Phys. Chem. Chem. Phys. 12 (2010) 11197.

CHAPTER 2

Large-area molecular junctions

This chapter provides an overview of the experimental procedure to fabricate and characterize large-area molecular junctions, the experimental testbed used throughout this thesis. The standard process flowchart is described, highlighting the features that make large-area molecular junctions a versatile testbed for the characterization of various materials.

2.1 The history of large-area molecular junctions

Large-area molecular junctions were developed in the University of Groningen and Philips Research Lab in Eindhoven, [1,2] adding to the variety of metal-molecule-metal geometries employed to measure the conductance through individual molecules or self-assembled monolayers (SAMs) of alkanethiols. Other techniques include scanning tunneling microscopy, conductive probe atomic force microscopy, break junctions, hanging mercury drop junctions, nanotransfer printing, nanopores, nanoparticle bridges and networks, lift-off/float-on, nanowires, large-area junctions with different interlayers, liquid eutectic top contacts and crossed wires. [3–29]

The main advantage of large-area molecular junctions over the aforementioned techniques is the potential to be upscaled and integrated in circuits, while providing a 100% yield of working devices. More than 20000 molecular junctions can be fabricated simultaneously on a single 6-inch wafer in a semi-automated procedure. [2] The breakthrough of this technology was the incorporation of a layer of poly(3,4-ethylenedioxythiophene):poly(4-styrenesulfonic acid) (PEDOT:PSS) on top of the SAM. The highly conducting polymer interlayer acts as a protective cushion during the evaporation of the top gold contact, preventing short-circuit formation, [30,31] resulting in highly stable and reproducible molecular junctions.

The large-area molecular junctions geometry can be used to incorporate any active layer (self-assembled monolayer, polymer or small molecule thin films) in an enclosed, well-defined area between two metal electrodes.

2.2 The basic geometry

A cross-section of the general structure of a large-area molecular junction is shown in Figure 2.1, where the active layer is sandwiched between two electrodes, enclosed in an insulating matrix defined in photoresist. The junctions are formed on a silicon wafer on top of which patterned bottom gold electrodes have been evaporated. Subsequently, a photoresist layer is spincoated and patterned by conventional lithography, creating circular vertical interconnects (vias, or holes) on top of the bottom electrodes. The active layer is deposited and the top layer of PEDOT:PSS is spincoated. Finally, the junction is finished by evaporating the top gold electrodes and using them as a self-aligned mask to etch away the redundant PEDOT:PSS. The basic experimental workflow is summarized in the flowchart shown in Figure 2.2. The basic components of a large-area molecular junction are described in detail in the following sections.

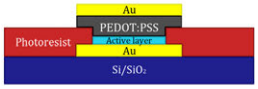

Figure 2.1: Schematic cross-section of a large-area molecular junction. The junction is processed in an insulating photoresist matrix to protect the device from degradation in ambient conditions and to allow for the variation of device area. A top contact of the highly conducting PEDOT:PSS is spincoated on top of the active layer.

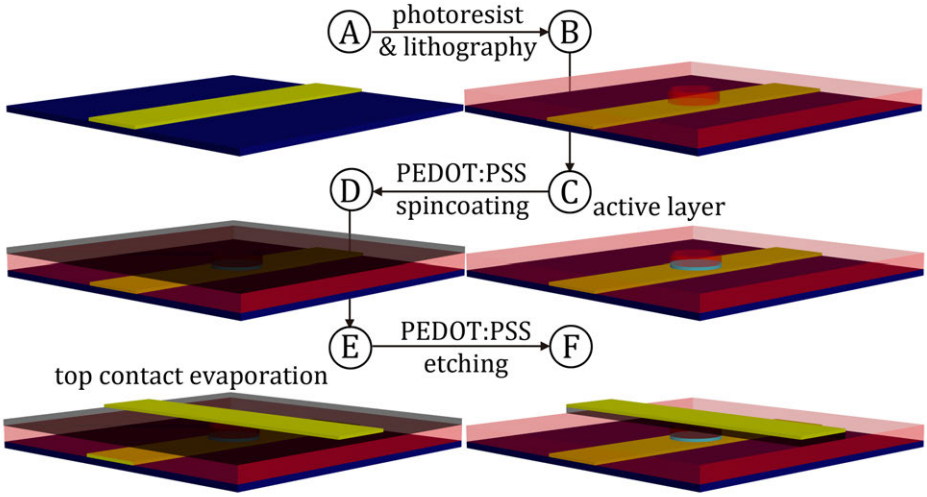

Figure 2.2: Processing steps of large-area molecular junctions. (a) Gold electrodes are vapor-deposited on a silicon wafer. (b) A photoresist layer is spincoated and holes are photolithographically defined in the photoresist. (c) The active layer is deposited. (d) A thin film of the highly conductive polymer PEDOT:PSS is spincoated as a top electrode. (e) The junction is completed by vapor-deposition of gold through a shadow mask and (f) etching away of the redundant PEDOT:PSS to prevent parasitic cross-talk and leakage.

2.2.1 The bottom electrodes

A 4-inch silicon wafer with a 500 nm thermally grown oxide is passivated using hexamethyldisilazane (HMDS), which promotes adhesion of the spincoated photoresist. A 1 nm layer of chromium is thermally evaporated through a shadow mask in a home-built evaporation system, which is placed in a glove box to exclude contaminants from ambient atmosphere. The evaporation rate for this chromium layer is 0.005 - 0.01 nm/s. Evaporation of 60 nm of gold through the same mask follows at a slow initial rate, which is increased to 1 nm/s during evaporation. An increased evaporation rate leads to a smaller grain size and an overall uniform layer, since the mobile gold atoms

have less time to re-arrange over the surface. [32]

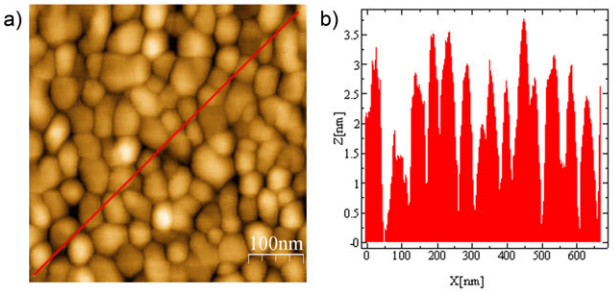

Figure 2.3: (a) AFM image (tapping mode) of a 60 nm gold layer evaporated on a Si/SiO_2 and 1 nm chromium adhesion layer (scan size 500 nm). (b) Cross-sectional profile of the layer.

An AFM image of a 60 nm thick gold layer evaporated over the 1 nm adhesion layer of chromium is shown in Figure 2.3. The root-mean-square (rms) roughness for this layer is 1.2 nm over an area of 0.25 μm^2. Image was acquired in tapping mode using a Multimode AFM (Digital Instruments) with a Nanoscope IV controller and analyzed using WSxM 4.0 Develop 12. [33]

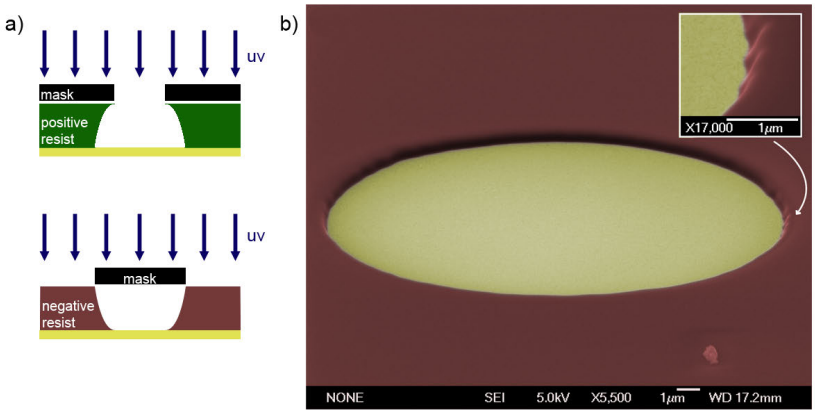

Figure 2.4: (a) Profiles of negative and positive photoresist after overexposure with UV light. (b) A colorized scanning electron micrograph of a circular via of 20 μm diameter in negative photoresist. The bottom gold electrode is colored yellow.

2.2.2 Photolithographic definition of holes

The two-terminal devices are defined in an insulating matrix of photoresist, which helps define the active area of the junction, protects the junction from the environment and prevents parasitic leakage currents. The negative photoresist (MA1400 or

L6000.5, Microresist) is spincoated on the wafer after the evaporation of the bottom contacts, resulting in a layer of approximately 570 nm. A negative photoresist is preferred over a positive one, because of the resulting negative profile after overexposure, as schematically depicted in Figure 2.4a. Since the top contact fabrication involves spincoating of the conductive polymer PEDOT:PSS and evaporation of gold, a continuous top electrode is ensured when the pore has a negative edge profile. Figure 2.4b shows this negative profile in a circular hole with a diameter of 20 μm, in a micrograph taken with a scanning electron microscope.

After a pre-bake step to remove any remaining solvents, the photoresist layer is exposed to UV light under a mask-aligner, to crosslink the photoresist and define the device pattern. Circular vertical interconnects (vias, or holes) with diameters ranging between 1 and 100 μm are defined on top of the bottom gold contacts.

Following exposure, the wafer is immersed in the developer to remove the non-crosslinked areas of the photoresist. A hard bake step follows, to render the photoresist insoluble in the solvents used during the deposition of the active layer. This step is performed in a vacuum oven, which is heated slowly from room temperature to 200 $^{\circ}C$, to ensure that the photoresist layer's features remain intact. The wafer is kept for about two hours at 200 $^{\circ}C$. A last step, before the active layer, involves the cleaning of the bottom gold contacts to remove any possible photoresist residuals. This is done in a PDC plasma cleaner (Harrick). The wafer is subsequently immersed in ethanol to reduce the gold electrodes and remove any contaminating adsorbents. A clean bottom gold electrode is essential for the deposition of the active layer by, for example, promoting the formation of well-ordered, close-packed self-assembled monolayers of molecules.

2.2.3 The active layer

The large-area molecular junctions geometry is a versatile testbed to assess the electrical properties of a variety of active layers. The active area is well defined in an insulating matrix of photoresist and is free from parasitic currents. The absence of leakage in tandem with the high stability of the junctions allows for electrical characterization at a wide field and temperature range. Charge transport can be measured through monolayers of molecules that readily self-assemble on gold (**Chapters 3** to **6**), or thin films of small molecules and polymers (**Chapters 7** and **8**). The self-assembled monolayers are formed from molecules dissolved in an appropriate solvent. The SAM solution is applied in a Teflon box where the wafer is subsequently immersed for at least 36 hours, under nitrogen atmosphere. When the wafer is removed from the

SAM solution, it is thoroughly rinsed with the pure solvent, toluene and iso-propanol to remove any remaining molecules. The wafer is then dried in a dry spinner. Thin layers of small molecules can be applied by either spincoating, dropcasting or even direct evaporation. The processing details of the deposition of the active layers used in this thesis are given in each respective chapter.

2.2.4 The top electrode

The fabrication of the top electrode in the large-area molecular junctions includes the breakthrough of this technology, the use of the PEDOT:PSS interlayer. PEDOT:PSS, a water-based suspension of poly(3,4-ethylenedioxythiophene) stabilized with poly(4-styrenesulphonic acid) (Figure 2.5), is hydrophilic and consists of big macromolecules that are unable to penetrate through the close-packed and typically hydrophobic alkane-based SAMs or thin films of polymers and small molecules. It acts as a highly conductive interlayer that protects the active layer during the evaporation of the top gold contact. The microstructure of thin films of PEDOT:PSS has been investigated using scanning tunneling microscopy. The thin films of PEDOT:PSS consist of spherical grains of PEDOT-rich cores surrounded by PSS-rich shells. [34–36] The workfunction of PEDOT:PSS is comparable to that of gold, amounting to $\sim 5\ eV$.

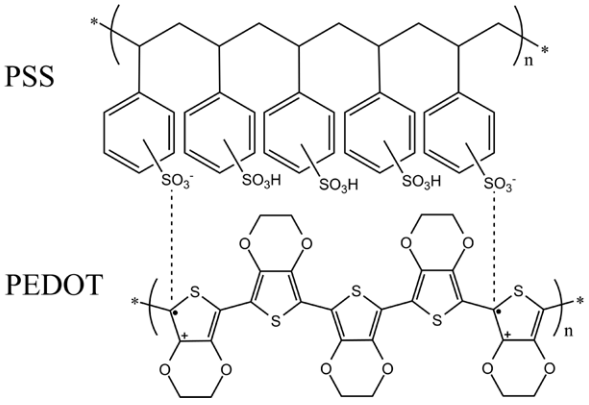

Figure 2.5: The structure of PEDOT:PSS.

In this thesis the commercially available formulations PHCV4 and PH500 from Clevios and ICP1020 from Agfa are used. Various blends based on these products can be prepared, using different additives such as the non-ionic fluoro-surfactant Zonyl FSO-100 (DuPont) which decreases the surface tension of PEDOT:PSS and improves wetting, or dimethyl sulfoxide (DMSO) which increases the conductivity

of PEDOT:PSS.[37] The PEDOT:PSS solution is prepared $\sim$ 12 hours before spin-coating, which is done in ambient conditions, resulting in a layer of a thickness of approximately 90 nm. The wafer is then immediately transferred to a vacuum oven for at least one hour, where the film dries in a dynamic vacuum at room temperature. To facilitate the contact to the top electrode, 150 nm of gold are evaporated on top of the dried PEDOT:PSS film. This gold layer also serves as a mask for the final step, in which redundant PEDOT:PSS is etched away with reactive ion etching (O_2 plasma), eliminating any parasitic currents from top to bottom electrode.

Pictures of different wafers containing large-area molecular junctions used in this thesis are presented in Figure 2.6. In Figure 2.6b a wafer prepared according to the experimental procedure described above on a 4-inch wafer, containing 260 junctions with diameters ranging between 1 μm and 100 μm, is shown. Substrates in Figures 2.6a,c are examples of wafers fabricated at Philips Research Lab in a semi-automatic process on 6-inch wafers. Figure 2.6c depicts one of the thirty identical 2×3 cm pieces defined by laser cutting on a 6-inch wafer. Each piece contains 110 junctions. The 6-inch wafer shown in Figure 2.6a consists of 62 identical "dies", containing different devices amongst which discrete molecular junctions with diameters ranging between 1 and 50 μm and strings of devices of 5 μm, resulting in the simultaneous fabrication of more than 20000 molecular junctions on a single wafer with a yield of 100%. The insets show composite optical microscope pictures of the corresponding junctions for each type of substrate, all in the same scale (scale bar: 200 μm).

2.3 Basic characterization

Large-area molecular junctions are two-terminal devices developed to measure accurately and reproducibly the charge transport through self-assembled monolayers of molecules. Experimentally, the absolute value of the current density (J) has been investigated as a function of applied voltage (J-V characteristics) and temperature (J-T characteristics). With the expansion of the nature of the active layer to include thin films of semiconducting polymers (**Chapter 7**) and other materials (ferroelectric, magnetic, see **Chapter 8**), the systematic study of the $J(V,T)$ characteristics and other properties (*viz.* dielectric, ferroelectric, magnetic) of these materials becomes possible at unprecedented temperature and field ranges, offered by the stable and leakage-free junctions. The large number of simultaneously fabricated devices allows for the collection of statistically reliable measurements.

Direct-current (DC) measurements were performed using a Keithley 4200 Semi-

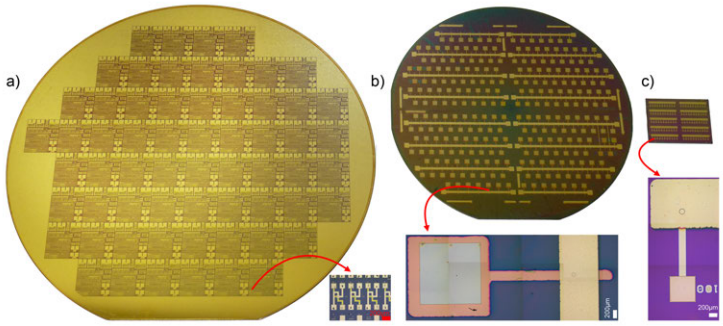

Figure 2.6: Three different large-area molecular junctions layouts used in this thesis. (a) A 6-inch wafer fabricated in Philips Research Lab in Eindhoven. (b) A 4-inch wafer and (c) 2×3 wafer piece from a 6-inch wafer containing 30 identical pieces, fabricated in Philips Research Lab. The corresponding insets show composite optical microscope pictures of the junctions in each type of substrate, all in the same scale (scale bar: 200 μm).

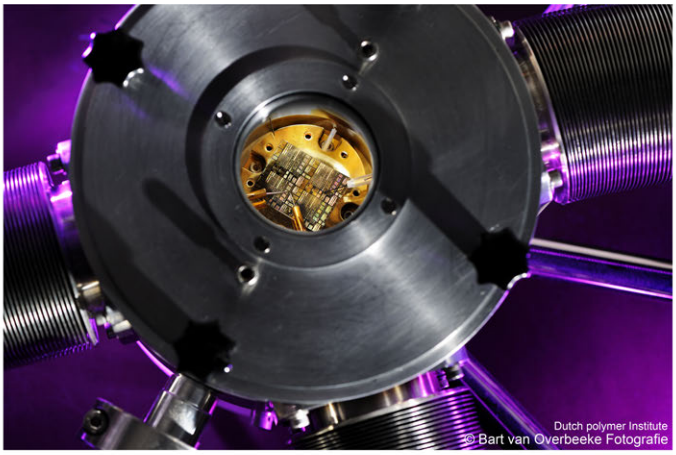

Figure 2.7: Electrical characterization of large-area molecular junctions in a Janis probestation.

conductor Characterization System. All measurements were done in commercial and home-built probe stations under both ambient conditions and vacuum (Figure 2.7). The uptake of water in the PEDOT:PSS layer, which is hygroscopic, can influence the performance of the devices,[38] limiting the characterization bias window. Depending on the active layer the effect can be due to doping or electrochemical reactions at the electrode. Electrolysis of the water in the PEDOT:PSS layer eventually leads to breakdown of the junctions due to the inability of the formed gases to escape the photoresist-enclosed junctions, resulting in delamination of PEDOT:PSS from the

bottom contact.[39,40] Moreover, at high biases other breakdown mechanisms, such as structural changes that molecules and polymer chains undergo under high voltage or thermal stress can become important.[41–45] These breakdown mechanisms become more pronounced under prolonged application of bias. To investigate the transport properties at higher biases, the measurement time has to be minimized. Therefore we performed pulsed measurements, using a Keithley 2602 Source meter controlled through Test Script Builder or a Labview program, or a Keithley 4200 Semiconductor Parameter Analyzer equipped with the Keithley Pulse Measurement Unit. The characterization window was significantly extended (**Chapters 5**,**6** and **7**). Temperature-dependent measurements, both pulsed and DC, were performed in a cryogen-free micro-manipulated probestation (Janis Research Co.), equipped with a water-cooled closed-cycle Helium refrigerator (Sumitomo, SHI), allowing for characterization in the range of 25-300 K. The substrates were fixed on the sample table using Apiezon N vacuum grease for enhanced thermal contact and the actual temperature of the samples was monitored with a thermocouple.

In summary, large-area molecular junctions are two-terminal devices which allow the accurate and reproducible measurement of charge transport through layers ranging from self-assembled monolayers of molecules to bulk films. The properties can be measured systematically at unprecedented temperature and field ranges, offered by the stable and leakage-free junctions. The material of interest is sandwiched between two electrodes, enclosed in an insulating matrix defined in photoresist. The junctions are formed on a silicon wafer on top of which patterned bottom gold electrodes have been evaporated. Subsequently, a photoresist layer is spincoated and patterned by conventional lithography, creating circular vertical interconnects (vias, or holes) on top of the bottom electrodes. The active layer is deposited and the layer of PEDOT:PSS is spincoated on top. Finally, the junction is finished by evaporating the top gold electrodes and using them as a self-aligned mask to etch away the redundant PEDOT:PSS. Large-area molecular junctions are a versatile testbed for the characterization of various materials.

References

[1] H. B. Akkerman, P. W. M. Blom, D. M. de Leeuw, B. de Boer, Nature 441 (2006) 69.

[2] P. A. van Hal, E. C. P. Smits, T. C. T. Geuns, H. B. Akkerman, B. C. De Brito, S. Perissinotto, G. Lanzani, A. J. Kronemeijer, V. Geskin, J. Cornil, P. W. M. Blom, B. de Boer, D. M. de Leeuw, Nat. Nanotechnol. 3 (2008) 749. (including supporting info).

[3] W. Wang, T. Lee, M. A. Reed, Phys. Rev. B 68 (2003) 035416.

[4] V. B. Engelkes, J. M. Beebe, C. D. Frisbie, J. Am. Chem. Soc. 126 (2004) 14287.

[5] B. Xu, N. J. Tao, Science 301 (2003) 1221.

[6] M. Suzuki, S. Fujii, M. Fujihira, Japan. J. Appl. Phys. 45 (2006) 2041.

[7] W. Haiss, R. J. Nichols, H. van Zalinge, S. J. Higgins, D. Bethell, D. J. Schiffrin, Phys. Chem. Chem. Phys. 6 (2004) 4330.

[8] F. Chen, X. Li, J. Hihath, Z. Huang, N. J. Tao, J. Am. Chem. Soc. 128 (2006) 15874.

[9] L. Venkataraman, J. E. Klare, I. W. Tam, C. Nuckolls, M. S. Hybertsen, M. L. Steigerwald, Nano Lett. 6 (2006) 458.

[10] J. M. Beebe, V. B. Engelkes, L. L. Miller, C. D. Frisbie, J. Am. Chem. Soc. 124 (2002) 11268.

[11] X. D. Cui, A. Primak, X. Zarate, J. Tomfohr, O. F. Sankey, A. L. Moore, T. A. Moore, D. A. Gust, L. A. Nagahara, S. M. Lindsay, J. Phys. Chem. B 106 (2002) 8609.

[12] T. Morita, S. Linsday, J. Am. Chem. Soc. 129 (2007) 7262.

[13] R. L. York, P. T. Nguyen, K. Slowinski, J. Am. Chem. Soc. 125 (2003) 5948.

[14] E. A. Weiss, R. C. Chiechi, G. K. Kaufman, J. K. Kriebel, Z. Li, M. Duati, M. A. Rampi, G. M. Whitesides, J. Am. Chem. Soc. 129 (2007) 4336.

[15] F. Milani, C. Grave, V. Ferr, P. Samori, M. A. Rampi, ChemPhysChem 8 (2007) 515.

[16] C. Chu, J. S. Na, G. N. Parsons, J. Am. Chem. Soc. 129 (2006) 2287.

[17] K. T. Shimizu, J. D. Fabbri, J. J. Jelincic, N. A. Melosh, Adv. Mater. 18 (2006) 1499.

[18] T. W. Kim, G. Wang, H. Lee, T. Lee, Nanotechnology 18 (2007) 315204.

[19] M. A. Reed, C. Zhou, C. J. Muller, T. Burgin, J. M. Tour, Science 278 (1997) 252.

[20] J. Reichert, R. Ochs, D. Beckmann, H. Weber, M. Mayor, H. v. Lohneysen, Phys. Rev. Lett. 88 (2002) 176804.

[21] C. A. Martin, D. Ding, H. S. J. van der Zant, J. M. van Ruitenbeek, New J. Phys. 10 (2008) 065008.

[22] E. H. Huisman, M. L. Trouwborst, F. L. Bakker, B. de Boer, B. J. van Wees, S. J. van der Molen, Nano Lett. 8 (2008) 3381.

[23] C. M. Guedon, J. Zonneveld, H. Valkenier, J. C. Hummelen, S. J. van der Molen, Nanotechnology 22 (2011) 125205.

[24] D. Fracasso, H. Valkenier, J. C. Hummelen, G. C. Solomon, R. C. Chiechi, J. Am. Chem. Soc. 133 (2011) 9556.

[25] G. Wang, Y. Kim, M. Choe, T.-W. Kim, T. Lee, Adv. Mater. 23 (2010) 755.

[26] H. J. Yan, A. J. Bergren, R. L. McCreery, J. Am. Chem. Soc. 133 (2011) 19168.

[27] Y. L. Loo, R. L. Willett, K. W. Baldwin, J. A. Rogers, Appl. Phys. Lett. 81 (2002) 562.

[28] J. Kushmerick, J. G. amd Naciri, J. C. Yang, R. Shashidhar, Nano Lett. 3 (2003) 897.

[29] L. T. Cai, H. Skulason, J. G. Kushmerick, S. K. Pollack, J. Naciri, R. Shashidhar, D. L. Allara, T. E. Mallouk, T. S. Mayer, J. Phys. Chem. B 108 (2004) 2827.

[30] B. de Boer, M. M. Frank, Y. J. Chabal, W. Jiang, E. Garfunkel, B. Z., Langmuir 20 (2004) 1539.

[31] H. Haick, J. Ghabboun, D. Cahen, Appl. Phys. Lett. 86 (2005) 042113.

[32] Z. H. Liu, N. M. D. Brown, A. McKinley, J. Phys.: Condens. Matter 9 (1997) 59.

[33] I. Horcas, R. Fernandez, J. M. Gomez-Rodriguez, J. Colchero, J. Gomez-Herrero, A. M. Baro, Rev. Sci. Instrum. 78 (2007) 013705.

[34] M. Kemerink, S. Timpanaro, M. M. de Kok, E. A. Meulenkamp, F. J. Touwslager, J. Phys. Chem. B 108 (2004) 18820.

[35] U. Lang, E. Müller, N. Naujoks, J. Dual, Adv. Funct. Mater. 19 (2009) 1215.

[36] A. M. Nardes, M. Kemerink, A. J. Janssen, J. A. M. Bastiaansen, N. M. M. Kiggen, B. M. W. Langeveld, A. J. J. M. van Breemen, M. M. de Kok, Adv. Mater. 19 (2007) 1196.

[37] J. Y. Kim, J. H. Jung, D. E. Lee, J. Joo, Synth. Met. 126 (2002) 311.

[38] H. B. Akkerman, Large-area molecular junctions, Ph.D. thesis, University of Groningen, 2008.

[39] B. C. de Brito, E. C. P. Smits, P. A. van Hal, T. C. T. Geuns, B. de Boer, C. J. M. Lasance, H. L. Gomes, D. M. de Leeuw, Adv. Mater. 20 (2008) 3750.

[40] I. Katsouras, A. J. Kronemeijer, E. C. P. Smits, P. A. van Hal, T. C. T. Geuns, P. W. M. Blom, D. M. de Leeuw, Appl. Phys. Lett. 99 (2011) 013303.

[41] R. Haag, A. M. Rampi, R. E. Holmlin, G. M. Whitesides, J. Am. Chem. Soc. 121 (1999) 7895.

[42] D. J. Wold, C. D. Frisbie, J. Am. Chem. Soc. 123 (2001) 5549.

[43] J. Zhao, K. Uosaki, Appl. Phys. Lett. 83 (2003) 2034.

[44] S. A. DiBenedetto, A. Facchetti, M. A. Ratner, T. J. Marks, J. Am. Chem. Soc. 131 (2009) 7158.

[45] H. B. Akkerman, A. J. Kronemeijer, J. Harkema, P. A. van Hal, E. C. P. Smits, D. M. de Leeuw, P. W. M. Blom, Org. Electron. 11 (2010) 146.

CHAPTER 3

Binary self-assembled monolayers: Apparent exponential dependence of resistance on average molecular length

In this chapter we investigate the electrical transport through mixed self-assembled monolayers (SAMs) of alkanemonothiols and alkanedithiols in large-area molecular junctions. To disentangle the role of the molecular length and the interfacial composition, monothiol -monothiol, dithiol-dithiol, and monothiol-dithiol binary combinations are studied. In all cases, we find that the resistance of these mixed SAMs appears to depend exponentially on the average number of carbon atoms, thus resembling monocomponent SAMs, whose resistance is known to depend exponentially on molecular length. However, in monocomponent SAMs this behavior has a single-molecule tunneling origin, which is not directly relevant for mixtures. Furthermore, in certain mixed SAMs the resistance decreases with increasing average layer thickness (the case of monothiol-dithiol systems). We suggest an explanation for the observed dependence of the resistance in the mixed SAMs on their composition within an equivalent circuit model, based on a simple assumption concerning their microdomain structure. The simulated dependence is non-exponential and leads to a good agreement between calculated and measured resistances with only two fit parameters.

3.1 Binary SAMs in large-area molecular junctions

Molecules self-assembled in monolayers [1–3] (SAM) are used extensively to control macroscopic interfacial phenomena such as wetting, adhesion, friction and charge injection. [4–11] The properties can be tuned by using mixed monolayers where interfacial gradients are created by adjusting the chemical composition. Mixed SAMs also provide a means for incorporating single molecules that themselves do not readily self-organize. This has been applied in molecular electronics where individual molecules embedded in an insulating matrix have been addressed with scanning probe techniques. [12–14] The ultimate target is to use mixed SAMs as electronic components in molecular integrated circuits. Here we study the influence of composition on the electrical characteristics of binary ensembles of molecules. We use the previously developed technology of large-area molecular junctions, a highly reproducible molecular electronic testbed with a yield of almost unity. [15] Here, a SAM is formed on a gold bottom electrode inside a photolithographically defined vertical interconnect (via) in photoresist. The conductive polymer poly(3, 4-ethylenedioxythiophene):poly(4-styrenesulfonic acid), abbreviated as PEDOT:PSS, is spincoated on top of the SAM to fabricate the top electrode. Direct evaporation of metals on SAMs leads to short-circuit formations due to filamentary growth of metal particles. [16] The PEDOT:PSS protects the SAM when the gold top electrode is thermally evaporated and, thereby, prevents short circuit formation. The technology is suitable for up-scaling and integration. [17] More than 20000 molecular junctions were fabricated simultaneously on a single 150 mm wafer in a semi-automated process.

The electrical transport through SAMs of alkanemonothiols with a methyl end group (-CH_3), and alkanedithiols with a thiol end group (-SH), has been reported previously. [15,17] Alkanedithiols with a length of N carbon atoms (HS-C_NH_{2N}-SH) are abbreviated as CNDT and alkanemonothiols (C_NH_{2N+1}-SH) as CNMT. The transport mechanism is non-resonant tunneling. The transmission of a junction can be modeled with a multi-barrier tunnel [18] model yielding for the resistance of a single molecule, R, at low bias:

$$R = \frac{h}{2e^2} T^{-1} = 12.9\,k\Omega\, T_{Au-S}^{-1} T_{mol}^{-1} T_{SAMPEDOT}^{-1} \tag{3.1}$$

where h is the Planck constant, e is the elementary charge, T is the overall transmission probability and where T_{Au-S}, T_{mol} and $T_{SAMPEDOT}$ are the transmission probabilities for the gold sulfur bottom contact, the molecule itself and the SAM/PEDOT:PSS top contact, respectively. Rewriting in practical terms yields:

$$R = 12.9\,k\Omega\, r_{Au-S} r_{mol} r_{SAMPEDOT} \tag{3.2}$$

where r_{Au-S}, r_{mol} and $r_{SAMPEDOT}$ are dimensionless resistance contribution factors accounting for the resistance contribution of the bottom contact, the molecule and the top contact, respectively. The molecule contribution is given by $r_{mol} \propto e^{\beta n}$, where β is the decay coefficient and n the number of carbon atoms in the backbone. Note that the resistance behavior of the PEDOT:PSS layer itself in a junction is nontrivial,[19] and this can hold for the $r_{SAMPEDOT}$ contribution. Nevertheless, for a monocomponent SAM junction the $r_{SAMPEDOT}$ factor is constant and the dependence of the resistance on molecular length is found exponential.[15,17,20] This dependence derives from the r_{mol} single-molecule term, as long as the overall resistance is dominated by the molecule. The SAM junction resistance is then given by the single molecule resistance divided by the grafting density, under the plausible assumption that cooperative effects can be disregarded.

What about mixed SAMs? To investigate the contribution of both the length of the molecule and the nature of the end group we systematically studied the electric resistance of binary mixed monolayers of alkanemonothiols and alkanedithiols. First, we kept the end group constant in the series of mixed monothiols and mixed dithiols, varying only the length of the molecule. Subsequently, we investigated mixed SAMs of an alkane*mono*thiol and an alkane*di*thiol. In this case, both the length of the molecule as well as the interfacial composition are varied.

3.2 Experimental

Large-area molecular junctions were prepared as described previously. The wafer was cut in several pieces using a diamond tip pen. This allowed the simultaneous processing of different mixed SAMs on a single wafer, thereby eliminating processing variations that can affect device performance.

The self-assembled monolayers were formed from molecules dissolved in ethanol. The series of molecules used in this work include 1-dodecanethiol (C12MT), 1- heptadecanethiol (C17MT), 1-octadecanethiol (C18MT) , 1-eicosanethiol (C20MT), 1, 12-dodecanedithiol (C12DT) and 1, 16-hexadecanedithiol (C16DT). All molecules except C17MT, C20MT, C12DT and C16DT were purchased from Sigma Aldrich. The synthesis of the other molecules was performed starting from the carboxylic acid, hydroxyl or bromide precursor, depending on the commercially available compounds.

Mixed solutions of various molar ratios between the two components were prepared

by mixing stock solutions of each component at the appropriate volume ratio. The wafer pieces were immersed in the solutions for at least 36 hours, under nitrogen. The concentration in ethanol was 3×10^{-3} M for the C12DT-C17MT system, 6×10^{-3} M for the C12MT-C18MT systems and 1×10^{-2} M for the other mixtures. The higher concentration is required to prevent formation of a looped phase when using longer alkanedithiols (C16DT).[21] After the self-assembly, the wafer pieces were thoroughly rinsed with ethanol, toluene and iso-propanol to remove any remaining alkanethiol molecules. Subsequently, the interlayer of PEDOT:PSS, a water-based suspension of poly(3, 4-ethylenedioxythiophene) and poly(4-styrenesulphonic acid), was spincoated. PEDOT:PSS acts as a highly conductive buffer layer that protects the SAM during subsequent evaporation of the top gold contact. Two blends were used. (a) Baytron® PH500, H.C. Starck GmbH & Co, filtered over a 1 μm Whatman® glass filter, in which 5% v/v dimethylsulfoxide was added to increase the conductivity[22] and (b) AGFA® ICP new type filtered over a 5 μm Whatman® glass filter. Blend (a) was used for the C12MT-C18MT system, while blend (b) was used for all other experiments. The PEDOT:PSS solution was spincoated, resulting in a layer thickness of about 90 nm. The wafer was then immediately transferred to a vacuum oven for at least 1 hour to dry the film. To facilitate contacting the top electrode, 100 nm of gold was evaporated through a shadow mask. This gold layer, apart from ensuring a better contact with the measurement probes, also serves as a self aligned mask for the removal of redundant PEDOT:PSS by reactive ion etching (O_2 plasma). This step eliminates any parasitic currents from top to bottom electrode.

Current-voltage (I-V) measurements were performed in two home-built probe stations using a Keithley 4200 Semiconductor Analyzer Characterization System. The probe stations were pressurized at 10^{-6}-10^{-7} $mbar$ for at least 6 hours before the measurements, to remove any water absorbed in the PEDOT:PSS layer. Devices were swept in the voltage range of 0 V to 1 V to -1 V and back to 0 V and the recorded current densities were averaged for all devices with different diameter. The normalized resistance (RS, resistance $\times$ area, $\Omega\mu m^2$) was then calculated at 0.1 V bias. The resistance scales linearly with device area for junctions of 5-100 μm in diameter, resulting in identical RS values.

Ellipsometric measurements, to verify that the segregation coefficient is unity and that the layer thickness linearly increases with composition, were performed using a V-VASE® ellipsometer (J.A. Woolam Co, Inc) equipped with an HS-190 high speed monochromatic system and controlled with a VB-400 module. All measurements were performed at the reflection geometry in the spectral range from 350 nm to 500 nm

with a step of 3 nm, at an angle of incidence of 65°-75° with a step of 5° and 10 revisions/measurement. Acquired data were analyzed using WVASE32® software. The index of refraction for monothiols and dithiols was taken equal as 1.45. The layer thickness derived as a function of composition in solution for the C12DT-C17MT mixed SAMs is presented in Figure 3.1. A linear dependence is found indicating that within experimental error the segregation coefficient is unity, as has been reported previously.[23] This conclusion is substantiated by the calculated layer thicknesses indicated by the fully drawn curve. The end points follow from the length of the molecule, calculated with Hyperchem 7.5, adding 2.3 $\AA$ for the S-Au bonds and taking an off-normal tilt angle of 30°. The fully drawn curve is obtained by a linear extrapolation between the end points and fits the data well. This analysis applies for all binary SAMs here investigated.

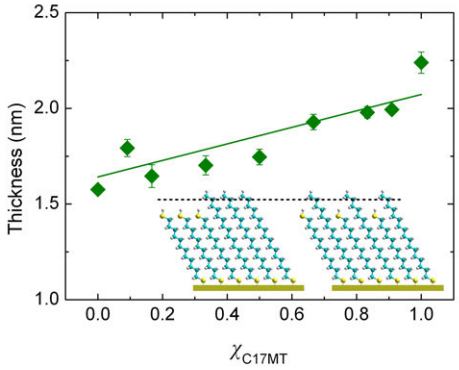

Figure 3.1: The thickness obtained from ellipsometry measurements on binary mixed SAMs of C12 dithiol and C17 monothiol (C12DT and C17MT), as a function of the fraction C17MT in solution, χ_{C17MT}. The fully drawn curve is a linear extrapolation between the end points, which have been calculated using Hyperchem 7.5.

For the sample preparation, a silicon wafer with 500 nm thermally grown oxide was rinsed with iso-propanol, dried in a dry spinner and coated with 1 nm Cr adhesion layer and 60 nm of Au, according to the procedure described above. The wafer was cut to pieces, which were transferred in nitrogen filled bottles for the ellipsometry measurements (1 reference point per piece). Subsequently, the pieces were treated in a plasma cleaner and immersed in the respective solutions to self-assemble the monolayers. Ellipsometry samples and molecular junctions were prepared simultaneously from the same solutions. The thickness of the SAMs was determined by averaging at least 3 different measurements on each piece.

3.3 Results and discussion

3.3.1 "Walking along the lines"

The simplest binary SAM in terms of molecular interactions is a mixture of alkanemonothiols, in which the chemical composition of the end group is similar to that of the main chain. The mixed monolayers of C12MT and C18MT is studied first. In Figure 3.2 the normalized resistance, RS, is presented on a semi-logarithmic scale as a function of the mole fraction of C18MT in the SAM solution. Each data point represents the average value of about 40 junctions. The data can be fitted with a straight line in semi-logarithmic coordinates that might indicate an exponential dependence of the normalized resistance on the composition in the SAM solution. Note that the segregation coefficient was verified to be unity, meaning that the composition of the SAM is the same as that of the solution (See Experimental Section). The chemical structures of the end points are schematically depicted in Figure 3.2. A variation in composition translates as a linear variation in average layer thickness. Figure 3.2 shows that the resistance increases with layer thickness exponentially.

As a next step, we turn to the resistance of a series of mixed monothiol-dithiol monolayers, namely C17MT with the dithiol C12DT. In this series both the average thickness and the interfacial composition are varied simultaneously. The normalized resistance is presented in Figure 3.3 on a semi-logarithmic scale as a function of the mole fraction of C17MT in solution. Each data point represents the average value over about 20 junctions. As in the case of the mixed monothiols we observe that the normalized resistance appears to depend exponentially on composition. However, the dithiol, which is the shorter of the two molecules, has a higher resistance in monocomponent SAM than the monothiol, which is longer (their chemical structures are schematically depicted in Figure 3.3). Therefore, Figure 3.3 unambiguously shows that the resistance of the mixed C12DT-C17MT SAM decreases with increasing average layer thickness.

To complete this study, we fabricated all the binary monolayers of 4 components, *viz.* two alkanemonothiols C17MT and C20MT and two alkanedithiols C12DT and C16DT, except for the C12DT-C20MT mixed SAM. In this latter system, the big difference in the number of carbons is expected to lead to a non-unity segregation factor due to preferential adsorption.[24–26] The normalized resistances are presented in Figure 3.4 on a semi-logarithmic scale as a function of average number of atoms, as calculated from the mole fraction in solution assuming a segregation coefficient of

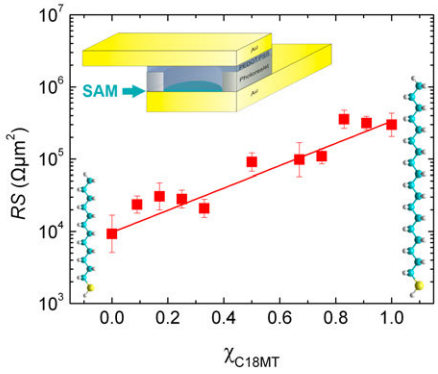

Figure 3.2: Normalized resistance, RS, of binary mixed SAMs of C12 and C18 monothiols (C12MT and C18MT), as a function of mole fraction of C18MT in solution, χ_{C18MT}. The solid red line represents an exponential fit to the data. The inset shows a schematic cross section of the junction. The chemical structures of the end points are included to illustrate that the resistance increases with increasing layer thickness.

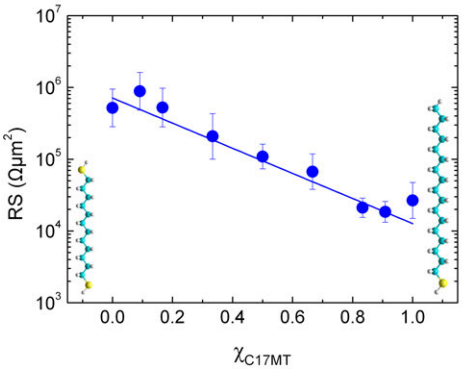

Figure 3.3: Normalized resistance, RS, of binary mixed SAMs of C12 dithiol and C17 monothiol (C12DT and C17MT), as a function of mole fraction of C17MT in solution, χ_{C17MT}. The solid blue line represents an exponential fit to the data. The chemical structures of the end points are included to illustrate that the resistance decreases with increasing layer thickness.

unity. The resistances of all binary SAMs can be fitted with straight lines that might indicate an exponential dependence on the average number of atoms.

The constructed resistance diagram of Figure 3.4 shows a trapezoidal correlation. The mixed monothiol C17MT-C20MT SAM and the mixed dithiol C12DT-C16DT SAM exhibit the same slope, yielding parallel lines. Throughout each of these two series, the contributions to the resistance from the top and bottom contacts are constant. The resistance changes only due to a different number of carbon atoms. The

contribution of the top contact is reflected in the series C16DT-C17MT. The average number of atoms in the mixed SAM is constant, while the interfacial composition is varied. The resistance systematically varies with composition over more than two orders of magnitude. The simultaneous effect of molecular length and nature of the end group is observed along the C12DT-C17MT and C16DT-C20MT lines. For both these series an apparently exponential dependence on the average number of atoms is found. The slope, however, is different because the change in the number of atoms at the end points is different; hence the corresponding lines in the trapezoid are not parallel.

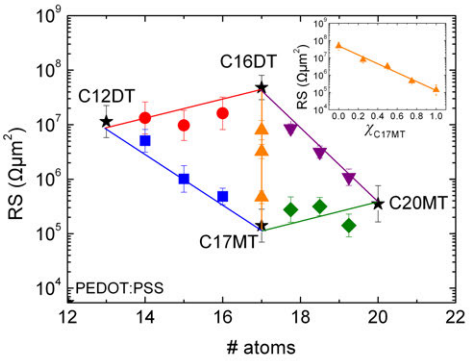

Figure 3.4: Geometric resistance diagram showing a trapezoidal correlation. Normalized resistance, *RS*, of all binary mixed SAMs based on the end points C12DT, C16DT, C17MT and C20MT, as a function of average number of atoms. The fully drawn curves are a guide to the eye. The inset shows the normalized resistance of the C16DT-C17MT mixed SAMs as a function of the mole fraction of C17MT in solution. The vertical axis starts at 5×10^3 $\Omega\mu m^2$, the value for the corresponding PEDOT:PSS only junction.

3.3.2 Apparent exponential dependence

As a matter of fact, the experimental results leading to the diagram in Figure 3.4 are quite puzzling. The first hypothesis to consider is that in a mixed SAM the overall resistance is given by the resistance of all its constituent individual molecules connected in parallel, *i.e.* as in a monocomponent SAM. It is easy to show that the behavior this hypothesis predicts contradicts experiment. Indeed, addition of significantly more conductive molecules would quickly reduce the resistance of a mixed SAM already when their fraction is low, because they would act as "shorts". On the other hand, a low share of less conductive molecules has no spectacular effect. The dependence of resistance on composition simulated in Figure 3.5 and Figure 3.6 is far from both the

experimental points and from the straight line in semi-logarithmic coordinates. We are forced to conclude that not every molecule in the mixed SAM carries current fully and independently. Another extreme hypothesis would be that molecular composition of the SAM is irrelevant, it just serves as an effective medium (spacer) that only modifies the average width of the tunneling barrier between the contacts. Such a model seems compatible with the exponential dependence on average thickness found. We note that for MT-MT and DT-DT mixed SAMs the slope obtained amounts to 3.54 per fraction. The difference between the end points is 6 carbon atoms, yielding a slope of 0.6 per carbon atom. Apparently, both systems exhibit the same length dependence with a decay coefficient of about 0.6 per carbon atom. This value corresponds to the one derived in Figure 3.2 and to published decay constants for alkane based molecules of 0.5 - 1.2.[15,17,20] The resistance changes only due to a different number of carbon atoms, according to Equation 3.2, where molecular contribution is given by $r_{mol} \propto e^{\beta n}$, where β is the constant decay coefficient and n in this case is the average number of carbon atoms.

Whatever the possible physical justification of this model, not all the observed facts are compatible with it. Note that the absolute value for the resistances of the mixed monothiols is different from that of the mixed dithiols. According to Equation 3.2, this offset originates from the different end groups, -CH_3 versus -SH, yielding a different top contact contribution, $r_{SAMPEDOT}$.[16,17,20,27–34] The numbers imply a more transparent contact barrier, *i.e.* a higher transmission coefficient, for the methyl/PEDOT:PSS interface as for the thiol/PEDOT:PSS interface. We note that this behavior is counterintuitive: the water-based suspension PEDOT:PSS is expected to be repelled by the hydrophobic methyl end group of the alkanemonothiols, yielding a less intimate physical contact. Therefore the absolute resistance of a dithiol SAM is expected to be lower than that of a monothiol SAM, contrary to what is experimentally observed; at the moment, we have no explanation for this fact. This difference is significant enough to make certain monocomponent SAMs of longer MT less resistive than those of DT with shorter molecules. Consequently, a systematic resistance decrease with increasing average layer thickness for certain monothiol-dithiol mixed SAMs (Figure 3.4) was observed, which contradicts the effective medium model and stresses the importance of microscopic structure of the junction.

3.3.3 A phenomenological model for the mixed SAM resistance

The consideration in the previous section demonstrates that a viable model for mixed SAMs should take into account their microstructure in a realistic way, assum-

ing that the resistance can be calculated as for an equivalent circuit of a parallel resistor network. With this in mind, we propose a microdomain model, which by parameterization of the microstructure explains the resistance data.

A mixed monolayer is a dynamic system formed at room temperature at relatively low concentrations. Though full phase segregation is thermodynamically favorable, the SAM will nevertheless contain phases with kinetically-formed compositions [35] where domains of different sizes coexist probably even with single molecules. For the purpose of an equivalent circuit of a mixed SAM composed of molecules A and B, we limit the model to four parallel resistances, per molecule: (i) A-domain, (ii) A-single, (iii) B-domain and (iv) B-single. The difference in effective resistance of the same molecule as single or a domain member is supposed to reflect contact and conformational issues, rather than mutual influence of the molecules that we consider irrelevant. Indeed, the longer molecules likely act as pillars and only they are fully contacted by PEDOT:PSS, preventing all short molecules from being equally well contacted and fully contribute to the current. On the other hand, the longer molecules trapped into the shorter molecule domains can hardly stand straight but rather adopt bent conformations. Consequently, "domain" in this context signifies an ensemble of molecules vast enough to be fully contacted (*i.e.* the fraction of molecules at its boundaries being relatively small), while "singles" might as well apply to groups of a few molecules. Therefore, the resistance of the A and B in domains corresponds to that of the monocomponent SAMs of A and B, respectively, while the resistances of A and B singles have to be parameterized.

We need now a model for the composition of a *mixed* SAM in terms of domains and singles for both components. It has been known that alkanethiol SAM formation is a two-stage process, the initial fast step being diffusion-limited adsorption and the second slow step reorganization of the primary monolayer described as surface crystallization. [36] For a mixed monolayer, we suppose that only a part of the molecules of each type will assemble into domains, while the rest will be in the form of singles. It is reasonable to assume that the shares of the domains and singles depends on the composition of the SAM. Let the molecular composition of the monolayer be characterized by the mole fraction of A denoted by χ; the fraction of B is then $1-\chi$, $\chi = 0$ corresponds to pure B and $\chi = 1$ corresponds to pure A. When $\chi \to 0$, all molecules B are expected to be organized in domains, while for $\chi \to 1$ practically all molecules B are single: a view supported by previously reported STM data. [37] We suppose further that a certain number of molecules, n, must meet to form a critical nucleus leading to the formation of a domain, which is more likely to occur when there are

more molecules of a given component in the mixed monolayer, hence at a higher mole fraction of this component. Within such a probabilistic approach, the population, of A and B arranged in domains is, χ^n and $(1-\chi)^n$ respectively. The population of singles is then $\chi - \chi^n$ for A and $(1-\chi) - (1-\chi)^n$ for B. The resistance of the mixed SAM as a function of composition is then given by:

$$\frac{1}{R} = \frac{\chi^n}{R_{A-domain}} + \frac{(1-\chi^{n-1})\chi}{R_{A-single}} + \frac{(1-\chi)^n}{R_{B-domain}} + \frac{(1-\chi)[1-(1-\chi)^{n-1}]}{R_{B-single}} \tag{3.3}$$

For the mixed SAMs of Figure 3.5, the molecule A is C18 monothiol and the molecule B is C12 monothiol. The resistances of each of the domains, $R_{A-domain}$ and $R_{B-domain}$, are taken equal to that of the corresponding end points, *viz.* the pure single component SAMs. As in the case of a perfectly mixed monolayer, the top inset of Figure 3.5, we assume that the single molecules C12 monothiol embedded in domains of C18 monothiols, are not contacted by the PEDOT:PSS top contact. Therefore they do not contribute to the overall resistance. Only when organized in sufficiently large domains the short molecules contribute to the overall resistance, as schematically depicted in the lower inset of Figure 3.5. The only parameters left are the exponent n and the resistance of a single molecule C18 monothiol in domains of C12 monothiol, $R_{A-single}$. Fitting the experimental data with Equation 3.3 (fully drawn red curve in Figure 3.5) yields $n = 2.3$ and $R_{A-single} = 43$. The resistance of single C18MT molecules in domains of C12MT, $R_{A-single}$, is in the same order of magnitude as the C18MT domains.

Parameterization of the microstructure can also explain the observed resistance behavior of the mixed C12DT-C17MT system of Figure 3.3, where the resistance actually decreases with increasing average layer thickness. The resistances are replotted in Figure 3.6 where the values are normalized to the pure C17MT SAM. Similarly as above, we take the resistances of the domains equal to that of the corresponding end points, the pure monocomponent SAMs. The contribution of the short single molecules is again disregarded. The only parameters left in Equation 3.3 are the exponent n and the resistance of a single molecule C17 monothiol in domains of C12 dithiol, $R_{A-single}$. The dashed black curve in Figure 3.6 is calculated assuming that the resistance for single C17MT molecules is the same as that in domains. Contrary to Figure 3.5, this assumption does not lead to a fit to the data. This is because C17MT molecules are highly conductive in comparison with C12DT molecules and constitute electric shorts in a C12DT domain. A fitting of both n and $R_{A-single}$ yields a good

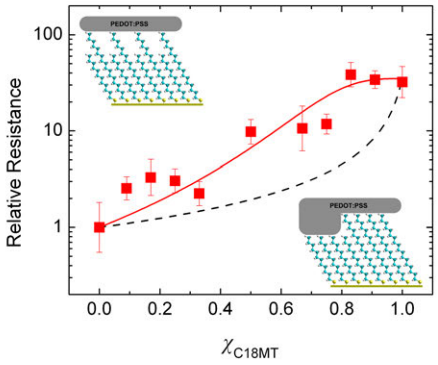

Figure 3.5: Relative resistance of binary mixed SAMs of C12 and C18 monothiols (C12MT and C18MT), as a function of mole fraction of C18MT in solution, χ_{C18MT}, taken from Figure 3.2 and normalized to the end point C12MT. The insets show the two cases of the mixed SAM microstructure. The top left inset depicts intermixing and the bottom right inset depicts phase separation. The dashed black line is calculated assuming that all the molecules of each component have the same resistance equal to their resistance in their respective monocomponent SAMs and are connected in parallel in the mixed SAMs. The solid red line is calculated by parameterization of the microstructure using Equation 3.3.

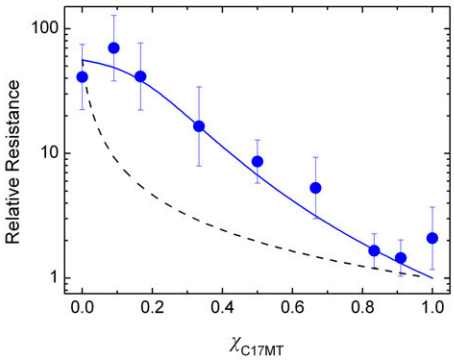

Figure 3.6: Relative resistance of binary mixed SAMs of C12 dithiol and C17 monothiol (C12DT and C17MT), as a function of mole fraction of C17MT in solution, χ_{C17MT}, as taken from Figure 3.3 and normalized to the end point C17MT. The dashed black line is calculated assuming that all the molecules of each component have the same resistance equal to their resistance in their respective monocomponent SAMs and are connected in parallel in the mixed SAMs. The blue line is calculated by parameterization of the microstructure using Equation 3.3.

agreement, however, with $n = 3.3$ and the relative resistance of the single C17MT molecule equal to 27, an order of magnitude higher than when organized in domains.

This approximately twenty-fold increase in the resistance of single long monothiols

can be related to their molecular conformation. It has been shown that the resistance of an alkane molecule increases an order of magnitude when gauche defects are introduced.[38,39] The emergence of defects can be due to conformational disorder, whose origin in a mixed SAM has been described previously.[26,35] Close to the gold surface, the mixed SAM is ordered. The free volume introduced into the outer part of the longer molecules in the monolayer by the presence of the shorter chains makes it disordered and liquid-like. The loss of lateral and orientational order implies the existence of gauche defects. We note that the degree of conformational disorder in the longer molecules depends on their share in the mixed SAM. At low fraction the gauche densities per molecule are higher,[35] meaning that most of the longer molecules exist as singles, in agreement with the assumption that the domain fraction depends on the monolayer composition.

Conformational changes, or gauche defects, affect the charge transport through a molecule directly,[38–41] by reducing the periodicity. Indirectly, the resistance can be affected by the presence of bent molecules via altered interface energy of a methyl- to a methylene terminated interface,[35,42] as well as by diminishing the electronic coupling of the shorter SAM domains to the top contact.[43] For the monothiol/dithiol SAMs, the presence of gauche defects can be inferred from analysis. On the other hand, conformational disorder in mixed monothiols does not manifest in our electric measurements as the single long molecules already have a higher resistance.

Relatively small values for n support the hypothesis that the dependence of the normalized resistance on the fraction is non-exponential, but follows a power law. Moreover, as simple as our model might be, it embodies some tracts of nucleation and growth phenomena. The assumption of a critical nucleus size of 1-2 molecules might be reasonable,[44] although weaker intermolecular interactions can lead to critical nucleus sizes larger than two.[45,46] The different interactions between the components in the two systems, owing to their different chemical structures, could explain the variation in the value of n. A more rigorous treatment could account for the dynamics of the binary SAM in order to relate the trend to the critical nucleus size.

3.4 Summary and conclusions

We have investigated the electrical transport through mixed self-assembled monolayers in large-area molecular junctions. The SAM is formed on a gold bottom electrode inside a photolithographically defined interconnect in photoresist. The conducting polymer PEDOT:PSS is used as top contact. To investigate the contribution of

both the length of the molecule and the nature of the end group on the resistance, we systematically studied the charge transport through mixed monolayers of alkanemonothiols and alkanedithiols. We verified by ellipsometry measurements that the segregation coefficient is unity for all investigated binary SAMs. To disentangle the role of the length of the molecule and the interfacial composition, we prepared mixed monolayers of all different binary combinations of two monothiols and two dithiols. The end group is fixed in a series of mixed monothiols and in a series of mixed dithiols.

A trapezoidal correlation in semi-logarithmic resistance-composition coordinates has been obtained (Figure 3.4). The straight lines seem to indicate an exponential dependence on composition, or on the average molecular length, also in the case of mono-and dithiol mixed SAMs where resistance can decrease with increasing layer thickness, as the longer component is more conductive in monocomponent SAM. However mathematically simple, exponential dependence is difficult to justify physically for mixed monolayers, unlike the case of monocomponent SAMs where this dependence has a single-molecule tunneling origin.

We search for the origin of the resistance-composition dependence in mixed SAMs in an equivalent circuit model based on their microdomain structure, for which we suggest a simple model. In essence, we suppose that the effective resistance of a molecule can differ depending on whether it is isolated (that is, trapped within an alien molecular domain) or belongs to a domain of the same molecules, due to contact and conformational issues. The simulated dependence is non-exponential and leads to a good agreement between calculated and measured resistances with only two fit parameters.

References

[1] J. C. Love, L. A. Estroff, J. K. Kriebel, R. G. Nuzzo, G. M. Whitesides, Chem. Rev. 105 (2005) 1103. (and references therein).

[2] M. D. Porter, T. B. Bright, D. L. Allara, C. E. D. Chidsey, J. Am. Chem. Soc. 109 (1987) 3559.

[3] C. Vericat, M. E. Vela, G. A. Benitez, J. A. M. Gago, X. Torrelles, R. C. Salvarezza, J. Phys.: Condens. Matter 18 (2006) R867.

[4] P. E. Laibinis, G. M. Whitesides, J. Am. Chem. Soc. 114 (1992) 1990.

[5] A. Ulman, An introduction to ultrathin organic films: From Langmuir-Blodgett to self-assembly, Academic Press, INC, San Diago, 1991.

[6] C. Pale-Grosdemange, E. S. Simon, K. L. Prime, G. M. Whitesides, J. Am. Chem. Soc. 113 (1991) 12.

[7] D. L. Allara, A. F. Heburd, F. J. Padden, R. G. Nuzzo, D. R. Falcone, J. Vac. Sci. Technol. A 1 (1983) 376.

[8] V. DePalma, N. Tillman, Langmuir 5 (1989) 868.

[9] C. E. D. Chidsey, Science 251 (1991) 919.

[10] G. K. Rowe, S. E. Creager, Langmuir 7 (1991) 2307.

[11] B. de Boer, A. Hadipour, M. M. Mandoc, T. van Woudenbergh, P. W. M. Blom, Adv. Mater. 17 (2005) 621.

[12] G. K. Ramachandran, T. J. Hopson, A. M. Rawlett, L. A. Nagahara, A. Primak, Lindsay, Science 300 (2003) 1413.

[13] A. S. Blum, J. G. Kushmerick, D. P. Long, C. H. Patterson, J. C. Yang, J. C. Henderson, Y. X. Yao, J. M. Tour, R. Shashidhar, B. R. Ratna, Nat. Mater. 4 (2005) 167.

[14] Z. J. Donhauser, B. A. Mantooth, T. P. Pearl, K. F. Kelly, S. U. Nanayakkara, P. S. Weiss, Jpn. J. App. Phys. 41 (2002) 4871.

[15] H. B. Akkerman, P. W. M. Blom, D. M. de Leeuw, B. de Boer, Nature 441 (2006) 69.

[16] T. W. Kim, G. Wang, H. Lee, T. Lee, Nanotechnology 18 (2007) 315204.

[17] P. A. van Hal, E. C. P. Smits, T. C. T. Geuns, H. B. Akkerman, B. C. De Brito, S. Perissinotto, G. Lanzani, A. J. Kronemeijer, V. Geskin, J. Cornil, P. W. M. Blom, B. de Boer, D. M. de Leeuw, Nat. Nanotechnol. 3 (2008) 749. (including supporting info).

[18] G. Wang, T. W. Kim, H. Lee, T. Lee, Phys. Rev. B 76 (2007) 205320.

[19] A. J. Kronemeijer, E. H. Huisman, I. Katsouras, P. A. van Hal, T. C. T. Geuns, P. W. M. Blom, S. J. van der Molen, D. M. de Leeuw, Phys. Rev. Lett. 105 (2010) 156604.

[20] H. B. Akkerman, B. de Boer, J. Phys:Condens. Matter 20 (2008) 013001. (and references therein).

[21] H. B. Akkerman, A. J. Kronemeijer, P. A. van Hal, D. M. de Leeuw, P. W. M. Blom, B. de Boer, Small 4 (2008) 100.

[22] J. Y. Kim, J. H. Jung, D. E. Lee, J. Joo, Synth. Met. 126 (2002) 311.

[23] J. P. Folkers, P. E. Laibinis, G. M. Whitesides, Langmuir 8 (1992) 1330.

[24] S. F. Chen, L. Y. Li, C. L. Boozer, S. Y. Jiang, Langmuir 16 (2000) 9287.

[25] K. Heister, D. L. Allara, K. Bahnck, S. Frey, M. Zharnikov, M. Grunze, Langmuir 15 (1999) 5440.

[26] C. D. Bain, G. M. Whitesides, J. Am. Chem. Soc. 111 (1989) 7164.

[27] J. M. Seminario, L. M. Yan, Int. J. Quantum Chem. 102 (2005) 711.

[28] H. Haick, O. Niitsoo, J. Ghabboun, D. Cahen, J. Phys. Chem. C 111 (2007) 2318.

[29] F. Chen, X. Li, J. Hihath, Z. Huang, N. J. Tao, J. Am. Chem. Soc. 128 (2006) 15874.

[30] B. Kim, J. M. Beebe, Y. Jun, X. Y. Zhu, C. D. Frisbie, J. Am. Chem. Soc. 128 (2006) 4970.

[31] F. Tao, S. L. Bernasek, Chem. Rev. 107 (2007) 1408. (and references therein).

[32] P. E. Laibinis, G. M. Whitesides, D. L. Allara, Y. T. Tao, A. N. Parikh, R. G. Nuzzo, J. Am. Chem. Soc. 113 (1991) 7152.

[33] H. Basch, R. Cohen, M. A. Ratner, Nano Lett. 5 (2005) 1668.

[34] X. L. Li, J. He, J. Hihath, B. Q. Xu, S. M. Lindsay, N. J. Tao, J. Am. Chem. Soc. 128 (2006) 2135.

[35] P. E. Laibinis, R. G. Nuzzo, G. M. Whitesides, J. Phys. Chem. 96 (1992) 5097.

[36] A. Ulman, Chem. Rev. 96 (1996) 1533.

[37] G. E. Poirier, Chem. Rev. 97 (1997) 1117.

[38] C. Li, I. Pobelov, T. Wandlowski, A. Bagrets, A. Arnold, F. Evers, J. Am. Chem. Soc. 130 (2008) 318.

[39] M. Fujihira, M. Suzuki, S. Fujii, A. Nishikawa, Phys. Chem. Chem. Phys. 8 (2006) 3876.

[40] M. Paulsson, C. Krag, T. Frederiksen, M. Brandbyge, Nano Lett. 9 (2009) 117.

[41] K. Tagami, M. Tsukada, e-J. Surf. Sci. Nanotechnol. 2 (2004) 186.

[42] A. Ulman, S. D. Evans, Y. Shnidman, R. Sharma, J. E. Eilers, J. C. Chang, J. Am. Chem. Soc. 113 (1991) 1499.

[43] R. L. York, K. Slowinski, J. Electroanal. Chem. 327 (2003) 550.

[44] I. Doudevski, D. K. Schwartz, Phys. Rev. B 60 (1999) 14.

[45] M. Brinkmann, S. Graff, F. Biscarini, Phys. Rev. B 66 (2002) 165430.

[46] S. Verlaak, S. Steudel, P. Heremans, D. Janssen, M. S. Deleuze, Phys. Rev. B 68 (2003) 195409.

CHAPTER 4

Organic field-effect transistors as a testbed for molecular electronics: A combined study with large-area molecular junctions

The contact resistance of a transistor using self-assembled monolayer (SAM)-modified source and drain electrodes depends on the SAM tunnel resistance, the height of the injection barrier and the morphology at the contact. To disentangle the different contributions, we have combined here transmission line measurements in transistors with transport measurements of SAMs in large-area molecular junctions. The tunnel resistance of the SAM has been independently extracted in two-terminal large-area molecular junctions. We show that the tunneling resistance of the SAM can be added linearly to the contact resistance of the transistor with bare Au electrodes, to account for the increased contact resistance in the SAM-modified transistor. The manifestation of the SAM in the contact resistance shows that transistors can potentially be used as an experimental testbed for molecular electronics.

4.1 FETs as a gauge for molecular electronics

The building block of organic electronic integrated circuits is the field-effect transistor (FET). Applications are envisaged in smart labels and active matrix displays.[1,2] The performance of the transistor depends on both charge injection and the transport of injected charges through the organic semiconductor.[3] The charge transport in organic semiconductors is theoretically well understood.[4–8] Experimentally, charge carrier mobilities close to unity ($cm^2V^{-1}s^{-1}$) have been reported both for holes and electrons.[9,10] A remaining challenge is understanding of the charge injection mechanism.

To inject charge carriers the Fermi level of the metal electrode has to be aligned with either the lowest unoccupied molecular orbital (LUMO) or the highest occupied molecular orbital (HOMO) of the organic semiconductor.[11,12] An offset between these levels yields an injection barrier, the presence of which deteriorates charge injection.[13–16] To reduce the injection barrier the workfunction of the electrodes has been modified by using polar self-assembled monolayers.[17] This dipole layer can be described as two parallel sheets of charge separated by the length of the molecule. The change in workfunction of the modified electrode follows from classical electrostatics.[18] By adapting the dipole moment of the molecule the workfunction can be tuned in a range of about 2 eV.

Although control of charge injection with SAMs in FETs has led to improved performance, enhancement of the extracted field-effect mobility and reduction of the contact resistance,[16,19] the role of SAMs on the FETs performance is still elusive. In a thorough study, Stoliar *et al.* have investigated pentacene FETs with Au electrodes functionalized with alkanethiols. The extracted mobility increased with chain length up to $n = 8$ (n being the number of methylene units), and decreased exponentially for n larger than 8.[20] This non-monotonic behavior, together with a clear odd-even fluctuation in the extracted mobility, has been explained as the result of the interplay between a decreased hole injection barrier due to the dipole moment of the SAM, the tunneling assisted by the SAM and by an improved morphology of the pentacene at the interface with the SAM.

Firstly, we note that the mobility extracted from transistors is rather tolerant for injection barriers. Pentacene has been investigated using transistors with source and drain electrodes with widely different workfunctions: Au, Cu, Ni. The saturated output currents differed by less than an order of magnitude. Experimentally, injection barriers as high as 1 eV can be surmounted.[21–24]

Moreover, deposition of organic materials that tend to form crystalline domains is particularly sensitive to the surface energy of the substrate. Application of a SAM alters the surface energy and can therefore change the morphology of the deposited semiconductor.[25,26] Changes in device mobility upon application of a SAM are therefore not necessarily due to a change in injection barrier but can be due to a different morphology.[27–30]

Finally, insertion of a SAM on the electrodes introduces an additional resistance. The extra resistance depends on the molecular structure of the SAM, conjugated or non-conjugated, and its molecular length.[31–33] The resistance increases with the molecular length, L, of the molecule as $R \propto e^{\beta L}$, where the tunneling decay coefficient β depends on the energy gap between the HOMO and the LUMO.[34,35] Although the charge transport through single molecules has typically been investigated in break junctions, in scanning probe geometries and in large-area molecular junctions, Stoliar *et al.* extracted the decay coefficient β from transistor measurements.[20] However, how the SAMs resistance manifests in the overall resistance of the transistor remains unclear. It can be a simple series resistance or it can be a multiplication factor for the contact resistance.

In this chapter, we combine electrical measurements in large-area molecular junctions with those in FETs to disentangle the different contributions of a SAM-modified electrode in the extracted mobility of a transistor. We used aliphatic SAMs because they are the benchmark for self-assembly. Aromatic SAMs can be applied to modify workfunction and improve device performance. Therefore we speculate that the mechanism described for aliphatic SAMs would be same for aromatic SAMs. In order to eliminate the morphological complications, we used an amorphous semiconducting polymer. The electrode workfunction was tuned in opposite directions using SAMs with opposite dipole moments. We substantiate the effect of the SAM on the source-drain electrodes by investigation of the contact resistance of the FET using the transmission line method (TLM). We further corroborate the role of the resistance of the SAM in a FET by utilizing two-terminal large-area molecular junctions to independently extract the tunneling resistance of the used SAMs. We demonstrate that in a first order approximation the tunneling resistance of the SAM can be added linearly to the contact resistance of bare Au FETs, to account for the increased contact resistance in SAM-modified FETs. We tentatively propose that this result supports the claim that a FET can be used as an experimental testbed for molecular electronics.[20,33]

4.2 Experimental

Materials: Hexadecanethiol (HDT) was purchased from Aldrich and was distilled prior to use. Perfluorinated decanethiol (PFDT) was synthesized according to literature procedures.[36] Poly(2-methoxy-5-(2'-ethylhexyloxy)-1, 4-phenylene vinylene) (MEH-PPV), an amorphous semiconducting polymer, was synthesized in our laboratory via the Gilch method.[37] Poly(3, 4-ethylenedioxythiophene):poly(4- styrenesulphonic acid) (PEDOT:PSS) was purchased from AGFA. Chemical structures of all the compounds are given in Figure 4.1c.

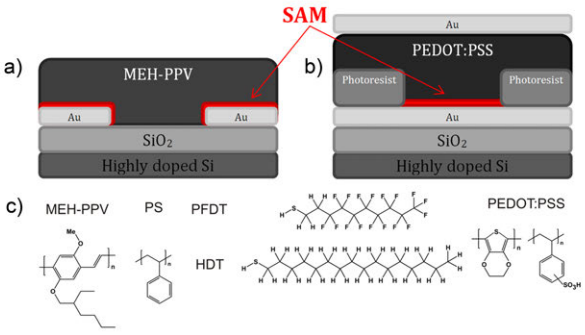

Figure 4.1: Schematic of (a) a field-effect transistor and (b) a large-area molecular junction. The self-assembled monolayer (SAM) is indicated in red. (c) Chemical structure of the materials used.

Device fabrication: FET test substrates (Figure 4.1a) were fabricated on 150 mm highly p-type doped Si wafers with 250 nm thermally grown silicon oxide. Using conventional lithography, Au source and drain contacts (150 nm) were patterned with finger geometry with 5 nm of Ti as an adhesion layer. The channel length varied from 5 μm to 40 μm while the channel width was kept constant at 10000 μm. Prior to use, the FET test substrates were treated with the primer hexamethyldisilazene (HMDS). HDT and PFDT were dissolved in ethanol with a concentration of 1 mM. The FET substrates were then immersed into the solution for 36 hours. After the self-assembly process, the substrates were thoroughly rinsed with ethanol, toluene, and 2-propanol, respectively and then spin dried. MEH-PPV solution (dry toluene, 5 mg/ml) was then spincoated onto the FET substrates. The film thickness was kept at 100 nm. All spincoating and evaporation processes were performed in a nitrogen-filled glove box.

Large-area molecular junctions (Figure 4.1b) were manufactured as described pre-

viously. On 100-mm Si wafers with a 500 nm thermally grown oxide treated with HMDS, Au bottom electrodes of 60 nm (rms roughness was $\backsim$ 0.7 nm over an area of 0.25 μm^2) were thermally evaporated through a shadow mask with 1 nm of Cr as an adhesion layer. Vertical interconnects, ranging from 5 μm to 100 μm in diameter, were defined in a 570 nm layer of negative photoresist, ma-N1410 (micro resist technology GmbH) using conventional UV-lithography. SAM formation was identical to that of the FETs. After self-assembly, a 90 nm interlayer of PEDOT:PSS was spincoated on to the substrate and dried in dynamic vacuum. PEDOT:PSS acts as a highly conductive buffer layer that protects the SAM during evaporation of the 100 nm thick top Au contact. The top Au layer ensures better contact with the measurement probes and serves as a self-aligned mask for the removal of redundant PEDOT:PSS by reactive ion etching (O_2 plasma). This step eliminates any parasitic currents from the top to the bottom electrode.

For workfunction measurements, Au substrates were prepared by thermal evaporation of 150 nm of Au on thermally grown SiO_2 substrate with 1 nm of Cr as an adhesion layer. After the self-assembly process the workfunction of bare and SAM-modified metals were measured using a Kelvin probe in a nitrogen-filled glove box. Device characterization: Electrical measurements on FETs were all carried out in a probe station under high vacuum (10^{-6} $mbar$) with a Keithley 4200-SCS Semiconductor Characterization System. In the case of large-area molecular junctions, the probe station was pressurized at 10^{-6}-10^{-7} $mbar$ for at least 6 hours before the measurements to remove any residual water absorbed in the PEDOT:PSS layer.[38] The recorded current densities were averaged for approximately 40 devices with different diameters.

4.3 Results and discussion

4.3.1 FETs and molecular junctions characterization

We measured large-area molecular junctions with self-assembled monolayers of both PFDT and HDT, processed in identical conditions. In large-area molecular junctions the tunneling resistance can be evaluated by measuring the tunneling current.[31,32] Figure 4.2 shows the tunneling current density versus applied voltage for PFDT and HDT junctions. The values are averaged over more than 40 devices. We calculated the normalized resistance in the Ohmic regime (RS, resistance $\times$ area, $\Omega\mu m^2$) at 0.1 V bias, corresponding to an electric field of 70 MV/m. The resistance scales linearly with

device area for junctions of 5-100 μm in diameter, resulting in identical RS values. For HDT and PFDT SAMs the corresponding tunnel resistances were determined as $2.7 \times 10^6\ \Omega\mu m^2$ and $9.7 \times 10^5\ \Omega\mu m^2$, respectively.

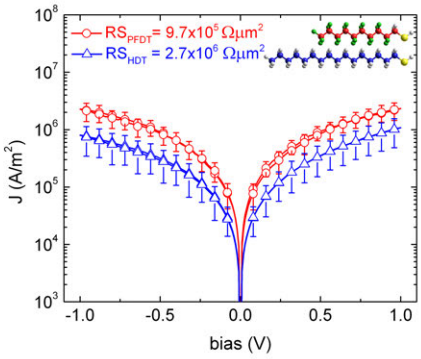

Figure 4.2: Current density versus voltage as measured in large-area molecular junctions for PFDT and HDT. The values are averaged over more than 40 devices. The normalized resistance values (RS) and the corresponding structures of the molecules are indicated.

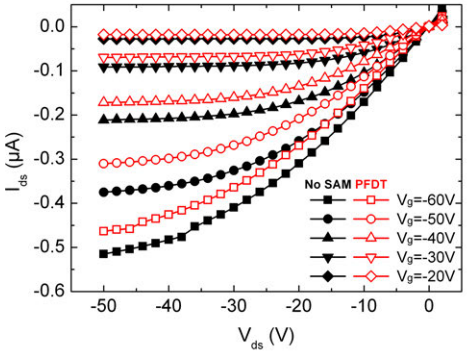

Figure 4.3: Output characteristics of field-effect transistors with bare Au and PFDT-modified Au source-drain electrodes in a bottom contact, bottom gate (BC/BG) configuration.

We used bottom contact / bottom gate (BC/BG) transistors to extract the contact resistance in the FETs as a function of gate bias. In the coplanar BC/BG structure, charges are directly injected into the accumulation layer at the semiconductor/dielectric interface, whereas in the staggered bottom contact / top gate (BC/TG) configuration, the source and drain electrodes are separated from the channel by the semiconducting layer, which yields a series resistance. Direct evaluation of SAMs tun-

nel resistance in BC/TG is then hampered by the presence of the additional resistance. Moreover, the current crowding effect in BC/TG impedes a good estimation of the effective contact area.[39]

To unambiguously rule out the influence of an injection barrier, we first focus on PFDT-treated Au electrodes. The workfunction of bare Au was measured as 4.7-4.8 eV and that of the PFDT-treated Au electrode as 5.5 eV. The HOMO energy of MEH-PPV is approximately 5.1 eV. Therefore both bare Au and Au/PFDT electrodes form an Ohmic contact with MEH-PPV for hole injection.

The output characteristics are presented in Figure 4.3. There is no hysteresis. The mobility determined for both transistors in the linear regime at small source-drain bias is comparable and amounts to 3×10^{-4} $cm^2V^{-1}s^{-1}$, in good agreement with reported mobility values. A similar value for the saturated mobility was determined from the transfer characteristics (not shown), which shows that the channel resistance of the transistors with bare Au and Au/PFDT electrodes is the same.

Figure 4.3 shows that the output current using Au/PFDT electrodes for all gate voltages is smaller than that using bare Au electrodes. The total device resistance is comprised of the channel resistance plus the contact resistances. To verify that the lower output current for Au/PFDT originates from an increased contact resistance, we derived the contact resistance via the transmission line method by using transistors with various channel lengths.[16,40] The contact resistances derived from the TLM scaling analysis are presented in Figure 4.4 as a function of gate bias. The contact resistance decreases with increasing negative gate bias as commonly observed.[24,41,42] At low bias the charges are injected into an undoped semiconductor yielding a high contact resistance. With increasing gate bias the semiconductor gets electrostatically doped, and the contact resistance decreases. The contact resistance has been presented as a function of mobility.[41]The determined value of the contact resistance in accumulation of about 10^8 Ωm is lower than expected for a transistor with a mobility of 3×10^{-4} $cm^2V^{-1}s^{-1}$, confirming the absence of any injection barrier. Figure 4.4 shows that the contact resistance increases when the Au source/drain electrodes are modified with a PFDT SAM. In order to relate the calculated contact resistance with the measured resistance of the PFDT SAM in molecular junctions, we renormalized the contact resistance to the injection area in transistors. The renormalized contact resistance (presented in Figure 4.4 right axis) is taken as the contact resistance times the thickness of the accumulation layer which is typically estimated as about 2 nm.[43,44]

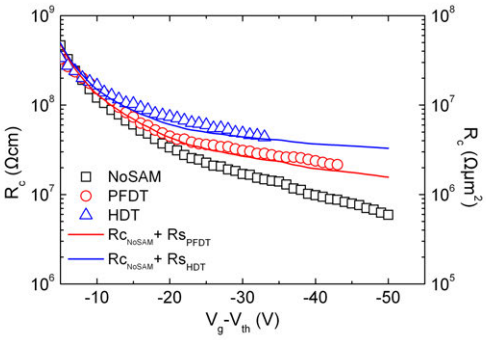

Figure 4.4: Contact resistance of BC/BG transistors with bare Au and Au/PFDT - Au/HDT electrodes as a function of gate bias. The contact resistances were derived from transmission line measurements using various channel lengths after correction for threshold voltage shifts. The channel width was kept constant at 10000 μm. The solid lines represent the summation of the tunnel resistance of corresponding SAM in molecular junctions with the contact resistance of the transistor with bare Au electrodes.

4.3.2 Reconstructing the contact resistance

In a simple approximation, we can reconstruct the contact resistance of the PFDT-modified transistors by simply adding the tunnel resistance of the PFDT SAM as measured in large-area molecular junctions, to the renormalized contact resistance as determined in transistors using bare Au electrodes. The calculated curve is presented in Figure 4.4 by the red line. A good agreement with the extracted contact resistance of the PFDT-modified transistor is obtained. At low gate bias, the contact resistance is dominated by charge injection into the undoped semiconductor. At higher gate bias, in accumulation, the contact resistance is dominated by the series resistance of the SAM.

To substantiate the analysis above, we varied the chemical nature of the SAM. We investigated transistors with HDT-modified Au electrodes. The workfunction amounted to 4.1 eV yielding an injection barrier with MEH-PPV of approximately 1 eV. The contact resistance as a function of gate bias was obtained from TLM analysis and presented in Figure 4.4. Despite the barrier of about 1 eV, the values are comparable to those of bare Au and PFDT-treated electrodes. Transistors are tolerant for injection barriers due to the image-force lowering of the barrier caused by the high electric field at the source contact.[45] We added the measured tunnel resistance of HDT molecular junctions to that of renormalized contact resistance using bare Au electrodes. The blue line in Figure 4.4 shows that a good agreement is obtained with

the extracted contact resistance of transistors using HDT-modified electrodes. We note that the agreement is surprising because resistance and Ohm's law are based on scattering and diffusive transport rather than tunneling. A tentative explanation is given below.

The absolute value of the resistance in a molecular junction depends on the nature of the electrical contacts to the molecule.[46–48] Strongly-coupled chemisorbed contacts yield lower resistances than weakly-coupled physisorbed contacts.[49,50] Furthermore, the metal workfunction and the composition of the chemical anchoring group can change the resistance.[50–53] Here we have determined the SAM resistance in molecular junctions that consist of a chemisorbed Au-S bottom contact, an alkane backbone and a physisorbed SAM/PEDOT:PSS top contact. The junction thickness is smaller than the electron coherence length and, therefore, Ohm's law is not obeyed. The electrical transport is by non-resonant tunneling. The resistance of a single molecule follows from *e.g.* multi barrier models yielding a resistance that is factorized with the contacts.

The total resistance of the transistor is the sum of the channel resistance and the contact resistance. At low bias the resistance is dominated by the channel resistance of the semiconductor. At high gate bias, however, the contact resistance dominates. In accumulation the semiconductor channel is electrostatically "doped" by the gate voltage. Therefore, at sufficiently high gate voltage there are so many charge carriers in the channel that the semiconductor becomes degenerate and it starts acting like an electrode at the SAM modified contact. The contact at low gate bias can be treated as a metal-insulator-semiconductor (MIS) tunnel junction. At high gate bias, however, the contact behaves as a MIM tunnel junction, similar as in the large-area molecular junctions.[54] Here we add the absolute value of the SAM resistance as a series resistance to the total resistance of the transistor without SAM. The resistance of the molecular junction is factorized with the PEDOT:PSS resistance.[55] However, when using highly conductive PEDOT:PSS and optimized processing the absolute resistance derived agrees with that of break junction and c-AFM measurements.[56] The agreement obtained here might be due to the fact that the junction consists of metal/SAM/doped semiconductor. Therefore, the SAM resistance is clearly manifested in the contact resistance of the transistors. Hence a SAM-modified transistor can be used as an experimental testbed for molecular electronics as first proposed by Stoliar *et al.*[20]

4.4 Summary and conclusions

The contact resistance of a transistor using SAM-modified source and drain electrodes depends on the SAM tunnel resistance, the height of the injection barrier and the morphology at the contact. To disentangle the different contributions, we have combined transmission line measurements in transistors with transport measurements of SAMs in large-area molecular junctions. In order to eliminate the morphological complications, we have used in the transistor an amorphous semiconducting polymer, MEH-PPV. To unambiguously rule out the influence of an injection barrier we have focused on PFDT-treated Au electrodes. Both bare Au and Au/PFDT electrodes form an Ohmic contact with MEH-PPV for hole injection. However, the output current using Au/PFDT electrodes is slightly lower than that using bare Au electrodes due to higher contact resistance. The absolute value of the contact resistance in combination with the extracted device mobility confirms the absence of any injection barrier.

The tunnel resistance of the PFDT SAM has been independently extracted in two-terminal large-area molecular junctions. We show that in first order approximation the tunneling resistance of the SAM can be added linearly to the contact resistance of the bare Au transistor, to account for the increased contact resistance in the PFDT-modified transistor. The analysis has been verified by using different SAMs.

The SAM-modified contact at low gate bias can be treated as a metal-insulator-semiconductor (MIS) tunnel junction. At high gate bias, however, the contact behaves as a MIM tunnel junction, similar as in the large-area molecular junctions.

The agreement obtained here shows that the SAM resistance is clearly manifested in the contact resistance of the transistors. Hence SAM-modified transistors can potentially be used as a gauge to measure electrical transport through single molecules.

References

[1] E. Cantatore, T. C. T. Geuns, G. H. Gelinck, E. van Veenendal, A. F. A. Gruijthuijsen, L. Schrijnemakers, S. Drews, D. M. de Leeuw, J. Solid-St. Circ. 42 (2007) 84.

[2] D. M. de Leeuw, E. Cantatore, Mat. Sci. Semicon. Proc. 11 (2008) 199.

[3] B. Crone, A. Dodabalapur, Y. Y. Lin, R. W. Filas, B. Z., A. LaDuca, R. Sarpeshkar, H. E. Katz, W. Li, Nature 403 (2000) 521.

[4] C. Tanase, E. J. Meijer, P. W. M. Blom, D. M. de Leeuw, Phys. Rev. Lett. 91 (2003) 216601.

[5] M. C. J. M. Vissenberg, M. Matters, Phys. Rev. B 57 (1998) 12964.

[6] H. Bässler, Phys. Stat. Sol. B 175 (1993) 15.

[7] W. F. Pasveer, J. Cottaar, C. Tanase, R. Coehoorn, P. A. Bobbert, P. W. M. Blom, D. M. de Leeuw, M. A. J. Michels, Phys. Rev. Lett. 94 (2005) 206601.

[8] H. Sirringhaus, Adv. Mater. 17 (2005) 2411.

[9] H. Yan, Z. Chen, Y. Zheng, C. Newman, J. R. Quinn, F. Dotz, M. Kastler, A. Facchetti, Nature 457 (2009) 679.

[10] Z. Chen, M. J. Lee, R. Shahid Ashraf, Y. Gu, S. Albert-Seifried, M. Meedom Nielsen, B. Schroeder, T. D. Anthopoulos, M. Heeney, I. McCulloch, H. Sirringhaus, Adv. Mater. 24 (2012) 647.

[11] G. Horowitz, P. Lang, M. Mottaghi, H. Aubin, Adv. Funct. Mater. 14 (2004) 1069.

[12] N. Koch, ChemPhysChem 8 (2007) 1438.

[13] K. Asadi, F. Gholamrezaie, E. C. P. Smits, P. W. M. Blom, B. de Boer, J. Mater. Chem. 17 (2007) 1947.

[14] I. H. Campbell, J. D. Kress, R. L. Martin, D. L. Smith, N. N. Barashkov, J. P. Ferraris, Appl. Phys. Lett. 71 (1997) 3528.

[15] S. Khodabakhsh, D. Poplavskyy, S. Heutz, J. Nelson, D. D. C. Bradley, H. Murata, T. S. Jones, Adv. Funct. Mater. 14 (2004) 1205.

[16] B. H. Hamadani, D. A. Corley, J. W. Ciszek, J. M. Tour, D. Natelson, Nano Lett. 6 (2006) 1303.

[17] B. de Boer, A. Hadipour, M. M. Mandoc, T. van Woudenbergh, P. W. M. Blom, Adv. Mater. 17 (2005) 621.

[18] J. C. Love, L. A. Estroff, J. K. Kriebel, R. G. Nuzzo, G. M. Whitesides, Chem. Rev. 105 (2005) 1103. (and references therein).

[19] H. Ma, H. L. Yip, F. Huang, A. K. Y. Jen, Adv. Funct. Mater. 20 (2010) 1371.

[20] P. Stoliar, R. Kshirsagar, M. Massi, P. Annibale, C. Albonetti, D. M. de Leeuw, F. Biscarini, J. Am. Chem. Soc. 129 (2007) 6477.

[21] D. J. Gundlach, L. Zhou, J. A. Nichols, T. N. Jackson, P. V. Necliudov, M. S. Shur, J. Appl. Phys. 100 (2006) 024509.

[22] E. C. P. Smits, T. D. Anthopoulos, S. Setayesh, E. van Veenendal, R. Coehoorn, P. W. M. Blom, B. de Boer, D. M. de Leeuw, Phys. Rev. B 73 (2006) 205316.

[23] L. Bürgi, M. Turbiez, R. Pfeiffer, F. Bienewald, H.-J. Kirner, C. Winnewisser, Adv. Mater. 20 (2008) 2217.

[24] T. D. Anthopoulos, C. Tanase, S. Setayesh, E. J. Meijer, J. C. Hummelen, P. W. M. Blom, D. M. de Leeuw, Adv. Mater. 16 (2004) 2174.

[25] M. Chiodi, L. Gavioli, M. Beccari, V. Di Castro, A. Cossaro, L. Floreano, A. Morgante, A. Kanjilal, Phys. Rev. B 77 (2008) 115321.

[26] Y. Ge, J. E. Whitten, J. Phys. Chem. C 112 (2008) 1174.

[27] C. Bock, V. Pham, U. Kunze, D. Kafer, G. Witte, A. Terfort, Appl. Phys. Lett. 91 (2007) 052110.

[28] K. Asadi, Y. Wu, F. Gholamrezaie, P. Rudolf, P. W. M. Blom, Adv. Mater. 21 (2009) 4109.

[29] D. J. Gundlach, J. E. Royer, S. K. Park, S. Subramanian, O. D. Jurchescu, B. H. Hamadani, A. J. Moad, R. J. Kline, L. C. Teague, O. Kirillov, C. A. Richter, J. G. Kushmerick, L. J. Richter, S. R. Parkin, T. N. Jackson, J. E. Anthony, Nat. Mater. 7 (2008) 216.

[30] F. Gholamrezaie, K. Asadi, R. A. H. Kichen, B. M. W. Langeveld-Voss, D. M. de Leeuw, P. W. M. Blom, Synth. Metals 161 (2011) 2226.

[31] H. B. Akkerman, P. W. M. Blom, D. M. de Leeuw, B. de Boer, Nature 441 (2006) 69.

[32] S. H. Choi, B. Kim, C. D. Frisbie, Science 320 (2008) 1482.

[33] S. Casalini, A. Shehu, S. Destri, W. Porzio, M. C. Pasini, F. Vignali, F. Borgatti, C. Albonetti, F. Leonardi, F. Biscarini, Org. Electron. 13 (2012) 789.

[34] A. Salomon, D. Cahen, S. Linsday, J. Tomfohr, V. B. Engelkes, C. D. Frisbie, Adv. Mater. 15 (2003) 1881.

[35] H. B. Akkerman, B. de Boer, J. Phys:Condens. Matter 20 (2008) 013001. (and references therein).

[36] C. Naud, P. Calas, H. Blancou, A. Commeyras, J. Fluorine Chem. 104 (2000) 173.

[37] K. Asadi, J. Wildeman, P. W. M. Blom, D. M. de Leeuw, IEEE Tran. Elec. Dev. 57 (2010) 3466.

[38] I. Katsouras, A. J. Kronemeijer, E. C. P. Smits, P. A. van Hal, T. C. T. Geuns, P. W. M. Blom, D. M. de Leeuw, Appl. Phys. Lett. 99 (2011) 013303.

[39] T. J. Richards, H. Sirringhaus, J. Appl. Phys. 102 (2007) 094510.

[40] D. J. Gundlach, L. Jia, T. N. Jackson, IEEE Electron Device Lett. 22 (2001) 571.

[41] E. J. Meijer, G. H. Gelinck, E. van Veenendal, B.-H. Huisman, D. M. de Leeuw, T. M. Klapwijk, Appl. Phys. Lett. 82 (2003) 4576.

[42] F. Torricelli, J. R. Meijboom, E. C. P. Smits, A. K. Tripathi, M. Ferroni, S. Federici, G. H.

Gelinck, L. Colalongo, Z. M. Kovács-Vajna, D. M. de Leeuw, E. Cantatore, IEEE Trans. Electronic Devices 58 (2011) 2610.

[43] G. Horowitz, M. E. Hajlaoui, R. Hajlaoui, J. Appl. Phys. 87 (2000) 4456.

[44] C. Tanase, E. J. Meijer, P. W. M. Blom, D. M. de Leeuw, Org. Electron. 4 (2003) 33.

[45] J. J. Brondijk, F. Torricelli, E. C. P. Smits, P. W. M. Blom, D. M. de Leeuw, Org. Electron. 13 (2012) 1526.

[46] K. W. Hipps, Science 294 (2001) 536.

[47] J. G. Kushmerick, Mater. Today 8 (2005) 26.

[48] D. Vuillaume, S. Lenfant, Microelectron. Eng. 70 (2003) 539.

[49] X. D. Cui, A. Primak, X. Zarate, J. Tomfohr, O. F. Sankey, A. L. Moore, T. A. Moore, D. A. Gust, G. Harris, S. M. Lindsay, Science 294 (2001) 571.

[50] V. B. Engelkes, J. M. Beebe, C. D. Frisbie, J. Am. Chem. Soc. 126 (2004) 14287.

[51] F. Chen, X. Li, J. Hihath, Z. Huang, N. J. Tao, J. Am. Chem. Soc. 128 (2006) 15874.

[52] J. M. Beebe, V. B. Engelkes, L. L. Miller, C. D. Frisbie, J. Am. Chem. Soc. 124 (2002) 11268.

[53] Y. S. Park, A. C. Whalley, M. Kamenetska, M. L. Steigerwald, M. S. Hybertsen, C. Nuckolls, L. Venkataraman, J. Am. Chem. Soc. 129 (2007) 15768.

[54] S. M. Sze, Physics of semiconductor devices, Willey, New Jersey, 2007.

[55] A. J. Kronemeijer, I. Katsouras, E. H. Huisman, P. A. van Hal, T. C. T. Geuns, P. W. M. Blom, D. M. de Leeuw, Small 7 (2011) 1593.

[56] P. A. van Hal, E. C. P. Smits, T. C. T. Geuns, H. B. Akkerman, B. C. De Brito, S. Perissinotto, G. Lanzani, A. J. Kronemeijer, V. Geskin, J. Cornil, P. W. M. Blom, B. de Boer, D. M. de Leeuw, Nat. Nanotechnol. 3 (2008) 749. (including supporting info).

CHAPTER 5

Extending the voltage window in the characterization of electrical transport of large-area molecular junctions

A large bias window is required to discriminate between different transport models in large-area molecular junctions. Under continuous DC bias, the junctions irreversibly break down at fields over 9 MV/cm*. We show that, by using pulse measurements, we can reach electrical fields of* 35 MV/cm *before degradation. The breakdown voltage is shown to depend logarithmically on both duty cycle and pulse width. A tentative interpretation is presented based on electrolysis in the polymeric top electrode. Expanding the bias window using pulse measurements unambiguously shows that the electrical transport exhibits not an exponential but a power-law dependence on bias.*

5.1 Breakdown in large-area molecular junctions

Single molecules or an ensemble of molecules have been incorporated in various molecular junction architectures, which allowed measuring the electrical transport through the molecules.[1] The transport mechanism, however, remains elusive.[2–5] Commonly, non-resonant tunneling has been used to explain the transport.[2,3,6–8] The current density in this case increases exponentially with applied bias. Recently, a power-law dependence has been reported.[4,5] To discriminate between the suggested models, a large bias window is needed. However, characterization at high bias is hampered by irreversible breakdown of the junctions. The origin can be structural changes that the molecules undergo under high voltage, thermal stress or electrochemical reactions at the electrode.[9–14] These breakdown mechanisms become more pronounced under prolonged application of bias. To eliminate the bias degradation the measurement time has to be minimized. Here we use pulsed measurements in large-area molecular junctions. We vary the duty cycle and pulse width, compare the pulsed and DC current densities, and we determine the breakdown voltage as a function of duty cycle. We show that we are able to extend the bias window, which allows us to discriminate between different electrical transport models in molecular junctions.

5.2 Experimental

We use the previously developed technology of large-area molecular junctions, a reproducible molecular electronic testbed with yield of almost unity to measure the electrical transport through self-assembled monolayers (SAMs).[15] More than 20000 molecular junctions were fabricated simultaneously on a single 6-inch wafer according to a previously reported semi-automated procedure.[16] On a 6-inch Si monitor wafer with a 500 nm SiO_2 passivation layer a 60 nm Au bottom electrode was sputtered onto a Ti adhesion layer and structured by standard photolithography. Vertical interconnects ranging from 1 μm to 50 μm in diameter were defined in insulating photoresist by conventional spin coating and UV lithography. 1-dodecanethiol (C12MT) was dissolved in ethanol using a concentration of 3×10^{-3} M. The self-assembled monolayer was formed inside the vertical interconnects by immersing the wafer in the solution for at least 36 hours under N_2 atmosphere. Subsequently, the conducting polymer PEDOT:PSS, a water-based suspension of poly(3, 4-ethylenedioxythiophene) stabilized with poly(4-styrenesulphonic acid), AGFA Na-free (Agfa-Gevaert), was spincoated. Finally, a 100 nm gold top contact electrode was thermally evaporated and structured

by photolithography. This top contact is utilized as a self-aligned reactive ion etching mask for the removal of the redundant PEDOT:PSS. A schematic presentation of the junction, the layout and a picture of a finished wafer is shown in Figure 5.1.

The normalized resistance (RS, in $\Omega\mu m^2$) at 0.5 V bias was measured in four-point probe geometry in a semi-automatic probe station. DC and pulsed I-V measurements were performed in a probe station (Janis Research Co.) using a Keithley 4200 Semiconductor Parameter Analyzer and a Keithley 2602 Source System controlled through Test Script Builder.

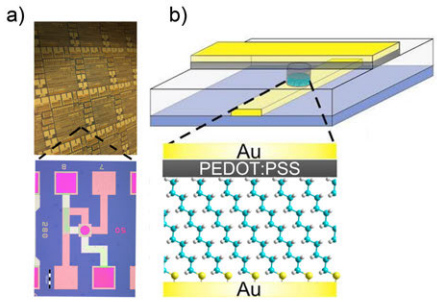

Figure 5.1: (a) Photograph of a 6-inch wafer, showing the repeating units, "dies" and the device layout of a discrete molecular junction (scale bar is 100 μm). (b) A schematic cross-section of the molecular junction.

5.3 Results and discussion

5.3.1 Extending the voltage window

The current as a function of DC bias for a typical C12MT large-area molecular junction in air is presented in Figure 5.2. At low bias the current is Ohmic. At higher bias, however, a negative differential resistance is observed. The current then decreases with increasing bias. Furthermore, the measurement shows a huge hysteresis. The diode irreversibly breaks down. Consecutive DC voltage sweeps on a pristine junction show that hysteresis already manifests at low bias, at 1 V to 2 V, and that after each subsequent measurement the junction has deteriorated. The degradation is slower when the junction is measured in vacuum, but still prohibits application of high DC bias.

To extend the bias window we performed pulse measurements. The pulse train used is presented in the inset of Figure 5.3a. It consists of sequential voltage pulses that

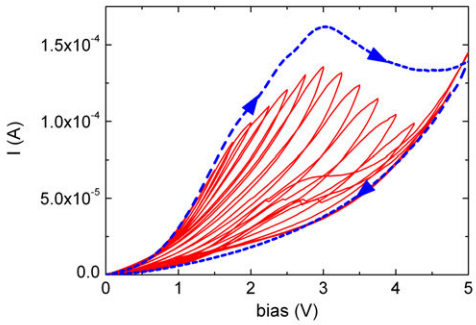

Figure 5.2: Current-voltage traces of a C12MT molecular junction measured in air. The device diameter is 10 μm. The dotted blue line represents the DC measurement directly to 5 V, showing pronounced hysteresis and breakdown of the junction. The inner loops represent consecutive voltage sweeps from 0.25 V to 5 V with a step of 0.25 V on a similar but pristine junction.

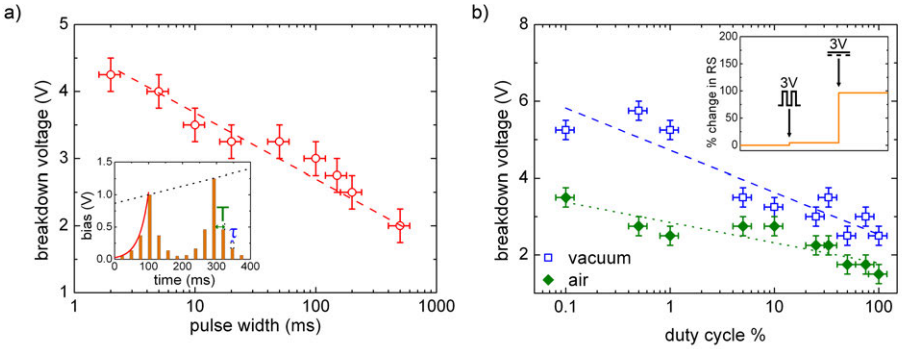

Figure 5.3: (a) Breakdown voltage as a function of pulse width for 10 μm diameter C12MT molecular junctions measured in vacuum. The duty cycle was fixed at 10%. The inset shows part of the pulse train used. The sequential voltage pulses increase and decrease exponentially around a peak voltage. The peak voltage increases linearly from 0.25 V to 6 V with a step of 0.25 V. (b) Breakdown voltage as a function of duty cycle for similar C12MT junctions in vacuum and in air. The pulse width was fixed at 2 ms. The inset shows the change in the normalized resistance of the junction as a result of pulsed and DC measurements at 3 V.

increase exponentially to a peak voltage and subsequently decrease similarly. The next pulse train goes to higher peak voltages. This specific pulse train was chosen to check the reversibility and to determine the breakdown voltage. To determine the onset of junction degradation we varied the duty cycle and the pulse width. Figure 5.3a shows the breakdown voltage as a function of pulse width at a fixed duty cycle of 10%. Each point represents a pristine junction measured in vacuum. The reproducibility

is reflected in the limited scatter in the breakdown voltage, which was taken as the onset of hysteresis in the measurements. The breakdown voltage is logarithmically dependent on pulse width.

Figure 5.3b shows the breakdown voltage as a function of duty cycle for a fixed pulse width of 2 ms for measurements in vacuum and in air. The breakdown voltage increases when the duty cycle decreases; the breakdown voltage is logarithmically dependent on duty cycle. At 100% duty cycle the breakdown voltage is similar to the value measured under DC bias. The highest breakdown voltage in vacuum corresponds to a breakdown field of about 35 MV/cm. For measurements in air, a similar logarithmic dependence is observed. However, to obtain breakdown voltages as high as those in vacuum, the duty cycle and pulse width have to be reduced by 2-3 orders of magnitude, which is beyond reach of the experimental setup. The inset of Figure 5.3b shows the difference between pulse- and DC bias. The normalized resistance is measured at low DC bias before and after application of 3 V using pulses and DC. The pulse train causes no change in resistance. Subsequent DC measurement at 3 V, however, causes a 100% change in resistance.

Figure 5.3 shows that the breakdown voltage is logarithmically dependent on both duty cycle and pulse width. Alkanethiol SAMs have been reported to undergo dielectric breakdown at fields ranging from 4 MV/cm to 20 MV/cm.[9–12] However, PEDOT:PSS degrades at even lower DC biases. Various mechanisms such as water-assisted dedoping[17] and electrochemical oxidation have been reported. In the last case the breakdown is due to electrolysis of residual water in the PEDOT:PSS.[13] At a bias above about 2 V water is oxidized. The gases formed cannot escape because the junction is enclosed in photoresist and sandwiched between a bottom and top electrode (Figure 5.1b). As a result, the pressure rises and the PEDOT:PSS delaminates from the SAM functionalized electrode. The contact area then decreases leading to a decrease in current. We note that under extreme bias conditions the junction can literally explode. The degradation depends on the amount of residual water; hence in air the onset of breakdown is at lower DC bias and deterioration is faster than in vacuum, as shown in Figure 5.3.

The junction breaks down due to an integrated Faradaic current that generates a volume of gas leading to delamination. The Faradaic current that is much smaller than the device current depends exponentially on the overpotential,[18] approximately equal to the applied bias. Hence the breakdown voltage for a given duty cycle depends logarithmically on pulse width as shown in Figure 5.3a. After each pulse the gas formed has to diffuse out of the junction. Hence for a fixed pulse width, a lower repetition rate

yields a higher breakdown voltage. The logarithmic dependence of breakdown voltage on duty cycle, Figure 5.3b, however is not yet fully understood. In first order, assuming that the diffusion coefficient is constant, diffusion of the generated volume of gas in the junction shows an exponential dependence on time.[19] The breakdown voltage increases with decreasing duty cycle. At very low duty cycle the junctions withstand fields as high as 35 MV/cm, indicating that the relevant breakdown mechanism at low voltages is electrolysis of water in the PEDOT:PSS layer and not a field-driven process.

5.3.2 Distinguishing between models

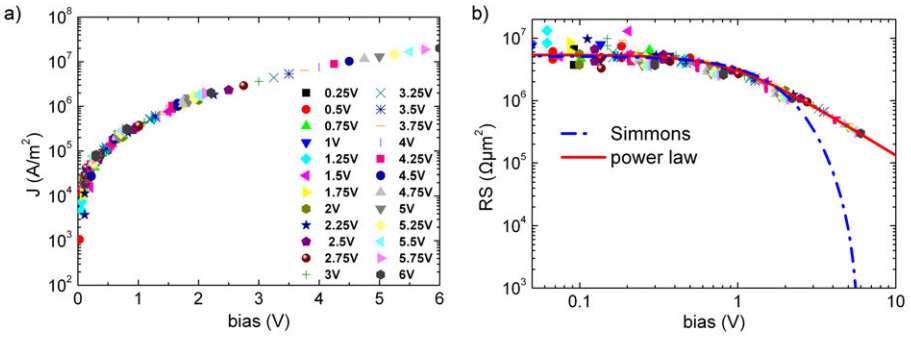

Figure 5.4: (a) Current density of a typical C12MT molecular junction as a function of bias as determined by pulse measurements. The pulse width was 2 ms and the duty cycle 1%. (b) Data replotted as normalized resistance as a function of voltage. The drawn curves are fits to the data. The blue line represents the Simmons model, tunneling through a rectangular barrier with image force included. The red line represents a power law dependence of resistance on bias.

Figure 5.4a shows the current density of a typical C12MT large-area molecular junction up to 6 V bias using pulse measurements. There is no hysteresis. At low bias, below 1 V, pulse- and DC measurements overlap, yielding identical values for the normalized resistance. Values derived from all pulse trains going up and down in bias collapse. The junction does not degrade. In Figure 5.4b the data are replotted as normalized resistance as a function of applied bias.

Commonly, non-resonant tunneling has been used to explain the transport. The Simmons model that describes tunneling through a rectangular barrier with image force included[2,7,20,21] is used to fit our data (dashed blue curve in Figure 5.4b). At low bias a good agreement is obtained. However, at high bias the Simmons model predicts an exponential decrease in normalized resistance, which is not observed. Recently,

a power-law dependence on applied bias has been reported.[4,5,22] The origin could be dissipative tunneling, such as environmental Coulomb blockade, but is still elusive. The fully drawn red line in Figure 5.4b is a fit of the data with a power law dependence on bias as discussed for PEDOT:PSS-only junctions in reference [4]. A good agreement is obtained over the whole bias range.

5.4 Summary and conclusions

Large-area molecular junctions of dodecanethiol irreversibly break down under continuous applied DC bias of about 1 V to 2 V. By using pulse measurements however the bias window could be expanded to more than 6 V. This corresponds to a breakdown field of 35 MV/cm, significantly larger than reported values of 20 MV/cm. The breakdown voltage is shown to depend logarithmically on both duty cycle and pulse width. The dependence is tentatively explained by electrolysis in the PEDOT:PSS layer as the breakdown mechanism. Expanding the bias window using pulse measurements has unambiguously shown that the electrical transport exhibits not an exponential but a power-law dependence on bias.

References

[1] H. Haick, D. Cahen, Progress in Surface Science 83 (2008) 217. (and references therein).

[2] H. B. Akkerman, R. C. G. Naber, B. Jongbloed, P. A. van Hal, P. W. M. Blom, D. M. de Leeuw, B. de Boer, Proc. Natl. Acad. Sci. 104 (2007) 11161.

[3] S. H. Choi, B. Kim, C. D. Frisbie, Science 320 (2008) 1482.

[4] A. J. Kronemeijer, E. H. Huisman, I. Katsouras, P. A. van Hal, T. C. T. Geuns, P. W. M. Blom, S. J. van der Molen, D. M. de Leeuw, Phys. Rev. Lett. 105 (2010) 156604.

[5] A. J. Kronemeijer, I. Katsouras, E. H. Huisman, P. A. van Hal, T. C. T. Geuns, P. W. M. Blom, D. M. de Leeuw, Small 7 (2011) 1593.

[6] R. E. Holmlin, R. Haag, M. L. Chabinyc, R. F. Ismagilov, A. E. Cohen, A. Terfort, A. M. Rampi, G. M. Whitesides, J. Am. Chem. Soc. 123 (2001) 5075.

[7] W. Wang, T. Lee, M. A. Reed, Phys. Rev. B 68 (2003) 035416.

[8] X. D. Cui, A. Primak, X. Zarate, J. Tomfohr, O. F. Sankey, A. L. Moore, T. A. Moore, D. A. Gust, L. A. Nagahara, S. M. Lindsay, J. Phys. Chem. B 106 (2002) 8609.

[9] R. Haag, A. M. Rampi, R. E. Holmlin, G. M. Whitesides, J. Am. Chem. Soc. 121 (1999) 7895.

[10] D. J. Wold, C. D. Frisbie, J. Am. Chem. Soc. 123 (2001) 5549.

[11] J. Zhao, K. Uosaki, Appl. Phys. Lett. 83 (2003) 2034.

[12] S. A. DiBenedetto, A. Facchetti, M. A. Ratner, T. J. Marks, J. Am. Chem. Soc. 131 (2009) 7158.

[13] B. C. de Brito, E. C. P. Smits, P. A. van Hal, T. C. T. Geuns, B. de Boer, C. J. M. Lasance, H. L. Gomes, D. M. de Leeuw, Adv. Mater. 20 (2008) 3750.

[14] H. B. Akkerman, A. J. Kronemeijer, J. Harkema, P. A. van Hal, E. C. P. Smits, D. M. de Leeuw, P. W. M. Blom, Org. Electron. 11 (2010) 146.

[15] H. B. Akkerman, P. W. M. Blom, D. M. de Leeuw, B. de Boer, Nature 441 (2006) 69.

[16] P. A. van Hal, E. C. P. Smits, T. C. T. Geuns, H. B. Akkerman, B. C. De Brito, S. Perissinotto, G. Lanzani, A. J. Kronemeijer, V. Geskin, J. Cornil, P. W. M. Blom, B. de Boer, D. M. de Leeuw, Nat. Nanotechnol. 3 (2008) 749. (including supporting info).

[17] J. Wang, F. Gao, N. C. Greenham, Appl. Phys. Lett. 97 (2010) 053301.

[18] A. J. Bard, L. R. Faulkner, Electrochemical Methods: Fundamentals and Applications, J. Wiley & Sons, Inc., New York, U.S.A., 1980.

[19] J. Crank, Diffusion In Polymers, Academic Press, London, U.K., 1968.

[20] J. G. Simmons, J. Appl. Phys. 34 (1963) 1793.

[21] J. G. Simmons, J. Appl. Phys. 34 (1963) 2581.

[22] J. D. Yuen, R. Menon, N. E. Coates, E. B. Namdas, S. Cho, S. T. Hannahs, D. Moses, A. J. Heeger, Nat. Mater. 8 (2009) 572.

CHAPTER 6

Universal scaling of the charge transport in large-area molecular junctions

In this chapter we investigate the charge transport through alkanes and para-phenylene oligomers in large-area molecular junctions. The molecules are self-assembled in a monolayer and contacted with a top electrode consisting of poly(3,4- ethylenedioxythiophene): poly(4-styrenesulfonic acid) (PEDOT:PSS). Using the technique described in ***Chapter 5****, the complete set of $J(V,T)$ characteristics of both saturated and π-conjugated molecules can be described quantitatively by a single equation with only two fit parameters. The derived parameters, in combination with a variation of the bulk conductivity of PEDOT:PSS, demonstrate that the absolute junction resistance is factorized with that of PEDOT:PSS.*

6.1 Charge transport in large-area molecular junctions

Understanding of the charge transport in molecular devices is essential for progress in the field of molecular electronics. The two main fundamental challenges to resolve are the dependence of conductance on molecular length and the origin of the absolute value of the conductance. Charge transport through single molecules has been determined in break junctions and in scanning probe geometries. For short alkanes and π-conjugated molecules an increase in the molecular length L results in an exponential increase in resistance, $R \propto e^{\beta L}$. The tunneling decay coefficient β depends on the energy gap between the highest occupied molecular orbital (HOMO) and the lowest unoccupied molecular orbital (LUMO).[1,2] The resistance is temperature-independent, which points to tunneling as the dominant transport mechanism.[3] For longer π-conjugated molecules ($L > 3\ nm$), a transition to temperature-dependent hopping conduction has been reported.[4] The absolute value of the resistance is ideally only determined by the molecular structure. However, in reality, the electrical contacts to the molecule strongly influence the measured resistance.[1,2,5–7] Firstly, strongly coupled chemisorbed contacts yield lower resistances than weakly coupled physisorbed contacts.[2,8,9] Secondly, the metal workfunction and the composition of the chemical anchoring group change the resistance.[9–12] Finally, differences in the coordination geometry of the chemical anchoring group at the metallic contact affect the resistance by virtue of a different electronic coupling.[13,14] Scanning probe geometries and break junctions[2,15] exhibit different coupling strengths to the contacts and therefore lead to dissimilar resistances for identical molecules. Hence an understanding of the electrical contacts is necessary to compare molecular conductance measurements.

To apply and integrate molecules into functional devices, macroscopic electrodes, preferably in a cross-bar geometry, are required. For this purpose, as described previously, we have developed large-area molecular junctions using self-assembled monolayers (SAMs).[16,17] As a top electrode the conducting polymer poly(3, 4- ethylenedioxythiophene): poly(4-styrenesulfonic acid) (PEDOT:PSS) is used. The geometry of the junction is schematically depicted in Figure 6.1a. A SAM is formed on a gold bottom electrode inside a vertical interconnect defined in photoresist. Subsequently, PEDOT:PSS is spincoated on top to make the electrical contact to the SAM. We have investigated saturated alkanes and conjugated *para*-phenylene oligomers with thiol or methyl end groups.[16–18] The current density-voltage (J-V) characteristics show clear molecular features as concluded from the exponential dependence of the junc-

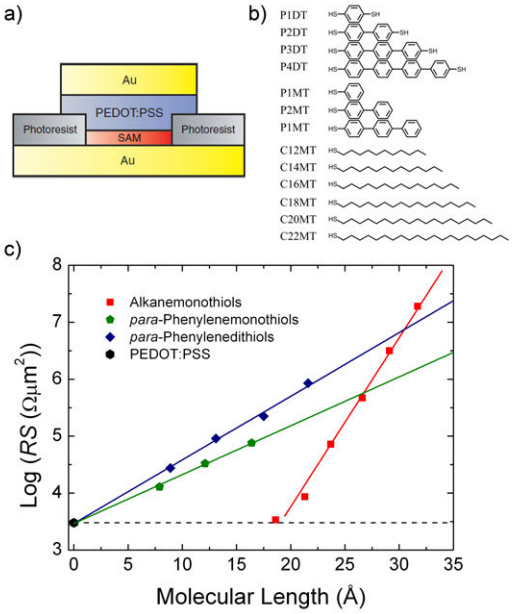

Figure 6.1: (a) Schematic representation of the geometry of a large-area molecular junction. (b) Chemical structure of the molecules investigated and their abbreviations. (c) Normalized resistance (RS) as a function of molecular length of the large-area molecular junctions. The dotted line represents the normalized resistance of the corresponding PEDOT:PSS-only diode.

tion resistance on molecular length. Tunneling decay coefficients for SAMs with thiol and methyl end groups have been determined as 0.26 and 0.20 $\mathring{A}^{-1}$ for conjugated *para*-phenylenes and as 0.66 and 0.73 $\mathring{A}^{-1}$ for saturated alkanes.[16–18] The origin of the absolute value of the resistance nevertheless remains unclear. The resistance of the junction is influenced by the composition of the PEDOT:PSS formulation and by the type of photoresist used. The molecular length dependence, however, remains unaffected. The charge transport, therefore, has been described with a multibarrier tunneling model yielding a factorized resistance, given by Equation 6.1:

$$R = \frac{h}{2e^2}T^{-1} = 12.9\,k\Omega\,T_{Au-S}^{-1}T_{mol}^{-1}T_{SAMPEDOT}^{-1} \tag{6.1}$$

where T is the overall transmission probability and T_{Au-S}, T_{mol} and $T_{SAMPEDOT}$ are the transmission probabilities of the molecule, the Au-S bond, and the SAM/PEDOT contact, respectively.[17] The molecular transmission is exponentially dependent on molecular length, $T_{mol} \propto e^{\beta L}$. However, a detailed understanding of the physics of T_{Au-S} and, especially, of $T_{SAMPEDOT}$ is missing. The SAM/PEDOT contact

is difficult to study experimentally since the interface is buried inside the junction. To analyze the electrical transport we first focused on large-area junctions without molecules, or so-called PEDOT:PSS-only diodes, as a reference.[19] The electrical transport was shown to exhibit a power-law dependence on both temperature and voltage, *viz.* $J \propto T^{a}$ at low voltage ($eV \ll kT$) and $J \propto V^{\beta}$ at low temperature ($eV \gg kT$), with $\beta = \alpha + 1$. Furthermore, all J-V curves at different temperatures can be normalized onto a single universal curve by plotting $J/T^{1+\alpha}$ versus eV/kT.[19] The universal curve is described by Equation 6.2:

$$J = J_0 T^{1+a} sinh\left(\gamma \frac{eV}{kT}\right) \left|\Gamma\left(1 + \frac{a}{2} + i\frac{eV}{\pi kT}\right)\right| \tag{6.2}$$

The parameter α is derived from the measurements, J_0 and γ are fit parameters, e is the elementary charge, k is the Boltzmann constant and Γ is the Gamma function. Equation 6.2 has been derived for dissipative tunneling in a biased double quantum well.[20,21] The electron tunnels between the two wells while coupled to an external heat bath of harmonic oscillators. The coupling can be due to, for instance, Coulomb interactions or polaronic effects. The origin of the scaling in the PEDOT:PSS-only diodes, however, remains elusive.

Here, we analyze in the same way the current-voltage characteristics of molecular junctions based on saturated alkanes and π-conjugated *para*-phenylene oligomers. The chemical structure and acronyms are presented in Figure 6.1b. The combined voltage and temperature dependencies have been measured. All junctions exhibit universal scaling of the $J(V,T)$ characteristics as described by Equation 6.2. The values of the derived parameters α, J_0 and γ are compared with those of the PEDOT:PSS-only diodes. The comparison shows that the resistance of the molecular junctions is factorized with the resistance of PEDOT:PSS. The additional factorization has been verified by deliberately varying the PEDOT:PSS conductance. Previously unresolved and poorly understood issues regarding large-area molecular junctions will be evaluated and discussed.

6.2 Experimental

Large-area molecular junctions were prepared as previously described. SAMs were formed inside the vertical interconnects under a N_2 atmosphere. Alkanethiols were dissolved in ethanol at a concentration of 3×10^{-3} M and thiolated *para*-phenylene oligomers were dissolved in SureSeal THF at 3×10^{-4} M. The wafers were immersed

in the solutions for 36 h. After self-assembly, the wafers were thoroughly rinsed with ethanol, toluene and isopropanol to remove any remaining molecules. Subsequently, the conducting polymer PEDOT:PSS, a waterbased suspension of poly(3, 4-ethylenedioxythiophene) stabilized with poly(4-styrenesulfonic acid), was spin-coated. PEDOT:PSS acts as a highly conductive layer that protected the SAM during evaporation of the top gold contact and prevents formation of shorts. After spin-coating, the layers were dried in a dynamic vacuum for at least 1 h. The layer thicknesses amounted to about 90 nm as measured with a Dektak surface profilometer. Three PEDOT:PSS formulations were used: Clevios PH500 (H. C. Starck), Clevios P HC V4 (H. C. Starck), and AGFA ICP new type (Agfa-Gevaert) mixed with 5% dimethyl sulfoxide (DMSO). The standard process flowchart was based on the AGFA ICP formulation. Next, auxiliary 100-nm gold top electrodes were thermally evaporated and structured by photolithography. To remove parasitic currents the redundant PEDOT:PSS was removed by reactive ion etching using an oxygen plasma. The top gold layer acted as a self-aligned etching mask. The normalized resistance (RS, in $\Omega\mu m^2$) at 0.5 V bias was measured in four-point probe geometry in a semi-automatic probe station. Temperature-dependent J-V measurements down to 25 K were performed on a representative subset of molecular junctions. Measurements were performed in a cryogenic probe station (Janis Research Co.) equipped with a Keithley 4200 semiconductor parameter analyzer. Control measurements at room temperature were performed afterwards to exclude permanent damage to the diodes. At room temperature the bias window was limited to ~ 1 V due to breakdown. At low temperatures (25-100 K), pulse measurements with a Keithley 2602 Source System controlled by a Labview program were used to increase the window up to 5 V. Pulse and DC measurements were identical in the overlapping bias voltage window.

6.3 Results and discussion

6.3.1 Universal scaling

Large-area molecular junctions were fabricated with conjugated monothiol and dithiol *para*- phenylene oligomers (P1MT-P3MT, P1DT-P4DT) and with saturated alkane monothiols (C18MT, C20MT, C22MT), presented in Figure 6.1b, according to previously reported procedures.[16–18] Figure 6.1c shows the normalized resistance for the investigated alkanes and *para*-phenylene oligomers (Figure 6.1b) on a semi-logarithmic scale as a function of the molecular length. For each series of molecules

the resistance increases exponentially with molecular length. The tunneling decay coefficients β are similar to previously reported values.[16–18] Figure 6.1c shows that the resistance of the *para*-phenylene oligomers extrapolates to the PEDOT:PSS-only resistance. The alkane-based junctions do not extrapolate to zero molecular length. Below molecular lengths of ~ 20 $\AA$ the resistance of the molecular junctions is indistinguishable from the PEDOT:PSS-only resistance. The offset might be explained by a series resistance in the order of the PEDOT:PSS-only resistance, as indicated by the dashed line in Figure 6.1c. The origin of the series resistance and the absence of the effect for the π-conjugated compounds are not yet understood. Preferential adsorption of the insulating aliphatic backbone of PSS on top of the alkanemonothiol monolayers by virtue of increased van der Waals interactions might explain the observation.

To understand the origin of the absolute value of the resistance, we performed a combined temperature- and voltage-dependent analysis of the measured electrical transport. Figure 6.2a shows, as a representative example, the temperature-dependent J-V measurements of a benzenedithiol (P1DT) junction from 300 K down to 25 K. The current density is symmetric versus bias voltage and nonlinear; the resistance decreases with increasing bias. Furthermore, the current density decreases when lowering the temperature. The current density at 0.1, 0.3, and 0.5 V bias is presented as a function of temperature in Figure 6.2b on a double logarithmic scale. The straight lines obtained indicate a clear power-law dependence on temperature. The slope decreases with increasing bias voltage.

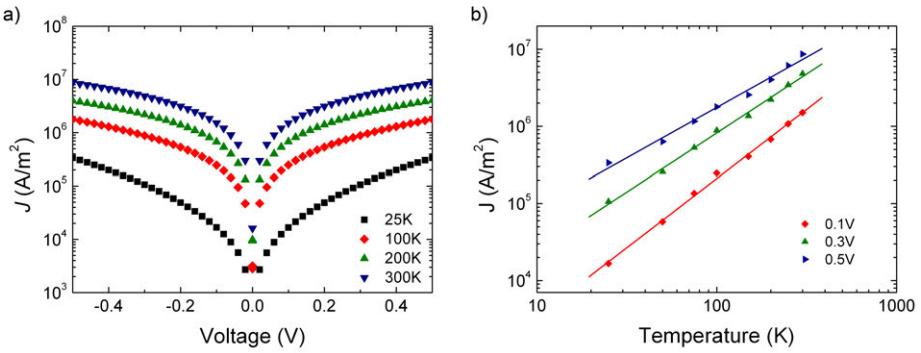

Figure 6.2: (a) Current density as a function of bias for a benzenedithiol (P1DT)-based junction as measured at temperatures between 25 and 300 K. (b) Current density of the P1DT junction at 0.1, 0.3, and 0.5 V bias as a function of temperature on a double logarithmic scale.

Extrapolation of the value of the slope to 0 V bias where $kT \gg eV$ yields the value of the parameter α. A value for α of 2.0 is obtained. The experimental data

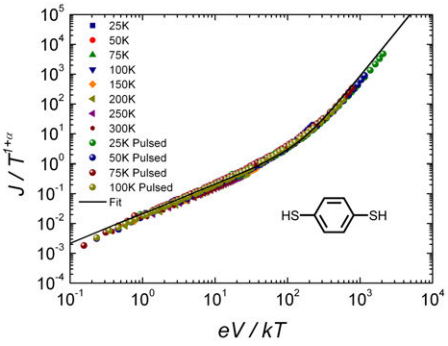

Figure 6.3: Scaled current density of a benzenedithiol (P1DT) junction presented on a double logarithmic scale as a function of eV/kT. Both DC measurements up to 0.5 V bias and pulse measurements up to 5 V are included. The solid curve is calculated with Equation 6.2 using $\alpha = 2.0$, $\gamma = 2.0 \times 10^{-2}$ and $J_0 = 1.1\ Am^{-2}$.

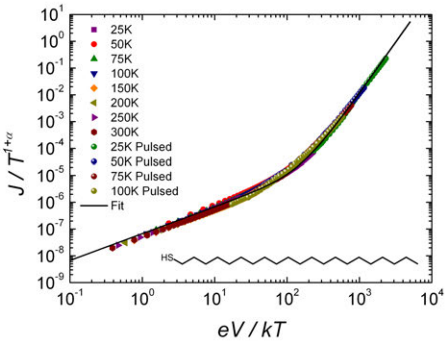

Figure 6.4: Scaled current density of a docosane (C22MT) junction presented on a double logarithmic scale as a function of eV/kT. Both DC measurements up to 0.5 V bias and pulse measurements up to 5 V are included. The solid curve is calculated with Equation 6.2 using $\alpha = 2.8$, $\gamma = 2.3 \times 10^{-2}$ and $J_0 = 1.9 \times 10^{-6}\ Am^{-2}$.

of Figure 6.2a can now be replotted as $J/T^{1+\alpha}$ versus eV/kT. Figure 6.3 shows that a single, smooth curve is obtained, with eV/kT spanning four orders of magnitude and the scaled current density spanning seven orders of magnitude. The solid line is calculated with Equation 6.2; a good agreement is obtained. There are only two fit parameters J_0 and γ. The value of $\gamma = 2.0 \times 10^{-2}$ determines the position of the knee in the curve while $J_0 = 1.1\ Am^{-2}$ fixes the absolute value. The other π-conjugated molecules show a similar scaling of the normalized current density versus eV/kT.

Similar scaling was observed for the alkanemonothiol junctions as well. As a typical example, Figure 6.4 shows the scaled current density as function of eV/kT for

Table 6.1: Parameters derived from the analysis of the electrical transport in large-area junctions by using Equation 6.2. The normalized resistance (RS), the power-law coefficient α, and the fit parameters J_0 and γ are shown. Furthermore, the value of $\pi\gamma^{-1}$, related to the number of microscopic tunneling events, is presented.

Junction Type	$RS_{0.1\,V}$ $[\Omega\mu m^2]$	α	γ	$\pi\gamma^{-1}$	J_0 $[Am^{-2}]$
PEDOT:PSS	3.0×10^3	1.3	2.5×10^{-2}	126	2.0×10^2
P1DT	2.8×10^4	2.0	2.0×10^{-2}	157	1.1
P2DT	9.1×10^4	2.1	1.9×10^{-2}	165	1.3×10^{-1}
P3DT	2.2×10^5	2.3	2.3×10^{-2}	137	7.7×10^{-3}
P4DT	8.5×10^5	2.4	3.3×10^{-2}	95	1.3×10^{-3}
P1MT	1.3×10^4	2.4	2.4×10^{-2}	131	7.0×10^{-2}
P2MT	3.3×10^4	2.2	2.2×10^{-2}	143	2.2×10^{-1}
P3MT	7.6×10^4	1.9	2.1×10^{-2}	150	5.8×10^{-1}
C18MT	2.7×10^5	1.6	2.5×10^{-2}	126	1.8×10^{-1}
C20MT	8.4×10^6	3.0	2.2×10^{-2}	143	4.0×10^{-6}
C22MT	1.9×10^7	2.8	2.3×10^{-2}	137	1.9×10^{-6}

docosanemonothiol (C22MT). A single, smooth curve is found. The solid line is calculated by Equation 6.2 with $\alpha = 2.8$ and using fit constants γ of 2.3×10^{-2} and J_0 of 1.9×10^{-6} Am^{-2}. A good agreement is obtained. The observation of temperature dependence is in contrast with previous reports in which, from measurements down to 200 K, temperature-independent transport was claimed.[16] We note that a decisive statement can only be made when measurements to lower temperatures are performed. For the specific type of PEDOT:PSS used the power-law dependence resulted in only minor changes in the electrical characteristics down to 200 K. For lower temperatures, however, the temperature dependence progressively increases.

The complete $J(V,T)$ characteristics of all large-area molecular junctions can be described using only three parameters, *viz.* α, γ and J_0. Table 6.1 summarizes the values for all molecular junctions and for the corresponding PEDOT:PSS-only diode. Table 6.1 shows that the values of γ for the molecular junctions are nearly constant. Furthermore, they are identical to that of the PEDOT:PSS-only diode from which we conclude that the value of γ in the molecular junctions is determined by PEDOT:PSS. The normalized resistance for the junctions varies over four orders of magnitude whereas α varies only between 2.0 and 3.0. The value of α determines the temperature dependence at low bias. Table 6.1 shows that the values of α and γ are essentially constant and the main difference between the junctions is the value of the prefactor J_0. When α is exactly the same for all junctions, the prefactor should scale linearly with RS at low bias. When compensated for the small differences in α, a one-to-one correspondence is indeed found. When variations in α can be disregarded, J_0 depends exponentially

on the molecular length. Therefore J_0 contains the molecular contribution.

6.3.2 Factorization with PEDOT:PSS

The similarity between the molecular junctions and the PEDOT:PSS-only diode implies that the temperature and voltage dependence originates from the PEDOT:PSS. The molecular contribution is only a length-dependent prefactor. Furthermore, the similarity suggests that the prefactor J_0 scales with the PEDOT:PSS resistance. To verify this factorization we varied the conductivity of PEDOT:PSS between 0.2 and 300 Scm^{-1}. Figure 6.5 presents the normalized resistance of alkanemonothiols as a function of molecular length for junctions containing two PEDOT:PSS formulations. For both series an identical length dependence is obtained. The difference is about an order of magnitude in the absolute value of the resistance. The inset of Figure 6.5 shows the dependence of the resistance of icosanemonothiol (C20MT) junctions on the bulk PEDOT:PSS conductivity. The obtained correlation implies that J_0 depends not only on the molecular length but also on the conductivity of PEDOT:PSS. Consequently, in the multibarrier tunneling model for the large-area junctions the factorization with the PEDOT:PSS resistance has to be explicitly included:

$$R = 12.9\,k\Omega\, T_{Au-S}^{-1} e^{\beta L} T_{SAMPEDOT}^{-1} T_{PEDOT:PSS}^{-1} \tag{6.3}$$

We note that a relation with the bulk conductivity of PEDOT:PSS has previously been suggested.[17] The current analysis unambiguously demonstrates this factorization.

Previously, we have used the Simmons model to interpret the electrical transport in molecular junctions.[22] A good description for the normalized resistance at low bias was obtained. At higher bias, however, the model underestimated the resistance. The discrepancy is due to the fact that the Simmons model is derived for an insulator sandwiched between two metallic electrodes. The current transport is by tunneling and depends exponentially on the applied bias. The transport in these large-area molecular junctions, however, is factorized with the PEDOT:PSS resistance. This polymer is a highly doped semiconductor and yields a power-law dependence on both bias and temperature. Factorization of the resistance of molecular junctions with PEDOT:PSS accounts for a number of previously poorly understood processing issues. The resistance of the junctions was shown to depend on the type of PEDOT:PSS used as contact and on the type of photoresist used to define the vias.[17] It has now been demonstrated that the influence stemming from PEDOT:PSS is actually the conductivity of the film. The dependence on the type of photoresist might be

explained by differences in surface tension, which lead to a modified morphology of the PEDOT:PSS film, effectively modifying $T^{-1}_{PEDOT:PSS}$.

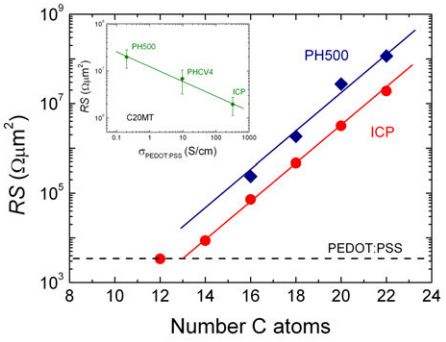

Figure 6.5: Normalized resistance versus molecular length of alkanemonothiol-based junctions fabricated with different PEDOT:PSS formulations. Data are reproduced from reference [17]. The inset shows the normalized resistance of icosanemonothiol (C20MT) junctions versus the (four-point probe) conductivity of the PEDOT:PSS formulation used to fabricate the junctions.

For large-area junctions the current density is constant, that is, the current scales with device area. For vias with a diameter smaller than 5 μm deviations can occur. The wetting of PEDOT:PSS on the SAM is different from that on the photoresist. The electrical contact at the perimeter of the vias can be different from that in the middle. This nonhomogeneity increases with decreasing diameter of the via. Hence the larger the via, the better is the scaling. The yield of junctions is in first order digital, either 100% or 0%. A junction is called shorted when the resistance coincides with the PEDOT:PSS-only resistance. The resistance of the junction is given by Equation 6.3. The inverse transmission prefactors cannot be smaller than unity. Hence, the resistance cannot be smaller than that of a PEDOT:PSS-only diode. Any higher value is counted as a functional junction. The quality of a wafer is therefore not assessed by the yield but by the parameter spread. The establishment of factorization and the dominant role of PEDOT:PSS on the transport in molecular junctions demonstrates that PEDOT:PSS cannot be regarded as a simple metallic electrode. Any change in the processing can yield different transmission factors and, hence, differences in the absolute value of the resistance. However, if the fabrication technology is strictly kept constant a clear signature of the molecular structure is observed. Consequently, large-area molecular junctions can yield valuable information on transport through functional molecules.

6.4 Summary and conclusions

Charge transport through monolayers of alkanes and *para*-phenylene oligomers has been investigated in large-area molecular junctions. The molecules are self-assembled in a monolayer on a gold bottom electrode and contacted with a PEDOT:PSS top electrode. The current density exhibits a power-law dependence on both temperature and bias, *viz.* $J \propto T^{\alpha}$ at low voltage ($eV \ll kT$) and $J \propto V^{\beta}$ at low temperature ($eV \gg kT$), with $\beta = \alpha + 1$. The value of α is unambiguously determined from the temperature dependence at low bias. For all molecules investigated replotting the scaled current density $J/T^{1+\alpha}$ as a function of eV/kT yields a single smooth curve spanning over orders of magnitude. With only two fit parameters, γ and J_0, the complete $J(V,T)$ characteristics can be quantitatively described. The prefactor J_0 depends on the molecular length. The values of α and γ are essentially constant for the molecular junctions and, furthermore, identical to those of the corresponding PEDOT:PSS-only diode. This similarity implies that the temperature and voltage dependence originates from PEDOT:PSS. The molecular contribution is only a length-dependent prefactor. Furthermore, by varying the type of PEDOT:PSS we have shown that J_0 depends on the bulk conductivity of PEDOT:PSS as well. Consequently, in a multibarrier tunneling model the factorization with the PEDOT:PSS resistance has to be explicitly included. The dominant role of the PEDOT:PSS contact explains the absolute value of the junction resistance and its relation to processing conditions.

References

[1] A. Salomon, D. Cahen, S. Linsday, J. Tomfohr, V. B. Engelkes, C. D. Frisbie, Adv. Mater. 15 (2003) 1881.

[2] H. B. Akkerman, B. de Boer, J. Phys:Condens. Matter 20 (2008) 013001. (and references therein).

[3] W. Wang, T. Lee, M. A. Reed, Phys. Rev. B 68 (2003) 035416.

[4] S. H. Choi, B. Kim, C. D. Frisbie, Science 320 (2008) 1482.

[5] K. W. Hipps, Science 294 (2001) 536.

[6] D. Vuillaume, S. Lenfant, Microelectron. Eng. 70 (2003) 539.

[7] J. G. Kushmerick, Mater. Today 8 (2005) 26.

[8] X. D. Cui, A. Primak, X. Zarate, J. Tomfohr, O. F. Sankey, A. L. Moore, T. A. Moore, D. A. Gust, G. Harris, S. M. Lindsay, Science 294 (2001) 571.

[9] V. B. Engelkes, J. M. Beebe, C. D. Frisbie, J. Am. Chem. Soc. 126 (2004) 14287.

[10] F. Chen, X. Li, J. Hihath, Z. Huang, N. J. Tao, J. Am. Chem. Soc. 128 (2006) 15874.

[11] J. M. Beebe, V. B. Engelkes, L. L. Miller, C. D. Frisbie, J. Am. Chem. Soc. 124 (2002) 11268.

[12] Y. S. Park, A. C. Whalley, M. Kamenetska, M. L. Steigerwald, M. S. Hybertsen, C. Nuckolls, L. Venkataraman, J. Am. Chem. Soc. 129 (2007) 15768.

[13] X. L. Li, J. He, J. Hihath, B. Q. Xu, S. M. Lindsay, N. J. Tao, J. Am. Chem. Soc. 128 (2006) 2135.

[14] C. Li, I. Pobelov, T. Wandlowski, A. Bagrets, A. Arnold, F. Evers, J. Am. Chem. Soc. 130 (2008) 318.

[15] B. A. Mantooth, P. S. Weiss, Proc. IEEE 91 (2003) 1785.

[16] H. B. Akkerman, P. W. M. Blom, D. M. de Leeuw, B. de Boer, Nature 441 (2006) 69.

[17] P. A. van Hal, E. C. P. Smits, T. C. T. Geuns, H. B. Akkerman, B. C. De Brito, S. Perissinotto, G. Lanzani, A. J. Kronemeijer, V. Geskin, J. Cornil, P. W. M. Blom, B. de Boer, D. M. de Leeuw, Nat. Nanotechnol. 3 (2008) 749. (including supporting info).

[18] A. J. Kronemeijer, E. H. Huisman, H. B. Akkerman, G. S. M., I. Katsouras, P. A. van Hal, T. C. T. Geuns, S. J. van der Molen, P. W. M. Blom, D. M. de Leeuw, Appl. Phys. Lett. 97 (2010) 173302.

[19] A. J. Kronemeijer, E. H. Huisman, I. Katsouras, P. A. van Hal, T. C. T. Geuns, P. W. M. Blom, S. J. van der Molen, D. M. de Leeuw, Phys. Rev. Lett. 105 (2010) 156604.

[20] H. Grabert, U. Weiss, Phys. Rev. Lett. 54 (1985) 1605.

[21] M. P. A. Fisher, A. T. Dorsey, Phys. Rev. Lett. 54 (1985) 1609.

[22] H. B. Akkerman, R. C. G. Naber, B. Jongbloed, P. A. van Hal, P. W. M. Blom, D. M. de Leeuw, B. de Boer, Proc. Natl. Acad. Sci. 104 (2007) 11161.

CHAPTER 7

Charge transport in poly(p-phenylene vinylene) at low temperature and high electric field

Charge transport in poly(2-methoxy, 5-(2' ethyl-hexyloxy)-p-phenylene vinylene) (MEH-PPV)-based hole-only diodes is investigated at high electric fields and low temperatures using a novel diode architecture. Charge carrier densities that are in the range of those in a field-effect transistor are achieved, bridging the gap in the mobility versus charge carrier density plot between polymer-based light-emitting diodes and field-effect transistors. The extended field range that is accessed allows us to discuss the applicability of current theoretical models of charge transport, using numerical simulations. Finally, within a simple approximation, we extract the hopping length for holes in MEH-PPV directly from the experimental data at high fields, and we derive a value of 1.0 ± 0.1 *nm.*

7.1 Charge transport measurements in conjugated polymers: limitations

Understanding and modeling charge transport in conjugated polymers is crucial to optimize the performance of organic semiconductor devices such as light-emitting diodes (OLEDs), field-effect transistors (OFETs) and solar cells.[1–8] Charge carrier transport in these materials has been under intense research in the past decades. The workhorses for polymeric light-emitting diodes are derivatives of poly(p-phenylene vinylene) such as poly(2-methoxy, 5-(2' ethyl-hexyloxy)-p-phenylene vinylene) (MEH-PPV). It has been shown that the transport of holes, which are the dominant charge carriers in this material, can be explained by a space-charge limited current (SCLC),[9,10] with a mobility originating from a hopping process between localized sites in a Gaussian density of states (DOS).[11] It has been demonstrated that the mobility depends on density, electric field and temperature.[12,13] A commonly used model to describe the charge transport is the Extended Gaussian Disorder Model (EGDM).[14] In this model the dependence of the mobility on carrier density governs the hole conduction at room temperature, whereas at low temperatures the field dependence dominates.

A general problem to experimentally validate charge transport models is that in conventional OLEDs the charge transport is measured only in a limited range of electric field and temperature. A typical example is presented in Figure 7.1, where the experimental current density of an MEH-PPV hole-only diode at room temperature (symbols) is presented as a function of electric field. The transport is typically measured in a field range between 1 MV/m and 30 MV/m. The solid lines in Figure 7.1 are simulations using a numerical drift-diffusion model based on the EGDM model. As an illustration of two extreme cases, the solid lines represent simulations where we have varied the lattice constant, *i.e.* 1 nm and 2 nm, keeping all other parameters fixed. It is observed that within the conventional characterization window of about 1-30 MV/m it is not possible to resolve which set of parameters best describes the experimental data. The two fits deviate but only at an inaccessible field range. An extension of the experimental measurement window is therefore required to truly validate charge transport models that have been proposed in recent years.

The shaded areas in Figure 7.1 at higher and lower fields are not easily accessible with standard measurement techniques and device geometries. Extension to higher fields is hampered by dielectric breakdown under continuous applied DC bias. At low electric fields reliable transport measurements are hampered by parasitic leakage currents that mask the diode current, especially at low temperatures, since the

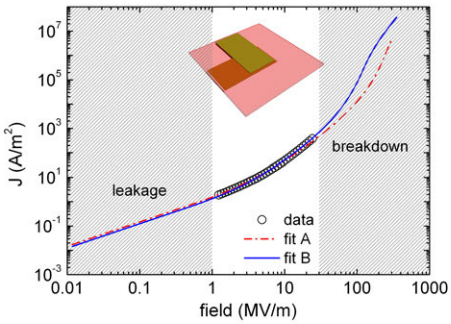

Figure 7.1: Current density as a function of applied electric field for an MEH-PPV hole-only diode. Measurements were performed at room temperature at electric fields between 1 and 30 MV/m. The solid lines are fits to the data using a numerical drift-diffusion model based on the Extended Gaussian Disorder Model. The solid lines are calculated using two extreme values for the lattice constant of 1 nm (fit A) and 2 nm (fit B). Inset shows the standard layout of an organic light-emitting diode.

device current decreases much faster with temperature than the parasitic currents. Here we characterize hole-only diodes of MEH-PPV at an unprecedented voltage and temperature range, by employing the previously developed technology of molecular junctions.[15] The diodes are defined in a matrix of insulating photoresist, eliminating the problem of parasitic leakage. Small device areas allow for higher biases to be applied before the current reaches the critical level at which the diodes break down. The application of short voltage pulses further extends the applied electric field range up to a maximum of 300 MV/m.[16] The resulting high field and low temperature measurements on hole-only diodes of MEH-PPV are used to test the ability of existing theoretical models to describe charge carrier transport in MEH-PPV at high fields. We use the achieved high carrier densities to address the charge carrier dependence of the mobility in the gap that exists between carrier densities in polymer-based light-emitting diodes and field-effect transistors. Finally, within a simple approximation we extract the hopping length directly from the experimental data at high fields.

7.2 Experimental

Molecular junctions were prepared as described previously on a 6-inch Si monitor wafer with a 500 nm thermally grown SiO_2 passivation layer.[15] A 60 nm Au bottom electrode was evaporated onto a Ti adhesion layer and patterned with I-line photolithography. Vertical interconnects (vias) ranging from 1 μm to 100 μm in diameter

were defined in insulating photoresist by conventional spincoating and UV-lithography. The wafer was divided by laser cutting in identical 2×3 cm pieces, each containing 110 junctions. The amorphous polymer poly(2-methoxy, 5-(2' ethyl-hexyloxy)-p-phenylene vinylene) (MEH-PPV), synthesized in our laboratory via the Gilch method, [17] was dissolved in toluene and spincoated in ambient conditions. A solution with a concentration of 4.5 mg/ml yielded layers of 115 nm and 85 nm when spincoated at 1000 rpm and 2000 rpm, respectively. A layer of 40 nm was obtained from a solution with a concentration of 2.5 mg/ml, by spincoating at 3000 rpm. The final thickness was measured on reference layers spincoated on clean glass slides using a Dektak profilometer. Subsequently, the conducting polymer PEDOT:PSS, a water-based suspension of poly(3, 4-ethylenedioxythiophene) stabilized with poly(4-styrenesulphonic acid), AGFA ICP1020 (Agfa-Gevaert), was spincoated from a formulation containing the nonionic Zonyl FSO-100 (DuPont) fluoro-surfactant. The conductivity amounted to 300 S/cm. The diodes were subsequently annealed for one hour at $85°C$ in dynamic vacuum. Finally, a 150 nm top gold contact was thermally evaporated through a shadow mask. This top contact is utilized as a self-aligned reactive ion etching mask for the removal of the redundant PEDOT:PSS. Stable and reproducible junctions were obtained.

DC and pulsed current measurements were performed in a cryogenic probe station (Janis Research Co.), using a Keithley 4200 Semiconductor Parameter Analyzer equipped with the Keithley Pulse Measurement Unit. The current through the junctions scaled with the lateral dimensions of the vias with only a small standard deviation. The transport of the diodes could be measured with DC biases between 1 mV and about 10 V, depending on the layer thickness. To circumvent electrical breakdown at higher DC bias, pulse measurements were applied (**Chapter 5**). The pulse width was set at 500 μs with a rise and fall time of 1 μs. At low temperature and with a low duty cycle of 10% the transport could be measured up to high biases of 13 V, 30 V and 40 V for the diodes with thickness of 40 nm, 85 nm and 115 nm respectively.

7.3 Results and discussion

7.3.1 Charge transport measurements and modeling

The current density as a function of electric field for MEH-PPV hole-only diodes, fabricated in the molecular junction architecture with MEH-PPV layer thicknesses of 40 nm, 85 nm and 115 nm, are presented in Figure 7.2a-c. The schematic diode

layout showing the difference to a conventional OLED geometry is shown in Figure 7.2d. The temperature was varied between 150 K and 300 K. The electrical transport could be measured over an electric field range of about 5 decades, from 0.01 MV/m up to 300 MV/m. The transport characteristics were nearly symmetric for negative and positive bias, showing that the highest occupied molecular orbital (HOMO) of the MEH-PPV layer is well aligned with the HOMO of the PEDOT:PSS top electrode and with the Fermi level of the bottom gold contact. The transport is Ohmic at low fields. Subsequently, with increasing field, a quadratic dependence of the device current on the voltage is observed indicating a space-charge limited (SCL) current, following Mott-Gurney's square law.[18] At even higher fields a deviation from the square-law dependence is observed. The deviation is due to the field and charge carrier density dependence of the mobility. At low bias the current density decreases with decreasing temperature. At higher fields the temperature dependence is weaker. At sufficiently high fields the temperature dependence disappears and the current density *vs.* electric field characteristics converge.

To describe the experimental data we used a numerical drift-diffusion model based on the commonly used Extended Gaussian Disorder Model (EGDM) of Pasveer *et al.*.[14,19] This model takes into account the density and field dependence of the mobility.[14] As both the electric field and the carrier density are non-uniform in a SCL diode, one has to resort to such a numerical model as the resulting mobility is highly non-uniform. The parameterization used by Pasveer *et al.*[14] is not valid for high charge-carrier densities, which are achieved in our thin layer diodes at high fields. We therefore performed numerical simulations using an improved parameterization, valid at high charge-carrier densities.[20] We chose a standard set of fitting parameters, previously used in literature to describe transport in MEH-PPV hole-only diodes.[14,21] Figure 7.3 shows the fits of the experimental data for the MEH-PPV diodes with a layer thickness of 85 nm. A magnification of the high field regime is given in the inset. We note that at low temperatures the simulation at high fields fails due to numerical issues. We observe that although the chosen model describes the experimental data well at the field range commonly used in other experiments, the fit to the data is rather poor at higher fields. Especially the calculated crossover at 200 MV/m is unrealistic.

7.3.2 Disentangling the dependence of mobility on field and carrier density

As a next step, we turn to a different theoretical description, developed by Vissenberg and Matters (VM), which is based on variable range hopping in an exponential

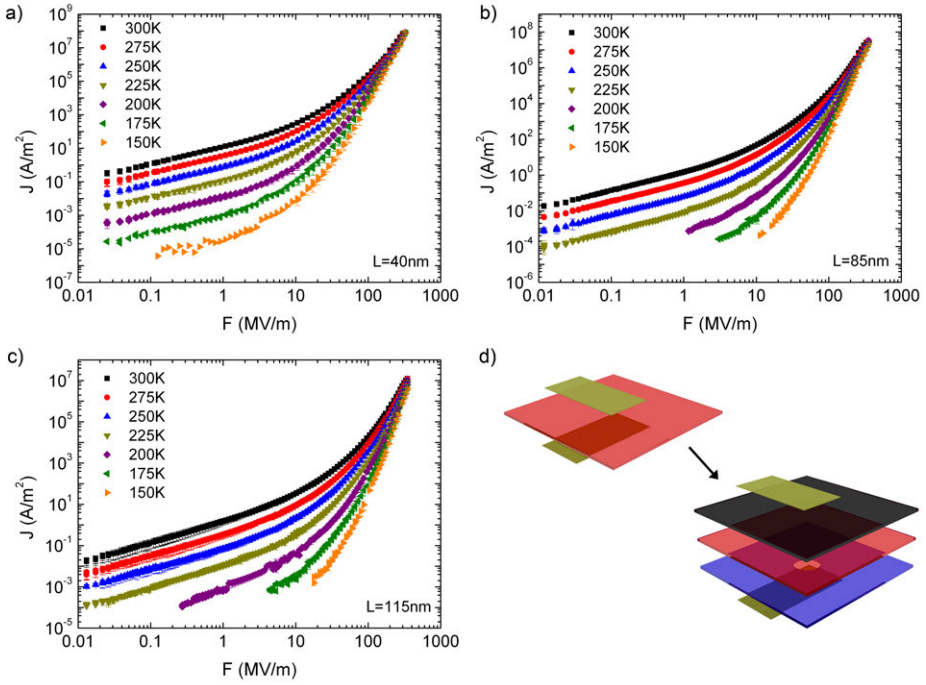

Figure 7.2: Current density as a function of applied electric field for MEH-PPV hole-only diodes fabricated in the large-area molecular junction geometry. The MEH-PPV layer thicknesses are (a) 40 *nm*, (b) 85 *nm* and (c) 115 *nm*. (d) Schematic of a standard LED structure and of the large-area molecular junction architecture, in which the extra photo-resist (blue) and PEDOT:PSS (black) layers are shown.

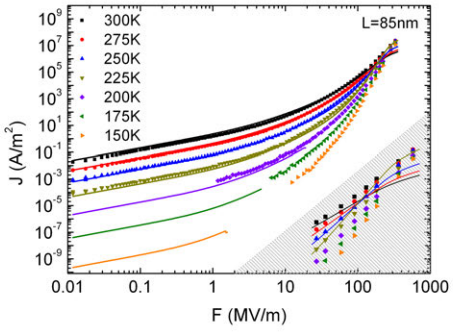

Figure 7.3: Current density as a function of applied electric field for an MEH-PPV hole-only diode with a layer thickness of 85 *nm* at temperatures between 150 *K* and 300 *K*. The solid lines are fits to the data using a numerical drift-diffusion model based on the Extended Gaussian Disorder Model. The inset shows a magnification of the cross-over at the high field regime.

density of states.[22] The model takes into account a charge carrier density dependent mobility, and it has been extensively used to model charge transport in organic field-effect transistors (FETs). Since in our SCL diodes similar high densities are obtained as in FETs, the VM model can also be tested. An important difference with FETs is that in our diodes a high voltage induces simultaneously a high electric field next to a high carrier density. Effects of the electric field on the mobility are not included in the VM model, since in organic FETs the electric field along the channel is very low due to the low applied source-drain bias and long channel length. It has been reported[13,14] that at room temperature the mobility is mainly dominated by charge density effects. With our new device structure we can investigate whether at room temperature the field dependence of the mobility can also be ignored at high voltages. In Figure 7.4 we show the room temperature J-V characteristics of the hole-only diodes of Figure 7.2 together with the J-V (dashed lines) characteristics following the VM transport model, as calculated with the numerical drift-diffusion simulator.[19] For clarity, only the data for the 40 nm and 85 nm diodes are plotted. We observe that only up to fields of approximately 10 MV/m the VM model gives a consistent description of the charge transport at room temperature. Above these fields we have to include a field dependence of the Poole-Frenkel type.[23] The mobility within this model exhibits a field enhancement that depends on the square root of the field exponentially, with a temperature and disorder dependent pre-factor γ.[11,24–29] Inclusion of a Poole-Frenkel factor $e^{\gamma\sqrt{F}}$, with a value for γ of 3.5×10^{-4} $(m/V)^{\frac{1}{2}}$, in the VM model gives a good description of the J-V characteristics in the full field range up to 300 MV/m (solid lines). The value for γ is in good agreement with previous reports.[11,24–29] We note that such a functional dependence of the mobility on the field cannot describe the convergence of the current density for different temperatures at high fields. Both the EGDM and VM with extended field-dependence models fail in this respect. The development of a charge transport model that consistently describes the charge transport at high electric field is a future challenge.

With the prefactor γ known, we can also disentangle the effects of carrier density and electric field on the charge carrier mobility. Similar to Tanase *et al.*[13] we extract the mobility as a function of charge carrier density directly from the J-V characteristics, disregarding the field effect. The values derived for MEH-PPV diodes with layer thicknesses of 40 nm, 85 nm and 115 nm are presented as a function of charge carrier density by the open symbols in Figure 7.5. Mobility values extracted for conventional MEH-PPV light-emitting diodes and for field-effect transistors by Craciun *et al.*[30] are included for comparison. The high mobility values extracted in our diodes demon-

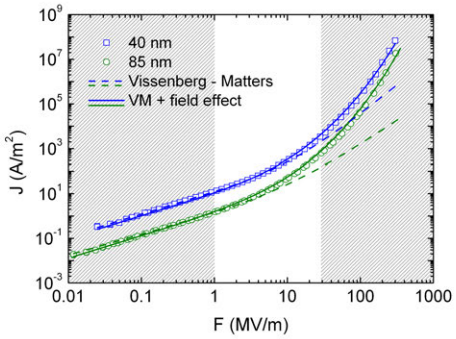

Figure 7.4: Current density as a function of applied electric field at room temperature for MEH-PPV hole-only diodes with a layer thickness of 40 *nm* and 85 *nm*. The dashed lines are the calculated characteristics following the Vissenberg-Matters transport model. The solid lines represent the calculated current density characteristics when a Poole-Frenkel factor $e^{\gamma\sqrt{F}}$ is included in the VM model.

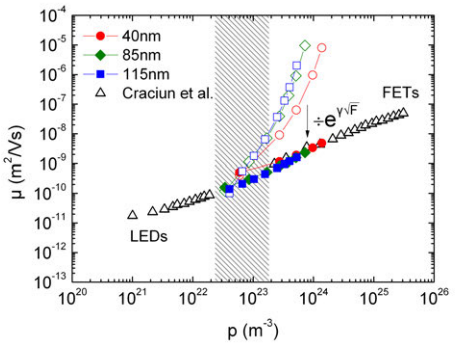

Figure 7.5: Mobility, μ, as a function of charge carrier density, p, extracted from MEH-PPV diodes with layer thicknesses of 40 *nm*, 85 *nm* and 115 *nm* (open symbols). Mobility values for MEH-PPV light-emitting diodes and field-effect transistors derived by Craciun *et al.*[30] are included for comparison (Δ). The solid symbols represent mobility values after correction for the field dependence, $e^{\gamma\sqrt{F}}$. The charge carrier density was extracted in each case from the middle of the MEH-PPV layer, at different applied fields.

strate that we have to correct for the field dependence, $e^{\gamma\sqrt{F}}$, as obtained from Figure 7.4. The solid symbols then represent the corrected, low field, mobility values. A good agreement with the data reported previously by Craciun *et al.*[30] is obtained. We observe that the gap between LEDs and FETs can be bridged without having to resolve exclusively to thin or doped polymer layers, as previously reported.[30,31] In contrast to these studies, the charge carrier density values in our devices do not simply approach, but overlap well with those achieved in a field-effect transistor. A unified

description is obtained.

7.3.3 Extracting the hopping length

The convergence of the current density data at high electric fields (Figure 7.2 and inset of Figure 7.3) can be used to extract directly from the experimental data a basic parameter of hopping transport, *viz.* the hopping length. A sufficiently large applied field is a strong perturbation to the thermal, diffusive motion of charge carriers. In a first order approximation, the J-V characteristics for different temperatures converge once the energy provided by the electric field can overcome the activation energy of the sequential hops between the localized sites in the polymer. The convergence field can then be used to estimate an average hopping length for the material. Using the approximation:

$$F_c \ell_{hop} = E_a \tag{7.1}$$

where F_c is the convergence field, ℓ_{hop} is the hopping length and E_a is the activation energy, one obtains the following relation between the convergence bias, V_c, and the thickness, L, of the polymer film in the diode:

$$V_c = \frac{E_a L}{\ell_{hop}} \tag{7.2}$$

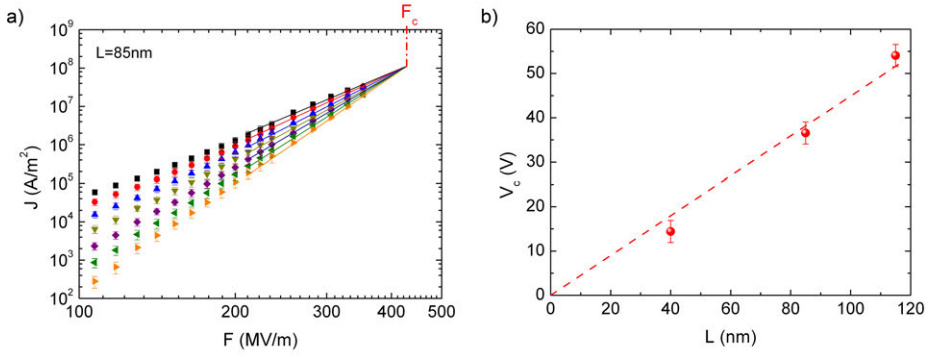

Figure 7.6: (a) Magnification of the high field regime for the current density versus electric field as a function of temperature of an MEH-PPV hole-only diode with a layer thickness of 85 *nm*. Solid lines represent a power-law extrapolation to estimate the convergence field, F_c. (b) Convergence voltage as a function of layer thickness for MEH-PPV hole-only diodes as a function of layer thickness. The dashed line is the linear fit to the data, using Equation 7.2.

From the current density-electric field characteristics of Figure 7.2, the convergence

field, at which the current density is independent of temperature, can be determined. We use a simple power-law extrapolation, as depicted in Figure 7.6a for the case of the diode with an 85 nm thick MEH-PPV layer. In Figure 7.6b the convergence voltages are presented as a function of film thickness. A linear dependence in agreement with Equation 7.2 is obtained. The slope is given by $\frac{E_a}{\ell_{hop}}$. Taking an activation energy for MEH-PPV of 0.45 eV,[30,32–34] we find an average hopping length ℓ_{hop} of 1.0 ± 0.1 nm. This value is in good agreement with hopping distances as reported for PPV-type semiconductors.[35,36]

7.4 Summary and conclusions

We have used the experimental testbed of large-area molecular junctions to characterize charge transport in MEH-PPV-based hole-only diodes at an unprecedented range of electric field and temperature. The data set presented here can be used as a benchmark to verify any theoretical charge transport model. We demonstrate that the commonly used transport model, *viz.* the Extended Gaussian Disorder Model, describes the experimental data well only in the field range that is conventionally used in experiments. The fit to the data is rather poor at higher fields. Similarly, the Vissenberg-Matters transport model consistently describes the charge transport at room temperature up to fields of approximately 10 MV/m. Above these fields we have to include a Poole-Frenkel type field dependence, $e^{\gamma\sqrt{F}}$, where the pre-factor γ depends on temperature and disorder. With the prefactor γ extracted at room temperature, we have disentangled the effects of carrier density and electric field on the charge carrier mobility. The gap between conventional LEDs and FETs has been bridged. However, the convergence of the current density for different temperatures at high fields is correctly described by neither the EGDM nor the VM with extended field-dependence. The development of a charge transport model that consistently describes the charge transport at high electric field is a future challenge. The convergence of the current density at high fields allows for the quantification of the energy provided by the electric field to overcome the activation energy of the sequential hops between the localized sites in the polymer. With a simple approximation, we have extracted directly from the experimental data at high fields a hopping length of 1.0 ± 0.1 nm for holes in MEH-PPV.

References

[1] J. H. Burroughes, D. D. C. Bradley, A. R. Brown, R. N. Marks, K. Mackay, R. H. Friend, P. L. Burns, A. B. Holmes, Nature 347 (1990) 539.

[2] G. Gustafsson, Y. Cao, G. M. Treacy, F. Klavetter, N. Colaneri, A. J. Heeger, Nature 357 (1992) 477.

[3] A. R. Brown, A. Pomp, C. M. Hart, D. M. de Leeuw, Science 270 (1995) 972.

[4] H. Sirringhaus, P. J. Brown, R. H. Friend, M. Nielsen, K. Bechgaard, B. M. W. Langeveld-Voss, A. J. H. Spiering, R. A. J. Janssen, E. J. Meijer, P. Herwig, D. M. de Leeuw, Nature 401 (1999) 685.

[5] R. H. Friend, R. W. Gymer, A. B. Holmes, J. H. Burroughes, R. N. Marks, C. Taliani, D. D. C. Bradley, D. A. Dos Santos, J. L. Bredas, M. Longlund, W. R. Salaneck, Nature 397 (1999) 121.

[6] S. E. Shaheen, C. J. Brabec, N. S. Sariciftci, F. Padinger, T. Fromherz, J. C. Hummelen, Appl. Phys. Lett. 78 (2001) 841.

[7] Y. Sun, N. C. Giebink, H. Kanno, B. Ma, M. E. Thompson, S. R. Forrest, Nature 440 (2006) 908.

[8] S. Reineke, F. Lindler, G. Schwartz, N. Siedler, K. Walzer, B. Lussem, K. Leo, Nature 459 (2009) 234.

[9] M. A. Lampert, P. Mark, Current injection in solids, Academic, New York, 1970.

[10] P. W. M. Blom, M. J. M. de Jong, J. J. M. Vleggaar, Appl. Phys. Lett. 68 (1996) 3308.

[11] H. Bässler, Phys. Stat. Sol. B 175 (1993) 15.

[12] C. Tanase, E. J. Meijer, P. W. M. Blom, D. M. de Leeuw, Phys. Rev. Lett. 91 (2003) 216601.

[13] C. Tanase, E. J. Meijer, P. W. M. Blom, D. M. de Leeuw, Phys. Rev. B 70 (2004) 193202.

[14] W. F. Pasveer, J. Cottaar, C. Tanase, R. Coehoorn, P. A. Bobbert, P. W. M. Blom, D. M. de Leeuw, M. A. J. Michels, Phys. Rev. Lett. 94 (2005) 206601.

[15] H. B. Akkerman, P. W. M. Blom, D. M. de Leeuw, B. de Boer, Nature 441 (2006) 69.

[16] I. Katsouras, A. J. Kronemeijer, E. C. P. Smits, P. A. van Hal, T. C. T. Geuns, P. W. M. Blom, D. M. de Leeuw, Appl. Phys. Lett. 99 (2011) 013303.

[17] K. Asadi, J. Wildeman, P. W. M. Blom, D. M. de Leeuw, IEEE Tran. Elec. Dev. 57 (2010) 3466.

[18] N. F. Mott, R. W. Gurney, Electronic processes in ionic crystals, Oxford University, London, 1940.

[19] L. J. A. Koster, E. C. P. Smits, V. D. Mihailetchi, P. W. M. Blom, Phys. Rev. B 72 (2005) 085205.

[20] L. Wang, H. Zhang, X. Tang, C. Mu, J. Li, Curr. Appl. Phys. 10 (2010) 1182.

[21] Y. Zhang, B. de Boer, P. W. M. Blom, Phys. Rev. B 81 (2010) 085201.

[22] M. C. J. M. Vissenberg, M. Matters, Phys. Rev. B 57 (1998) 12964.

[23] J. Frenkel, Phys. Rev. 54 (1938) 647.

[24] D. M. Pai, J. Chem. Phys. 52 (1970) 2285.

[25] W. D. Gill, J. Appl. Phys 43 (1972) 5033.

[26] P. W. M. Blom, Viss, Mater. Sci. Eng. B R27 (2000) 53.

[27] L. B. Schein, A. Peled, D. Glatz, J. Appl. Phys. 66 (1989) 686.

[28] P. M. Borsenberger, J. Appl. Phys. 68 (1990) 6263.

[29] M. A. Abkowitz, Phil. Mag. B 65 (1992) 817.

[30] N. I. Craciun, J. Wildeman, P. W. M. Blom, Phys. Rev. Lett. 100 (2008) 056601.

[31] J. J. Brondijk, F. Maddalena, K. Asadi, H. J. van Leijen, M. Heeney, P. W. M. Blom, D. M. de Leeuw, Phys. Status Solidi B 249 (2012) 138.

[32] H. Meyer, D. Haarer, H. Naarmann, H. H. Hohold, Phys. Rev. B 52 (1995) 2587.

[33] M. Kuik, L. J. A. Koster, G. A. H. Wetzelaer, P. W. M. Blom, Phys. Rev. Lett. 107 (2011) 256805.

[34] note. We extract the same activation energy from the temperature dependence.

[35] T. J. Savenije, J. E. Kroeze, M. M. Wienk, J. M. Kroon, J. M. Warman, Phys. Rev. B 69 (2004) 155205.

[36] H. C. F. Martens, P. W. M. Blom, H. F. M. Schoo, Phys. Rev. B 61 (2000) 7489.

CHAPTER 8

Outlook

In this outlook we have filled the holes with monolayers of DNA, spin-crossover compounds and the ferroelectric copolymer P(VDF-TrFE). The electrical transport has been measured and the preliminary data are presented. We show that dense monolayers of hybridized DNA molecules are obtained. However, the molecules are lying flat. The electrical data show that the charge transport is measured not along, but across the molecules. The conductance obtained indicates that the transport through DNA is due to non-resonant tunneling. Smooth thin films of a spin-crossover compound could be realized but the conductivity was too low to reliably identify a spin-crossover transition. The properties of ferroelectric capacitors with thick layers are in good agreement with literature data. Scaling down the thickness showed a gradual change in coercive field. Even ultra-thin films of about a few nanometers could be fabricated. The electrical transport data indicate the first ferroelectric tunnel junction, but more experiments are needed for verification. The examples presented unambiguously show that the technology is generic and versatile. The holes can be filled with unconventional semiconductors yielding scientifically interesting devices.

8.1 Introduction

The electrical transport through several classes of materials depends on the length scale. Interesting phenomena such as quantum confinement occur when one of the dimensions of the investigated system is in the order of a few nanometers. Experimental investigation of the scaling with the lateral dimensions requires a technology that can reproducibly address the electrical transport as a function of layer thickness varying from single molecules self-assembled in ultra-thin films to micrometer-thick films.

To measure the charge transport perpendicular through the films, they have to be sandwiched between two electrodes. As explained in **Chapter 1** we started from a previously developed technology for large-area molecular junctions. [1,2] The general structure of the junction consists of an active layer sandwiched between two electrodes, enclosed in an insulating matrix defined in photoresist. The junctions are formed on a thermally oxidized silicon wafer on top of which patterned bottom gold electrodes have been evaporated. Subsequently, a photoresist layer is spincoated and patterned by conventional I-line lithography, creating circular vertical interconnects (vias, or holes) on top of the bottom electrodes. The active layer is deposited and a layer of the conducting polymer poly(3, 4-ethylenedioxythiophene):poly(4-styrenesulphonic acid) (PEDOT:PSS) is spincoated on top. Ultra-thin films can be prepared by self-assembly, while thicker films can be made by spincoating. Finally, the junction is finished by evaporating top gold electrodes and using them as a self-aligned mask to etch away the redundant PEDOT:PSS. The key advantages are the use of the conducting polymer layer sandwiched between the active layer and the top electrode that prevents electrical shorts, and processing within the lithographically defined vertical interconnects (vias, or holes) that prevents both parasitic currents and cross-talk between different junctions. The active layer can vary from a monolayer to bulk films. The length scale varies between a few nanometers to a micrometer. The technique is simple, compatible with standard integrated circuit fabrication processes, and can be scaled up to any wafer size. [2]

The application of large-area molecular junctions for the characterization of electrical transport through various self-assembled monolayers (SAMs) has been discussed in **Chapters 3** through **6**. An example of thick films is shown in **Chapter 7**, which presents the charge transport through the well-known light emitting polymer, MEH-PPV, at an unprecedented range of electric field and temperature. Hence, the technology is generic and versatile. Any molecule can be applied to fill the holes. In a joint collaboration with CSIC in Barcelona, devices were made with electroactive

polychlorotriphenylmethyl (PTM) radical molecules. The data have been reported elsewhere.[3] In this outlook chapter, we focus on DNA, spin-crossover compounds and ferroelectrics. Preliminary data are presented in the next sections.

8.2 Junctions with DNA

Deoxyribonucleic acid (DNA) has been established as the most important biological polymer, since it carries genetic information. The answer to the question why such a complex molecule should be used in a field so different than the role that nature has assigned to it, can be sought in its unique features, which cannot be found in other polymers.

DNA possesses complementarity, the self-assembling ability that always forms specific hydrogen-bonded base pairs. Thanks to its self-assembling characteristics, which allow it to be highly integrated error-free with no need for microfabrication technologies, DNA is highly interesting as a functional nano-size material.

The DNA molecule can be viewed as a series of nitrogenous bases connected through a sugar-phosphate backbone. DNA in the cell functions as a double-stranded helix of B-form DNA, the structure of which was first determined by Watson and Crick[4] and is reproduced in Figure 8.1.

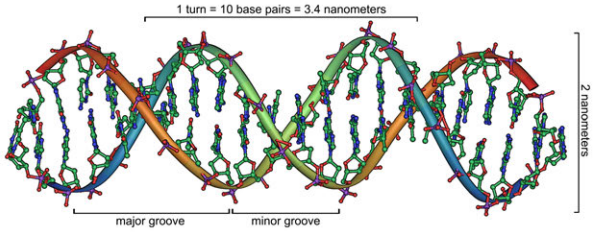

Figure 8.1: The structure of the double-stranded helix of B-DNA. Created by Michael Ströck.[5]

The polar sugar-phosphate backbones of each strand form the helical scaffold, with the nitrogenous bases in the interior of the molecule, their planes nearly perpendicular to the helical axis. The diameter of the B-DNA is ~ 20 Å, and the distance between base pairs is ~ 3.4 Å.

The nature of charge transport in DNA remains largely unresolved. DNA allegedly spans the whole spectrum of conductive behavior, having been reported to be an insulator, a semiconductor, a conductor and even a superconductor.[6–16] Before molecular

electronic applications that take advantage of DNA's complementarity can be envisioned, the ambiguity around DNA's charge transport properties should be lifted.

We have investigated whether a dense SAM of DNA molecules can be assembled onto an electrode and measured in large-area molecular junctions. The envisioned advantage of the junction geometry is that it offers a solvent- and stress-free environment. Furthermore, since the junctions are sealed, the SAM is protected from contamination.

The DNA molecules used in this study were oligomers with 14, 22 and 30 base pairs ($14mer$, $22mer$ and $30mer$ respectively). These DNA molecules were modified with a short alkyl spacer and a thiol termination, synthesized at the Polymer Chemistry and Bioengineering department of the Zernike Institute for Advanced Materials, at the University of Groningen.[17]

Fabrication of a dense self-assembled monolayer of DNA on gold is a long standing problem. For the chemical bonding with the substrate, the DNA molecules are modified with a thiol group that has a high affinity for gold. However, other interactions such as those of the base pairs and phosphate groups of DNA with the gold substrate prevail and result in monolayers of poor coverage.[18,19] The reported procedure to eliminate these interactions is passivation of the gold substrate with an incomplete monolayer of short alkylthiols. The short alkylthiol molecules compete with the weaker nonspecific interactions and prevent the target molecules from binding nonspecifically to the surface. The passivation step can be performed before or after the self-assembly of short, single-stranded DNA chains.[20,21]

We varied the length of the DNA linker between 3 and 6 carbon atoms, as well as the passivating molecules from 3-mercapto-1-propanol, 6-mercapto-1-hexanol, 1-mercaptohexane to 11-mercapto-1-undecanol. The substrate was passivated for different times, before or after the assembly of single-stranded DNA. Hybridization was always the last step. All these protocols did result in monolayers of DNA but the problem was that the grafting density was very low. Hence, the transport through DNA molecules could not be distinguished from that of PEDOT:PSS-only junctions.

Therefore, we used a reported alternative method,[21] *viz.* to self-assemble the hybridized DNA directly with the passivation step before or after the assembly. Numerous experiments showed that the most promising approach is to pre-treat the substrate for a very short time and self-assemble pre-hybridized double-stranded DNA.

Typical data are presented in Figure 8.2. The double-stranded DNA molecules contained one or two thiolated linkers. Three DNA molecules were used with 14, 22 and 30 base pairs with lengths of 4 nm, 7 nm and 10 nm, respectively.

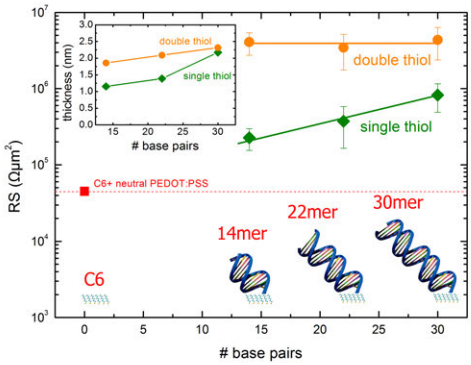

Figure 8.2: Normalized resistance as a function of the number of DNA base pairs as determined in large-area molecular junctions. The green and orange lines are for hybridized DNA molecules with a single and double thiol linker. The inset shows the corresponding layer thickness as measured by ellipsometry.

The green curve represents the normalized resistance of the DNA molecules with a single thiolated linker. The resistance is higher than that of the independently measured passivating dense layer of 1-hexanethiol. We note that the resistance of only the passivating film that has a low coverage can hardly be detected, it is comparable to the value of a PEDOT:PSS-only junction. The higher resistance is due to the presence of DNA. We note, however, that the resistance is hardly dependent on the length of the DNA molecule. For a dense monolayer with all DNA molecules perpendicular to the substrate an exponential dependence on length is expected. Here, however, we observe a change of only a factor of three. Furthermore, for the double thiolated DNA molecules there is no length dependence at all. The reason is unveiled by ellipsometry measurements as shown in the inset of Figure 8.2. The measured thickness is presented as a function of the number of base pairs. The layer thickness is much smaller than the length of the molecules, which, therefore, are not standing up. For the DNA molecules with the double linker (orange line) the layer thickness is almost independent of the length of the molecule. Actually, the value corresponds to the diameter of the DNA molecules. It can therefore be concluded that although we have a fully covered monolayer of molecules, they are not standing upright but are lying flat on the substrate. This is supported by the almost similar layer thickness for the longest DNA molecule with a single linker (green line). The smaller thickness for the shorter molecules is due to incomplete monolayer formation.

The morphology derived, *viz.* layers of DNA molecules lying flat on the surface, explains the electrical transport data. We measure the charge transport not along the

molecules but across their diameter. This automatically implies that the normalized resistance is identical for all fully-covered layers. The weak length dependence of the single thiolated molecules (green line) is due to incomplete coverage.

The diameter of B-DNA is 2 nm.[4] The normalized resistance value obtained is 5 $\times$ 10^6 $\Omega\mu m^2$, which is similar to that of alkanethiols of the same length. For instance, for a hexadecane-1-thiol (C16MT) with a length of 20.07 $\mathring{A}$ a resistance of 1 $\times$ 10^6 $\Omega\mu m^2$ has been reported.[2] The agreement shows that the charge transport mechanism is presumably non-resonant tunneling, which needs to be verified by temperature dependence measurements.

8.3 Junctions with spin-crossover compounds

Spin-crossover compounds, also named spin transition compounds, are functional switching materials able to change their spin state upon external stimuli. The phenomenon of spin-crossover (SCO) was discovered in 1931 and has been observed in octahedral coordination complexes of transition metals with an electronic configuration nd.[22] As shown in Figure 8.3 for an nd^6 configuration, the electrons occupy the crystal field splitted $t2g$ and eg orbitals in either a high spin or low spin state. The transition is triggered by external stimuli, such as temperature, pressure, light, magnetic field and yields a reversible change in physical properties such as color, magnetic susceptibility, thermal and electric conductivity, dielectric constant and mechanical properties.[23–27]

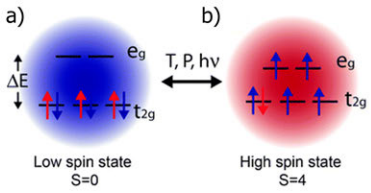

Figure 8.3: Scheme of nd^6 electron configuration in (a) low and (b) high spin state. Adapted from reference [28].

The switching is well understood.[29] As schematically shown in Figure 8.4, there are three types of transitions: (a) a gradual transition, (b) a transition showing a hysteresis loop and (c) a two-step transition. For data storage applications hysteresis is a prerequisite. The example of Figure 8.4b shows that the LS-to-HS transition occurs at a higher temperature than the HS-to-LS transition. The abrupt changes indicate that the metal complexes cooperate. A transition of one complex triggers

the transition of other complexes which implies that the transition from one spin state to the other spin state should depend on the length scale of the system under investigation. However, a testbed for the experimental verification of the scaling is missing.

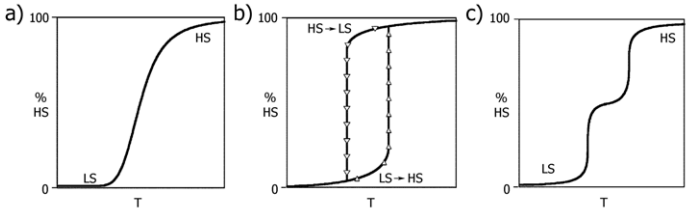

Figure 8.4: Three possible types of spin transition. As an example the percentage of high spin complex is plotted as a function of temperature. (a) a gradual transition, (b) a transition showing a hysteresis loop and (c) a two-step transition. Adapted from reference [30].

Electrical transport data are scarce. In 2011 the first spin-crossover system showing bistability and hysteresis effects at room temperature by applying a voltage bias was reported.[31] The authors accomplished this by creating nanoparticles covered with the spin-crossover material and placing them between two gold electrodes separated by approximately 5-10 nm. A switchable molecular device made by contacting individual nanoparticles between nanometer-spaced electrodes has been reported.[31] This nanoscale device exhibits switching and memory effects near room temperature as a consequence of the intrinsic bistability of the spin-crossover nanoparticle. Thus, a sharp increase in the conductance is observed upon heating above ca. 350 K, together with the presence of a thermal hysteresis as large as 30 K for a single-particle device, after which the conductance switches back to the original value. This confirms the existence of hysteretic spin-crossover effects in a single nano-object. Interestingly for molecular spintronics, the spin-crossover could also be induced by applying a voltage, showing that its magnetic state is controllable electrically.

We started working with the spin-crossover material $trans$-$[Fe(bapbpy)(NCS)_2]$. The chemical structure is presented in Figure 8.5a. The iron(II) nucleus is surrounded by NCS groups, and a tetradentate ligand abbreviated as *bapbpy*. The synthesis as well as extensive characterization has been reported elsewhere.[32] The magnetic susceptibility measurements as a function of temperature are reproduced in Figure 8.5b. The red curve represents the data for the crude powder and the green curve for material that was dissolved in a mixture of DMF and methanol, and recrystallized. The blue curve was measured for material recrystallized from a mixture of DMF and diisopropylether. The data are included to show the sensitivity of the properties on

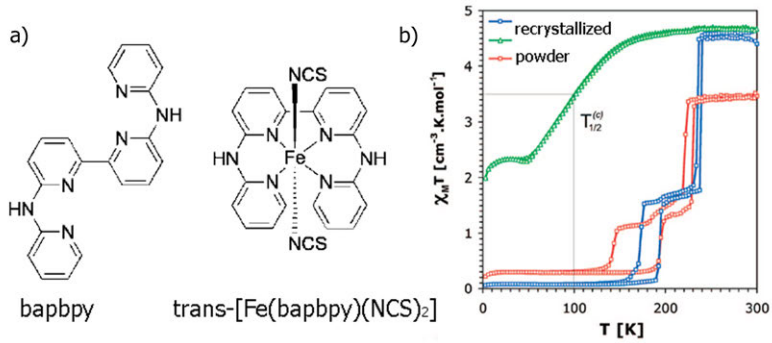

Figure 8.5: Spin-crossover compound. (a) Structure of the *bapbpy* ligand (left) and of *trans*-$[Fe(bapbpy)(NCS)_2]$ (right). (b) Magnetic susceptibility measurements reproduced from reference [32].

processing conditions.

We investigated fabrication of thin films by spincoating on glass substrates. Processing conditions such as concentration of *trans*-$[Fe(bapbpy)(NCS)_2]$ in DMF, substrate temperature and spin speed were varied deliberately. The optimal conditions turned out to be the maximum concentration of 12.5 mg/ml, a hot substrate and a low spinning speed of 500 rpm. This procedure yields uniform layers of approximately 60 nm. Adding polystyrene to the solution did not further improve the morphology or increase the layer thickness.

The spin-crossover compound was subsequently processed in large-area molecular junctions. The electrical transport was measured as a function of via size and temperature. The current density, however, was low, only 10^{-1} A/m^2. The conductivity was too low to reliably identify a spin-crossover transition. We note that many new, environmentally stable and processable, materials are being synthesized, and that there is progress in film deposition and patterning. Spin-crossover compounds that allow study of scaling of the transition as a function of layer thickness will emerge and materials for electrical data storage can be anticipated.

8.4 Ferroelectric tunnel junctions

A ferroelectric tunnel junction is a diode in which two metal electrodes are separated by a thin ferroelectric layer. The spontaneous polarization of the ferroelectric layer can be switched by an applied electric field. The electrical resistance strongly depends on the orientation of the electric polarization. This phenomenon is known

as tunneling electroresistance. A schematic band diagram is depicted in Figure 8.6a. There are at least three mechanisms responsible for the change in resistance by switching the ferroelectric polarization: (i) change in the electrostatic potential profile across the ferroelectric barrier; (ii) change in the transmission coefficient across interfaces; (iii) change in the attenuation constant of the barrier.

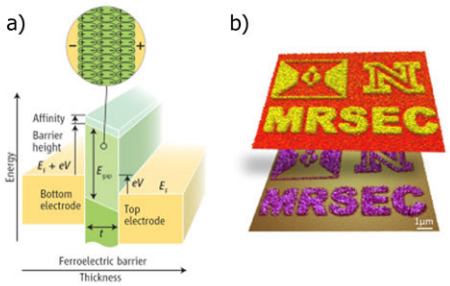

Figure 8.6: (a) Schematic band diagram of a ferroelectric tunnel junction. (b) Demonstration of tunneling electroresistance. Ferroelectric polarization pattern of a thin ferroelectric film in the form of the logotip (top) and the same pattern imaged by detecting the local tunneling current across the film by c-AFM (bottom). Adapted from reference [33].

In order to realize ferroelectric and multiferroic tunnel junctions a number of obstacles has to be overcome. In particular, parasitic effects such as local conductivity and transport via localized states have to be eliminated. In addition, the mechanisms of domain formation, nucleation and switching in nanoscale ferroelectrics and tunneling transport across polar thin film dielectrics have to be understood. Tremendous achievements in the field of complex oxide epitaxy and ultra-thin ferroelectric polymers in addition to the nanoscale characterization techniques during the last years make a promise that all these problems can be solved and the realization of ferroelectric tunnel junctions is just a matter of time.

We used the technology developed, to fabricate organic ferroelectric tunnel junctions. Ferroelectric polymers are ideal candidates for data storage in system-in-foil applications as they exhibit an intrinsic bistable, remanent polarization that can be repeatedly switched by an electric field.[34] Memories based on capacitors,[35] field-effect transistors[36,37] and ferroelectric-blend diodes[38–40] have been reported. The most commonly used organic ferroelectric is the random copolymer poly(vinylidene fluoride-trifluoroethylene) (P(VDF-TrFE)). The chemical structure is presented in the inset of Figure 8.7. This copolymer is widely applied for its ease of processing, the relatively large remanent polarization, low leakage currents due to a high electrical resistivity and switching times as short as 1 μs.

To benchmark the technology we started with thick ferroelectric films and characterized the capacitors obtained. We took the large-area junction technology developed and used a thick layer of P(VDF-TrFE). The current density and polarization as a function of bias for a film of about 400 nm are presented in Figure 8.7, for capacitors made with combinations of different electrodes. A remanent polarization of 70 mC/m^2 and a coercive field of 60 MV/m are obtained, both in good agreement with literature data. [41]

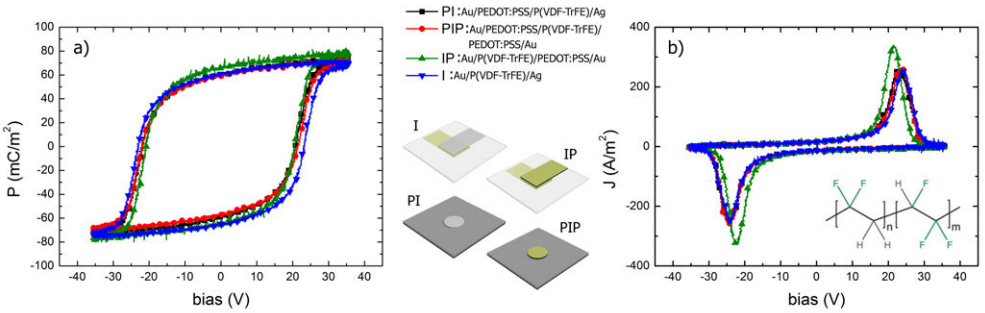

Figure 8.7: (a) Polarization and (b) current density of a 400 nm thick P(VDF-TrFE) film as a function of bias. The inset of (b) shows the chemical structure of P(VDF-TrFE). The capacitors with different electrode combinations (metal electrodes only, PEDOT:PSS as the top and/or bottom electrode) are schematically depicted in the center.

To fabricate thin ferroelectric films and tunnel junctions the process flowchart had to be adapted. Spincoated films of P(VDF-TrFE) are amorphous. To enhance the crystallinity and hence the ferroelectricity the films are typically annealed close to the melting temperature of about 140°C. On gold, however, thin films dewet and comprising capacitors are shorted. Hence, we used PEDOT:PSS electrodes instead. We carefully checked that for thick capacitors the ferroelectric properties are independent of the type of electrode, as shown in Figure 8.7. The PEDOT:PSS is spincoated over a pre-patterned substrate with Au electrodes. Subsequently, a very thin P(VDF-TrFE) film is spincoated on top and the whole stack is patterned by reactive ion etching. Then the photoresist is applied, the vias are defined and the top electrode is processed. The optimized process flowchart is presented in Figure 8.8. The additional steps cannot be circumvented as a very thin smooth film can only be obtained by spincoating on a substrate with negligible topography. We note that the annealing is done after the whole device is finished. Dewetting is then reduced by the presence of the top electrode. To prevent dewetting the annealing was performed under a N_2 pressure of 100 bar. It is as yet unclear if this high pressure is really needed.

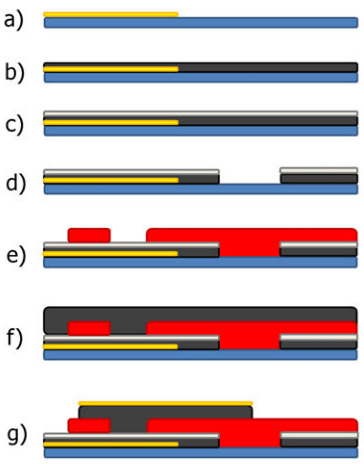

Figure 8.8: Adapted flowchart for ferroelectric tunnel junctions. (a) deposition of gold, (b) bottom PEDOT:PSS electrode spincoating, (c) P(VDF-TrFE) spincoating, (d) patterning of PEDOT:PSS and P(VDF-TrFE) by reactive ion etching, (e) photoresist spincoating and patterning with UV-lithography, (f) top PEDOT:PSS electrode spincoating and (g) deposition of top gold layer and removal of redundant PEDOT:PSS by reactive ion etching.

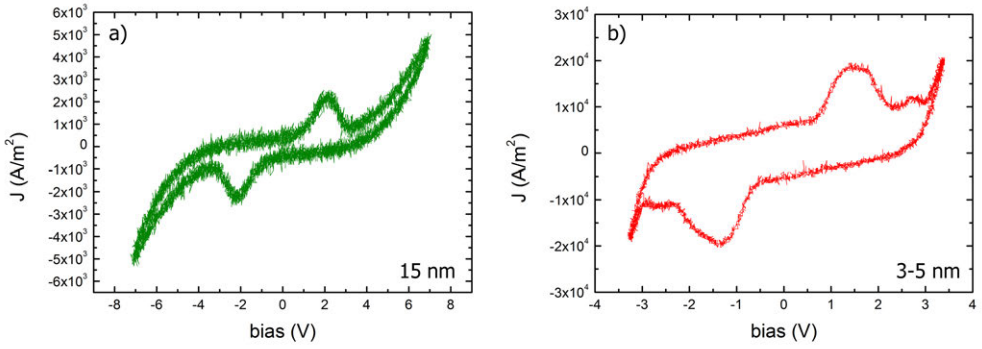

Figure 8.9: Current density as a function of voltage for ultra-thin P(VDF-TrFE) films of (a) 15 *nm* and (b) 3-5 *nm*. The current comprises the switching current of the thin ferroelectric superimposed on an almost exponential background current.

Current density-voltage measurements for films of 3-5 *nm* and of 15 *nm* are presented in Figure 8.9. The current comprises the switching current of the thin ferroelectric superimposed on an almost exponential background current. The voltage bias for the maxima in the switching current increases with decreasing thickness. In agreement to literature data, the coercive field gradually increases with decreasing thickness

from 60 MV/m for thick films to 350 MV/m for ultra-thin films of 4 nm.[42] We note that scaling of the voltage bias with the film thickness rules out Faradaic currents due to electrochemical oxidation and reduction of PEDOT:PSS. The polarization, as obtained by integration of the switching current after correction for the background current, yields a value slightly lower than as measured for thick film capacitors. The reason could be insufficient annealing of the P(VDF-TrFE) film. The background current could be measured up to about 10 V after which the device breaks down. The current could be due to the tunneling current through the P(VDF-TrFE) layer. However, the current has to be corrected for the PEDOT:PSS series resistance.

The current-voltage characteristics are symmetric while in first order approximation for a tunnel junction an asymmetric profile is expected. The origin could be due to the measurement protocol, single pulse measurements and c-AFM investigations are required instead of continuous measurements, or to parasitic leakage currents. Further experiments are required to verify the presence of a tunnel junction. However, the data presented here are very promising. It is clearly shown that with the technology developed ultra-thin ferroelectric capacitors can be made. The interest is not only scientific. Ferroelectric tunnel junctions with asymmetric current profiles can be non-destructively read-out. Functional ferroelectric tunnel junctions can be expected in the near future.

8.5 Summary and conclusions

In this outlook we have filled the holes with unconventional semiconductors and we have presented the preliminary data obtained. The holes were filled with monolayers of DNA, spin-crossover compounds and the ferroelectric copolymer P(VDF-TrFE). We used DNA molecules with different lengths, modified with short alkyl spacers and a thiol termination. We showed, from ellipsometry measurements, that dense monolayers of hybridized DNA molecules are obtained, which, however, are lying flat on the substrate. The electrical data show that the charge transport is measured not along, but across the molecules. The values obtained indicate that the transport through DNA is due to non-resonant tunneling. Thin films of the spin-crossover compound *trans*-$[Fe(bapbpy)(NCS)_2]$ have been fabricated. A processing protocol has been developed that did yield smooth thin films of about 60 nm. The conductivity was too low to reliably identify a spin-crossover transition. However, many new, environmentally stable and processable, materials are being synthesized and compounds that allow study of scaling of the transition as a function of layer thickness will emerge.

Furthermore, we filled the holes with the ferroelectric copolymer P(VDF-TrFE). The properties of capacitors with thick layers are in good agreement with literature data. Scaling down the thickness showed a gradual increase in coercive field. An optimized process flowchart was developed that allowed investigation of ultra-thin films of a few nanometers. The preliminary electrical transport data indicate a ferroelectric tunnel junction, but more experiments are needed for the unambiguous verification. The examples presented show that the technology is generic and versatile. The holes can be filled with unconventional semiconductors yielding scientifically interesting devices.

References

[1] H. B. Akkerman, P. W. M. Blom, D. M. de Leeuw, B. de Boer, Nature 441 (2006) 69.

[2] P. A. van Hal, E. C. P. Smits, T. C. T. Geuns, H. B. Akkerman, B. C. De Brito, S. Perissinotto, G. Lanzani, A. J. Kronemeijer, V. Geskin, J. Cornil, P. W. M. Blom, B. de Boer, D. M. de Leeuw, Nat. Nanotechnol. 3 (2008) 749. (including supporting info).

[3] C. D. Simão, Surface Self-Assembly of Electroactive molecules as Wires and Switches, Ph.D. thesis, Institut de Ciéncia de Materials de Barcelona - CSIC, 2011.

[4] J. D. Watson, F. H. C. Crick, Nature 171 (1953) 737.

[5] http://tinyurl.com/baev3eo.

[6] H.-L. Lee, H. Tanaka, Y. Otsuka, K.-H. yoo, J.-O. Lee, T. kawai, Appl. Phys. Lett. 80 (2002) 1670.

[7] H. W. Fink, C. Schönenberger, Nature 398 (1999) 407.

[8] P. J. de Pablo, F. Moreno-Herrero, J. Colchero, J. Gómez Herrero, P. Herrero, A. M. Baró, P. Ordejón, J. M. Soler, E. Artacho, Phys. Rev. Lett. 85 (2000) 4992.

[9] D. Porath, A. Bezryadin, S. de Vries, C. Dekker, Nature 403 (2000) 635.

[10] A. Y. Kasumov, M. Kociak, S. Guéron, B. Reulet, V. T. Volkov, D. V. Klinov, H. Bouchiat, Science 291 (2001) 280.

[11] Y. Zhang, R. H. Austin, J. Kraeft, E. C. Cox, N. P. Ong, Phys. Rev. Lett. 89 (2002) 198102.

[12] E. Braun, Y. Eichen, U. Sivan, G. Ben-Yoseph, Nature 391 (1998) 775.

[13] Y. Okahata, T. Kobayashi, K. Tanaka, M. Shimomura, J. Am. Chem. Soc. 120 (1998) 6165.

[14] P. Tran, B. Alavi, G. Gruner, Phys. Rev. Lett. 85 (2000) 1564.

[15] B. Hartzell, B. McCord, D. Asare, H. Chen, J. J. Heremans, V. Soghomonian, Appl. Phys. Lett. 82 (2003) 4800.

[16] Y. Maeda, T. Matsumoto, T. Kawai, ACS Nano 5 (2011) 3141.

[17] D. K. Prusty, DNA-Hybrid Materials: From Supramolecular Assembly to Applications in Catalysis and Biosensing, Ph.D. thesis, University of Groningen, 2012.

[18] R.-Y. Zhang, D.-W. Pang, Z.-L. Zhang, J.-W. Yan, J.-L. Yao, Z.-Q. Tian, B.-W. Mao, S.-G. Sun, J. Phys. Chem. B. 106 (2002) 11233.

[19] X. Michalet, Nano Lett. 1 (2001) 341.

[20] T. M. Herne, M. J. Tarlov, J. Am. Chem. Soc. 119 (1997) 8916.

[21] T. Aqua, R. Naaman, S. S. Daube, Langmuir 19 (2003) 10573.

[22] L. Cambi, A. Cagnasso, Atti. Accad. Naz. Lincei, CI. Sci. Fis., Mat. Nut., Rend 13 (1931) 809.

[23] E. Breuning, M. Ruben, J. M. Lehn, F. Renz, Y. Garcia, V. Ksenofontov, P. Gutlich, E. Wegelius, K. Rissasen, Angew. Chem., Int. Ed. 39 (2000) 2504.

[24] P. Gutlich, Y. Garcia, H. A. Goodwin, Chem. Soc. Rev. 29 (2000) 419.

[25] F. Varret, K. Boukheddaden, E. Codjovi, A. Goujon, Hyperfine Interact. 165 (2005) 37.

[26] O. Sato, Acc. Chem. Res. 36 (2003) 692.

[27] A. Bousseksou, G. Molnár, P. Demont, J. Menegotto, J. Mater. Chem. 13 (2003) 2069.

[28] M. Cavallini, I. Bergenti, S. Milita, G. Ruani, I. Salitros, Z. R. Qu, R. Chandrasekar, M. Ruben, Angew. Chem., Int. Ed. 47 (2008) 8236.

[29] P. Gütlich, H. A. Goodwin, Spin CrossOver in Transition Metal Compounds; Topics in Current Chemistry, Springer: Berlin, Germany, 2004.

[30] J. A. Real, A. B. Gaspar, M. C. Muñoz, Dalton Trans. (2005) 2062.

[31] F. Prins, M. Monrabal-Capilla, E. A. Osorio, E. Coronado, H. S. J. van der Zant, Adv. Mater. 23 (2011) 1545.

[32] S. Bonnet, G. Molnár, J. Sanchez Costa, M. A. Siegler, A. L. Spek, A. Bousseksou, W.-T. Fu, P. Gamez, J. Reedijk, Chem. Mater. 21 (2009) 1123.

[33] http://tinyurl.com/aj25yth.

[34] J. F. Scott, Ferroelectric Memories, Springer-Verlag, Berlin, 2000.

[35] R. C. G. Naber, K. Asadi, P. W. M. Blom, D. M. de Leeuw, B. de Boer, Adv. Mater. 22 (2010) 93.

[36] R. C. G. Naber, C. Tanase, P. W. M. Blom, G. H. Gelinck, A. W. Marshman, F. J. Touwslager, S. Setayesh, D. M. de Leeuw, Nat. Mater. 4 (2005) 243.

[37] M. A. Khan, U. S. Bhansali, H. N. alshareef, Adv. Mater. 24 (2012) 2165.

[38] K. Asadi, D. M. de Leeuw, B. de Boer, P. W. M. Blom, Nat. Mater. 2 (2008) 547.

[39] K. Asadi, M. Li, N. Stingelin, P. W. M. Blom, D. M. de Leeuw, Appl. Phys. Lett. 97 (2010) 193308.

[40] K. Asadi, M. Li, P. W. M. Blom, M. Kemerink, D. M. de Leeuw, Materials Today 14 (2011) 592.

[41] T. Furukawa, M. Date, E. Fukada, Y. Tajitsu, A. Chiba, Jap. J. Appl. Phys. 19 (1980) 109.

[42] R. C. G. Naber, P. W. M. Blom, D. M. de Leeuw, J. Phys. D: Appl. Phys. 39 (2006) 1984.

Summary

Microelectronics, with its applications weaved into almost every aspect of modern life, is the most common technology in the history of industrial engineering that is characterized by a length scale. There is however an emerging technology, envisioned already in the middle of the previous century, *viz.* nanotechnology. Nanotechnology can be defined as the fabrication and use of functional structures designed from atomic or molecular scale, with at least one characteristic dimension measured in nanometers. One nanometer, a billionth of a meter, is equal to a 50000th of the width of the average human hair. Designed and controlled fabrication and integration of nanomaterials and nanodevices is likely to be revolutionary for science and technology. Due to the variety of potential applications nanotechnology is a key technology for the future. Governments have invested billions of euros in its research.

As an example, molecular electronics is a branch of nanotechnology that uses single molecules, or nanoscale collections of single molecules, as electronic components. The major target of molecular electronics is to combine functional molecules into integrated circuits. Since single molecules are the smallest stable structures imaginable, molecular electronics provides a potential means to extend Moore's Law beyond the foreseen limits of small-scale conventional silicon integrated circuits.

Nevertheless, nanotechnology should not be simply considered a process of ultra-miniaturization. Phenomena at the nanometer scale are likely to constitute a completely new world. The nanometer size of the building blocks and functional units allows them to exhibit novel and significantly improved physical, chemical and biological properties. The changes in behavior are caused not only by the continuous modification of characteristics with diminishing size, but also by the emergence of totally new phenomena, such as quantum confinement and quantization of conductance. It is, therefore, important to investigate the properties of materials as a function of length scale. With an eye on electronic applications, research topics where the scaling of electrical properties with the lateral dimensions is interesting are for instance ferroelectrics and spin-crossover compounds for data storage applications and charge transport through single molecules for molecular electronics.

However, due to the difficulties in manipulating structures of such small size, char-

acterization of nanomaterials has proven to be a big challenge. New tools and approaches must be developed to meet the challenges. The investigation of the scaling with the lateral dimensions requires a technology that can reproducibly address the electrical transport of layers varying from single molecules self-assembled in ultra-thin films to bulk films.

In this thesis we employ and, when necessary, modify a previously developed technology of large-area molecular junctions, to address the scaling properties of a variety of systems. The dimensions of the investigated systems range from those of self-assembled monolayers of single molecules to those of bulk films. The junctions consist of an active layer sandwiched between metal electrodes. The structure is encased in an insulating matrix, pre-patterned with vias, or holes. By "filling the holes" with different materials we characterize their properties as a function of length scale, filling, at the same time, holes in the understanding of the behavior of these materials in the nano realm.

Large-area molecular junctions are two-terminal devices that allow the accurate and reproducible measurement of charge transport at unprecedented temperature and field ranges, offered by the stable and leakage-free junctions. An overview of the experimental procedure to fabricate and characterize large-area molecular junctions, the experimental testbed used throughout this thesis is presented in **Chapter 2**. The standard process flowchart is described, highlighting the features that make large-area molecular junctions a versatile testbed for the characterization of various materials.

In **Chapter 3** we investigate the electrical transport through mixed self-assembled monolayers (SAMs) of alkanemonothiols and alkanedithiols in large-area molecular junctions. To investigate the contribution of both the length of the molecule and the nature of the end group on the resistance, we systematically prepared mixed monolayers of all different binary combinations of two monothiols and two dithiols. The end group is fixed in a series of mixed monothiols and in a series of mixed dithiols. A trapezoidal correlation in semi-logarithmic resistance-composition coordinates has been obtained. The straight lines seem to indicate an exponential dependence on composition, or on the average molecular length, also in the case of mono- and dithiol mixed SAMs where resistance can decrease with increasing layer thickness, as the longer component is more conductive in the monocomponent SAM. However mathematically simple, exponential dependence is difficult to justify physically for mixed monolayers, unlike the case of monocomponent SAMs where this dependence has a single-molecule tunneling origin. We search for the origin of the resistance- composition dependence in mixed SAMs in an equivalent circuit model based on their microdomain structure, for which

we suggest a simple model. In essence, we suppose that the effective resistance of a molecule can differ depending on whether it is isolated (that is, trapped within an alien molecular domain) or belongs to a domain of the same molecules, due to contact and conformational issues. The simulated dependence is non-exponential and leads to a good agreement between calculated and measured resistances with only two fit parameters.

Chapter 4 discusses the contact resistance of a transistor using self-assembled monolayer (SAM)-modified source and drain electrodes. The contact resistance depends on the SAM tunnel resistance, the height of the injection barrier and the morphology at the contact. To disentangle the different contributions, we have combined transmission line measurements in transistors with transport measurements of SAMs in large-area molecular junctions. In order to eliminate the morphological complications, we have used in the transistor an amorphous semiconducting polymer, MEH-PPV. We show that in first order approximation the tunneling resistance of the SAM can be added linearly to the contact resistance of the bare Au transistor, to account for the increased contact resistance in the SAM-modified transistor. The analysis has been verified by using different SAMs. The SAM-modified contact at low gate bias can be treated as a metal-insulator-semiconductor (MIS) tunnel junction. At high gate bias however the contact behaves as a MIM tunnel junction, similar as in the large-area molecular junctions. The agreement obtained here shows that the SAM resistance is clearly manifested in the contact resistance of the transistors. Hence SAM-modified transistors can potentially be used as a gauge to measure electrical transport through single molecules.

In **Chapter 5** we use a large bias window to discriminate between different transport models in large-area molecular junctions. Under continuous DC bias, dodecanethiol junctions irreversibly break down at biases between 1 V and 2 V, corresponding to a field just over 9 MV/cm. We show that, by using pulse measurements, the bias window could be expanded to 6 V. This corresponds to a breakdown electrical field of 35 MV/cm, significantly larger than reported values of 20 MV/cm. The breakdown voltage is shown to depend logarithmically on both duty cycle and pulse width. The dependence is tentatively explained by electrolysis in the PEDOT:PSS layer as the breakdown mechanism. Expanding the bias window using pulse measurements has unambiguously shown that the electrical transport exhibits not an exponential but a power-law dependence on bias.

In **Chapter 6** we investigate the charge transport through alkanes and *para*-phenylene oligomers in large-area molecular junctions, using the technique developed

in **Chapter 5**. The molecules are self-assembled in a monolayer on a gold bottom electrode and contacted with a PEDOT:PSS top electrode. The current density exhibits a power-law dependence on both temperature and bias, *viz.* $J \propto T^{\alpha}$ at low voltage ($eV \ll kT$) and $J \propto V^{\beta}$ at low temperature ($eV \gg kT$), with $\beta = \alpha + 1$. The value of α is unambiguously determined from the temperature dependence at low bias. For all molecules investigated replotting the scaled current density $J/T^{1+\alpha}$ as a function of eV/kT yields a single smooth curve spanning over orders of magnitude. With only two fit parameters, γ and J_0, the complete $J(V,T)$ characteristics can be quantitatively described. The prefactor J_0 depends on the molecular length. The values of α and γ are essentially constant for the molecular junctions and, furthermore, identical to those of the corresponding PEDOT:PSS-only diode. This similarity implies that the temperature and voltage dependence originates from PEDOT:PSS. The molecular contribution is only a length-dependent prefactor. Furthermore, by varying the type of PEDOT:PSS we have shown that J_0 depends on the bulk conductivity of PEDOT:PSS as well. Consequently, in a multibarrier tunneling model the factorization with the PEDOT:PSS resistance has to be explicitly included. The dominant role of the PEDOT:PSS contact explains the absolute value of the junction resistance and its relation to processing conditions.

In **Chapter 7** the charge transport in MEH-PPV-based hole-only diodes is investigated at an unprecedented range of electric field and temperature. The data set presented can be used as a benchmark to verify any theoretical charge transport model. We demonstrate that the commonly used transport model, *viz.* the Extended Gaussian Disorder Model, describes the experimental data well only in the field range that is conventionally used in experiments. The fit to the data is rather poor at higher fields. Similarly, the Vissenberg-Matters transport model consistently describes the charge transport at room temperature up to fields of approximately 10 MV/m. Above these fields we have to include a Poole-Frenkel type field dependence, $e^{\gamma\sqrt{F}}$, where the pre-factor γ depends on temperature and disorder. With the prefactor γ extracted at room temperature, we have disentangled the effects of carrier density and electric field on the charge carrier mobility. The gap between conventional LEDs and FETs has been bridged. However, the convergence of the current density for different temperatures at high fields is correctly described by neither the Extended Gaussian Disorder Model nor the Vissenberg-Matters transport model with extended field-dependence. The development of a charge transport model that consistently describes the charge transport at high electric field is a future challenge. The convergence of the current density at high fields allows for the quantification of the energy provided by the electric

field to overcome the activation energy of the sequential hops between the localized sites in the polymer. With a simple approximation, we have extracted directly from the experimental data at high fields a hopping length of 1.0 ± 0.1 nm for holes in MEH-PPV.

Finally, **Chapter 8** provides an outlook on other topics of interest that can be investigated using the versatile experimental testbed of large-area molecular junctions, to arrive at molecular junctions with different functionality. The holes were filled with monolayers of DNA, spin-crossover compounds and the ferroelectric copolymer P(VDF-TrFE). We used DNA molecules with different lengths, modified with short alkyl spacers and a thiol termination. We show, from ellipsometry measurements, that dense monolayers of hybridized DNA molecules are obtained, which, however, are lying flat on the substrate. The electrical data show that the charge transport is measured not along, but across the molecules. The values obtained indicate that the transport through DNA is due to non-resonant tunneling. Thin films of the spin-crossover compound $[Fe(bapbpy)(NCS)_2]$ have been fabricated. A processing protocol has been developed that did yield smooth thin films of about 60 nm. The conductivity was too low to reliably identify a spin-crossover transition. However many new, environmentally stable and processable, materials are being synthesized and compounds that allow study of scaling of the transition as a function of layer thickness will emerge. We also filled the holes with the ferroelectric copolymer P(VDF-TrFE). The properties of capacitors with thick layers are in good agreement with literature data. Scaling down the thickness showed a gradually increase in coercive field. An optimized process flowchart was developed that allowed investigation of ultra-thin films of about a few nanometers. The preliminary electrical transport data indicate a ferroelectric tunnel junction, but more experiments are needed for the unambiguous verification.

The examples presented show that the technology of large-area molecular junctions is generic and versatile. The holes can be filled with unconventional semiconductors yielding scientifically interesting devices.

Samenvatting

Micro-elektronica, met zijn toepassingen verweven met bijna ieder aspect van het moderne leven, is de meest gangbare technologie in de geschiedenis van industriële techniek die wordt gekenmerkt door een lengteschaal. Er is echter een in opkomst zijnde technologie die reeds halverwege vorige eeuw is voorzien, namelijk nanotechnologie. Nanotechnologie kan worden gedefinieerd als het fabriceren en gebruikmaken van functionele structuren ontworpen op atomaire of moleculaire schaal, met ten minste één karakteristieke dimensie gemeten in nanometers. Een nanometer, een miljardste deel van een meter, staat gelijk aan een vijftigduizendste deel van de dikte van de gemiddelde menselijke haar. Ontwerp en gecontroleerde fabricage en integratie van nanomaterialen en nanoschakelingen zal waarschijnlijk van revolutionair belang zijn voor wetenschap en technologie. Vanwege de verscheidenheid aan mogelijke toepassingen is nanotechnologie een belangrijke technologie voor de toekomst. Overheden hebben miljoenen euro's geïnvesteerd in onderzoek hiernaar.

Moleculaire elektronica bijvoorbeeld is een tak van nanotechnologie die gebruikmaakt van afzonderlijke moleculen, of een verzameling van afzonderlijke moleculen op nanoschaal, als elektronische componenten. Het voornaamste doel van moleculaire elektronica is om functionele moleculen te gebruiken in geïntegreerde stroomkringen. Omdat afzonderlijke moleculen de kleinst denkbare stabiele structuren zijn biedt moleculaire elektronica een mogelijkheid om de wet van Moore uit te breiden voorbij de verwachte ondergrens voor het formaat van conventionele geïntegreerde stroomkringen op basis van silicium.

Toch moet nanotechnologie niet simpelweg worden opgevat als een ultraminiaturisatieproces. Verschijnselen op nanometerschaal vormen waarschijnlijk een compleet nieuwe wereld. Het nanometerformaat van de bouwstenen en functionele eenheden maakt het vertonen van nieuwe en aanmerkelijk verbeterde fysische, chemische en biologische eigenschappen mogelijk. De gedragsveranderingen worden niet alleen veroorzaakt door de doorlopende veranderingen van de karakteristieken bij afnemende grootte, maar ook door de opkomst van geheel nieuwe verschijnselen, zoals kwantuminsluiting en geleidingskwantisatie. Daarom is het belangrijk om de eigenschappen van materialen te onderzoeken als functie van de lengteschaal. Met het oog op elek-

tronische toepassingen zijn er onderzoeksonderwerpen waar de schaling van de elektrische eigenschappen met de laterale afmetingen interessant zijn, zoals ferro-elektrica en spin-omslag samenstellingen voor dataopslagtoepassingen en ladingstransport door afzonderlijke moleculen voor moleculaire elektronica.

Echter, door de complexiteit van het aanpassen van zulke kleine structuren is de karakterisering van nanomaterialen een grote uitdaging gebleken. Nieuwe hulpmiddelen en benaderingen moeten ontwikkeld worden om de uitdagingen aan te gaan. Het onderzoek naar de schaling met de laterale afmetingen vereist een technologie die reproduceerbaar het elektrische transport van lagen variërend van zelf-assemblerende, ultra-dunne lagen van afzonderlijke moleculen tot macroscopische lagen kan beschrijven.

In dit proefschrift gebruiken we en modificeren we wanneer noodzakelijk een eerder ontwikkelde technologie van moleculaire juncties met een groot oppervlak om de schalingseigenschappen van verscheidene systemen te onderzoeken. De afmetingen van de onderzochte systemen variëren van die van zelf-assemblerende monolagen tot die van macroscopische lagen. De juncties bestaan elk uit een actieve laag die tussen twee elektrodes geplaatst is. De structuur wordt omgeven door een isolerende matrix, waar vooraf gaten in zijn vervaardigd. Doormiddel van het vullen van deze gaten met verschillende materialen kunnen we hun eigenschappen karakteriseren als functie van hun lengteschaal, waarmee tegelijkertijd gaten in het begrip van het gedrag van deze materialen in de nanowereld worden gevuld.

Moleculaire juncties met een groot oppervlak zijn schakelingen met twee aansluitingen die betrouwbare en reproduceerbare metingen van landingstransport mogelijk maken in een ongekend temperatuur- en veldbereik, dankzij de stabiele en lekvrije juncties. Een overzicht van de experimentele procedure om moleculaire juncties met een groot oppervlak te vervaardigen en karakteriseren, de experimentele basis die door het gehele proefschrift wordt gebruikt, wordt gepresenteerd in **Hoofdstuk 2**. Het standaard stroomschema van het proces wordt beschreven, waarbij de eigenschappen die moleculaire juncties met een groot oppervlak tot een veelzijdige basis maken voor de karakterisering van verscheidene materialen naar voren worden gehaald.

In **Hoofdstuk 3** onderzoeken we het elektrische transport door gemengde zelf-assemblerende monolagen (self-assembled monolayer; SAM) van alkaanmonothiolen en alkaandithiolen in moleculaire juncties met een groot oppervlak. Om het aandeel van zowel de molecuullengte als de aard van de eindgroep op de weerstand te onderzoeken hebben we systematisch gemengde monolagen vervaardigd van alle verschillende binaire combinaties van twee monothiolen en twee dithiolen. De eindgroep is een

constante in een serie van gemengde monothiolen en een serie van gemengde dithiolen. Er is een trapezoïdale correlatie in enkel-logaritmische weerstand-samenstelling coördinaten gevonden. De rechte lijnen lijken te duiden op een exponentieel verband tussen de weerstand en de samenstelling of de gemiddelde molecuullengte, wat ook het geval is voor gemengde mono- en dithiol SAMs, waar weerstand kan afnemen bij toenemende laagdikte doordat het langere molecuul beter geleid in een SAM bestaande uit alleen dit molecuul. Hoewel dit exponentiële verband wiskundig gezien eenvoudig is, is het fysisch moeilijk te rechtvaardigen voor gemengde monolagen, in tegenstelling tot monocomponent SAMs, waarin dit verband een enkel-molecuul tunneling oorzaak heeft. We zoeken naar de oorzaak van het weerstand-samenstellingsverband in gemengde SAMs in een equivalente-stroomkring model gebaseerd op hun microdomeinstructuur, waarvoor we een simpel model voorstellen. In essentie veronderstellen we dat de effectieve weerstand van een molecuul kan afhangen van of het afgezonderd is (dat wil zeggen gevangen in vreemd moleculair domein) of dat het behoort tot een domein van dezelfde moleculen, uit contact- en samenstellingsoverwegingen. Het gesimuleerde verband is niet exponentieel en leidt tot een goede overeenkomst tussen berekende en gemeten weerstanden met slechts twee fitparameters.

Hoofdstuk 4 behandelt de contactweerstand van een transistor die gebruikmaakt van door SAMs gemodificeerde *source* en *drain* elektrodes. De contactweerstand hangt af van de tunnelweerstand van de SAM, de hoogte van de injectiebarriére en de morfologie aan het contact. Om de verschillende bijdragen te ontrafelen hebben we overdrachtslengtemetingen in transistors vergeleken met transportmetingen aan SAMs in moleculaire juncties met een groot oppervlak. Teneinde morfologische complicaties uit te sluiten hebben we een amorf halfgeleidend polymeer, MEH-PPV, gebruikt in de transistor. We tonen aan dat de tunnelweerstand van de SAM in eerste-orde benadering lineair kan worden opgeteld bij de contactweerstand van de niet gemodificeerde Au transistor om de toegenomen contactweerstand van de SAM-gemodificeerde transistor te verklaren. De analyse werd geverifieerd door gebruik te maken van verschillende SAMs. Het SAM-gemodificeerde contact kan bij lage spanning als een metaal-isolator-halfgeleider tunneljunctie worden behandeld. Bij hoge spanning gedraagt het contact zich echter als een metaal-isolator-metaal tunneljunctie, vergelijkbaar met het gedrag in moleculaire juncties met een groot oppervlak. De hier verkregen overeenkomst laat zien dat de SAM weerstand zich duidelijk manifesteert in de contactweerstand van de transistors. Derhalve kunnen SAM-gemodificeerde transistors mogelijk gebruikt worden als een meetinstrument om elektrisch transport door afzonderlijk moleculen te meten.

In **Hoofdstuk 5** gebruiken we een groot spanningsbereik om verschillende transportmodellen te onderscheiden in moleculaire juncties met een groot oppervlak. Onder continue gelijkspanning breken dodecaanthioljuncties onomkeerbaar af bij spanningen tussen de 1 V en 2 V, hetgeen overeenkomt met een veld van net meer dan 9 MV/cm. We laten zien dat het spanningsbereik kan worden uitgebreid tot 6 V wanneer gepulseerde metingen gebruikt worden. Dit komt overeen met een elektrisch veld van 35 MV/cm, aanmerkelijk groter dan gerapporteerde waardes van 20 MV/cm. De afbraakspanning hangt logaritmisch af van zowel de *duty cycle* als de pulsbreedte. Het verband wordt tentatief verklaard door elektrolyse in de PEDOT:PSS aan te wijzen als afbraakmechanisme. Het uitbreiden van het spanningsbereik door gebruik te maken van gepulseerde metingen heeft ondubbelzinnig aangetoond dat het elektrisch transport geen expontieel verband, maar een machtsverband heeft met de aangelegde spanning.

In **Hoofdstuk 6** onderzoeken we het ladingstransport door alkanen en parafenyleen oligomeren in moleculaire juncties met een groot oppervlak, gebruikmakend van de in **Hoofdstuk 5** ontwikkelde techniek. De moleculen worden door middel van zelf-assemblage aan gebracht op een onderelektrode van goud en in contact gebracht met een PEDOT:PSS bovenelektrode. De stroomdichtheid vertoont een machtsverband met zowel temperatuur als spanning, te weten $J \propto T^{\alpha}$ bij lage spanning ($eV \ll kT$) en $J \propto V^{\beta}$ bij lage temperatuur ($eV \gg kT$), met $\beta = \alpha + 1$. De waarde van α wordt ondubbelzinnig bepaald uit de temperatuursafhankelijkheid bij lage spanning. Voor alle onderzochte moleculen geeft het opnieuw uitzetten van de geschaalde stroomdichtheid $J/T^{1+\alpha}$ als functie van eV/kT in een grafiek een enkele gladde kromme die zich uitstrekt over enkele ordes van grootte. Met slechts twee fitparameters, namelijk γ and J_0, kunnen de gehele $J(V,T)$ karakteristieken kwantitatief worden beschreven. De voorfactor J_0 hangt af van de molecuullengte. De waardes van α en γ zijn in wezen constant voor de moleculaire juncties en bovendien identiek aan die voor de overeenkomstige diode met enkel PEDOT:PSS. De overeenkomst impliceert dat de temperatuurs- en spanningsafhankelijkheid veroorzaakt worden door PEDOT:PSS. De moleculaire bijdrage is slechts een lengteafhankelijke voorfactor. Voorts hebben we aangetoond dat J_0 afhangt van de geleidbaarheid van PEDOT:PSS, doormiddel van het variëren van het type PEDOT:PSS. Dientengevolge moet in een multi-barriére tunnel model het factoriseren met de PEDOT:PSS weerstand expliciet worden opgenomen. De dominante rol van het PEDOT:PSS-contact verklaart de absolute waarde van de junctieweerstand en zijn verhouding tot de procescondities.

In **Hoofdstuk 7** wordt het ladingstransport in op MEH-PPV gebaseerde diodes,

die enkel gaten transporteren, onderzocht in een ongekend bereik van elektrisch veld en temperatuur. De gepresenteerde dataset kan als maatstaf gebruikt worden om elk ladingstransportmodel te verifiëren. We tonen aan dat het gebruikelijke transportmodel, het Uitgebreide Gaussische Wanorde Model, de experimentele data slechts goed beschrijft in een veldbereik dat gewoonlijk gebruikt wordt in experimenten. De beschrijving van de data is vrij slecht bij hogere velden. Evenzo beschrijft het Vissenberg-Matters model het ladingstransport bij kamertemperatuur consistent tot velden tot ongeveer 10 MV/m. Boven deze velden moeten we een Poole-Frenkel veldafhankelijkheid toevoegen, $e^{\gamma\sqrt{F}}$, waarin de voorfactor γ afhangt van de temperatuur en de wanorde. Gebruikmakend van de voorfactor γ bepaald bij kamertemperatuur hebben we de effecten van ladingsdichtheid en elektrisch veld op de ladingsdragermobiliteit kunnen onderscheiden. De kloof tussen gebruikelijke LEDs en FETs is zodoende overbrugd. De convergentie van de stroomdichtheden wordt echter door noch het Uitgebreide Gaussische Wanorde Model noch het Vissenberg-Matters transportmodel, uitgebreid met veldafhankelijkheid, correct beschreven. De ontwikkeling van een ladingstransportmodel dat het ladingstransport bij hoge elektrische velden consistent beschrijft is een uitdaging voor de toekomst. De convergentie van de stroomdichtheden bij hoge velden staat het toe om de energie verschaft door het elektrisch veld om de activeringsenergie van opeenvolgende hops (ladingssprongen) tussen gelokaliseerde toestanden in het polymeer te overbruggen te kwantificeren. Met een eenvoudige benadering hebben we direct uit de experimentele data bij hoge velden een hopping afstand van 1.0 ± 0.1 nm voor gaten in MEH-PPV bepaald.

Ten slotte verschaft **Hoofdstuk 8** een vooruitzicht op andere onderwerpen van belang die kunnen worden onderzocht met de veelzijdige experimentele basis van moleculaire juncties met een groot oppervlak, om aan te komen bij moleculaire juncties met een verschillende functionaliteit. De gaten werden gevuld met monolagen van DNA, spin-omslag samenstellingen en het ferro-elektrische copolymeer P(VDF-TrFE). We hebben DNA moleculen van verschillende lengte gebruikt, aangepast met een korte alkylbrug en een thiol eindgroep. We laten zien met ellipsometriemetingen dat dichte monolagen van gehybridiseerde DNA moleculen worden verkregen, die echter plat op het substraat liggen. De elektrische data laten zien dat het ladingstransport niet in de richting van de moleculen wordt gemeten, maar dwars door de moleculen. De verkregen waardes wijzen erop dat transport door DNA toe te schrijven is aan niet-resonerende tunneling. Dunne films van de spin-omslagsamenstelling $[Fe(bapbpy)(NCS)_2]$ werden vervaardigd. Een fabricage-protocol werd ontwikkeld dat gladde dunne films van ongeveer 60 nm bewerkstelligde. De geleidbaarheid was te laag om betrouwbaar een

spin-omslag overgang vast te stellen. Echter worden er vele nieuwe, omgevingsstabiele en procesbare materialen gesynthetiseerd en samenstellingen die het toestaan de schaling van de omslagovergang te bestuderen als functie van de laagdikte zullen hun intrede doen. We hebben ook gaten gevuld met het ferro-elektrische polymeer P(VDF-TrFE). De eigenschappen van condensatoren met dikke lagen tonen een goede overeenkomst met literatuurgegevens. Het afschalen van de dikte vertoonde een geleidelijke toename in coërcitieve veldsterkte. Een geoptimaliseerd processtroomschema werd ontwikkeld dat onderzoek van ultradunne films van een paar nanometer dik mogelijk maakte. De voorlopige elektrisch-transportdata wijzen op een ferro-elektrische tunneljunctie, maar meer experimenten zijn nodig voor een ondubbelzinnige verificatie.

De gepresenteerde voorbeelden laten zien dat de technologie van moleculaire juncties met een groot oppervlak generiek en veelzijdig is. De gaten kunnen worden gevuld met ongebruikelijke halfgeleiders en zodoende worden wetenschappelijk interessante schakelingen bewerkstelligd.

List of publications

- I. Katsouras, C. Piliego, P. W. M. Blom and D. M. de Leeuw, *Transverse charge transport through DNA oligomers in large-area molecular junctions*, manuscript submitted
- M. Li, H. J. Wondergem, M. J. Spijkman, K. Asadi, I. Katsouras, P. W. M. Blom and D. M. de Leeuw, *Revisiting the δ-phase of poly(vinylidene-fluoride) for solution-processed ferroelectric thin films*, Nat. Mater. DOI:10.1038/nmat3577 (2013)
- K. van de Ruit, I. Katsouras, D. Bollen, T. van Mol, R. Janssen, D. M. de Leeuw and M. Kemerink, *The curious out-of-plane conductivity of PEDOT:PSS*, manuscript submitted
- I. Katsouras, A. Najafi, K. Asadi, A. J. Kronemeijer, A. J. Oostra, L. J. A. Koster, D. M. de Leeuw and P.W. M. Blom, *Charge transport in poly(p-phenylene vinylene) at low temperature and high electric field*, Org. Electron. in press
- K. Asadi, I. Katsouras, J. Harkema, F. Gholamrezaie, E. C. P. Smits, F. Biscarini, P. W. M. Blom and D. M. de Leeuw, *Organic field-effect transistors as a test-bed for molecular electronics: A combined study with large-area molecular junctions*, Org. Electron. 13 (2012) 2502
- I. Katsouras, A. J. Kronemeijer, E. C. P. Smits, P. A. van Hal, T. C. T. Geuns, P. W. M. Blom and D. M. de Leeuw, *Extending the voltage window in the characterization of electrical transport of large-area molecular junctions*, Appl. Phys. Lett. 99 (2011) 013303
- A. J. Kronemeijer, I. Katsouras, E. H. Huisman, P. A. van Hal, T. C. T. Geuns, P. W. M. Blom and D. M. de Leeuw, *Universal scaling of the charge transport in large-area molecular junctions*, Small 7 (2011) 1593
- I. Katsouras, V. Geskin, A. J. Kronemeijer, P. W. M. Blom and D. M. de Leeuw, *Binary self-assembled monolayers: Apparent exponential dependence of resistance on average molecular length*, Org. Electron. 12 (2011) 857
- A. J. Kronemeijer, E. H. Huisman, H. B. Akkerman, A. M. Goossens, I. Katsouras, P. A. van Hal, T. C. T. Geuns, S. J. van der Molen, P. W. M. Blom and D. M. de Leeuw, *Electrical characteristics of conjugated self-assembled monolayers in large-area molecular junctions*, Appl. Phys. Lett. 97 (2010) 173302

- A. J. Kronemeijer, E. H. Huisman, I. Katsouras, P. A. van Hal, T. C. T. Geuns, P. W. M. Blom, S. J. van der Molen and D. M. de Leeuw, *Universal scaling in highly doped conducting polymer films*, Phys. Rev. Lett. 105 (2010) 156604

Acknowledgements

A PhD can never be a one man's job. The problem is that in order to be fair I would have to acknowledge every single person that I have interacted with during my long stay in Groningen. I still have to apologize to the people that I will forget or not mention explicitly, but no one wants a tediously long, yet incomplete (I am no elephant), list of (probably misspelled) names. I want to believe that each one knows exactly how he/she contributed to the completion of this thesis.

I have to start with Bert de Boer, one of the main reasons I chose the MEPOS group to carry out my master thesis research in the first place. Bert, we only interacted for a bit more than a year, but I immediately recognized a dedicated and highly motivated scientist, a great supervisor and mentor. I was glad when you offered me a PhD position in the group. The news of your illness came as a shock. Your passing away was a tragedy for us all, the whole group suffered a great loss.

The group managed to survive with the help and the tremendous efforts of Paul Blom and Dago de Leeuw. Dago, working with you was the silver lining in the dark cloud that covered the group after the sad passing away of Bert. There's not a lot I can add to what has already been said by all the students that you have supervised over the years. I have learned so many things by your side, but most of all, in your own special way, you have helped me enjoy every moment of the PhD. Your help and interest goes beyond work, something that, for a supervisor, is atypical. But coming to think about it, so are you. I am grateful I was offered the chance to continue working with you in "Kafka country". Paul, I always appreciated your style, the relaxed and friendly way you shared profound knowledge during all work- and group- meetings. Your input and advice has been crucial in the completion of this thesis. I am looking forward to seeing the new group in Mainz growing in numbers and output, and I am grateful for being a part of it.

During the PhD I had the luck to be supervised by and work closely with some brilliant young scientists in our group. Hylke Akkerman, Kamal Asadi, Johan Brondijk, Eek Huisman, Jan-Anton Koster, Auke Kronemeijer, Martijn Kuik and Gert-Jan Wetzelaer, your guidance and help whenever I got stuck with something has been invaluable, I learned a lot from you all. You have been very patient with me and I am happy

that with some of you our interactions extended beyond the work environment.

In search of interesting materials to fill the holes with, a large number of collaborations was established both within and outside the Zernike Institute, as well as part of the European project ONE-P. I would like to acknowledge the help of all the people from Philips Research, Tom Geuns, Fatemeh Gholamrezaie, Paul van Hal, Mariane Li, Mark-Jan Spijkman and Edsger Smits. Conceptió Rovira and Claudia Simão are acknowledged for providing materials and for hosting me in Barcelona. Claudia, I can gladly reciprocate your words in your acknowledgements, thank you for everything. Jérôme Cornil, Colin van Dyck and Victor Geskin, we had a very fruitful collaboration and you helped me understand many aspects of the charge transport in our system. Our visits to Mons, although theoretically heavy, were always very informative. Victor, thank you for accepting to be present at the defense of the thesis. Martijn Kemerink and Kevin van de Ruit, I found our last-minute collaboration interesting to say the least. Sylvestre Bonnet and Sipeng Zheng from Leiden, and Laurence Lutsen and Wibren Oosterbaan from Hasselt/IMOMEC, thank you for providing us with interesting materials. Although short, our collaboration introduced me to many new topics. I would also like to thank Fabio Biscarini and Tobias Cramer from Bologna for all the interesting discussions during the ONE-P meetings, out of which a very fruitful collaboration begun. Fabio, it is a pleasure to have you in the committee of the defense. I would also like to acknowledge the efforts of the people from the Polymer Chemistry and Bioengineering group of Andreas Herrmann in Groningen. Deepak Prusty, we spent an enormous amount of time working (intermittently!) on the DNA project. I still believe we generated a lot of knowledge, which at least did not go wasted. Pavlo Gordiichuk, I really enjoyed working with you towards the end of the project, it is a pity we couldn't dedicate more time on it. I am thankful that we were able to help each other by passing on the contract of our house to you. I wonder if you will be working even harder now. Hennie Valkenier, thanks for adding large-area molecular junctions to the matrix. Vlad Pavelyev, onze samenwerking was kort, maar wel erg leuk, $\epsilon\upsilon\chi\alpha\rho\iota\sigma\tau\omega$! Beatriz Noheda and Jacob Baas, thank you for availing and helping with the mysterious and tricky black box. Beatriz, I appreciate agreeing to participate in the reading committee of my thesis although sadly you couldn't make it to the promotion. At this point I would also like to thank the other two members of the reading committee, professors Georges Hadziioannou from Bordeaux and Harold Zandvliet from TU/E.

I owe a great deal to Jan Harkema and Renate Hekkema. Jan, the work wouldn't have been possible without you; I always found it strange that many people did not

realize that. I find the way you organized and maintained the cleanroom so efficient that I am afraid that I am already spoilt. You were a pillar of the group at its most difficult times. Thank you so much for everything, you were always so kind and patient, speaking Dutch to me slow and clear! Renate, thank you for taking all the administrative work off my back, although I must apologize for annoying you with every little thing! You were always so friendly and positive though, I always enjoyed our little chats over cabbages and kings.

I also have to mention all the students that did some work with/for me, Timen Jansma, Ameneh Najafi, Jolt Oostra, Marco de Vries and Yitzi Wu. Thank you for your input and for, by putting me in the shoes of the supervisor, making me realize another thing that I need to try and do better.

I would also like to thank all the members of the MEPOS group for making it such a stimulating environment to "work" in, especially my roomies, Davood Abbaszadeh, Davide Bartesaghi, Irina Craciun, Francesco Maddalena and the guest star, Simone Fabiano.

Groningen would not have been the same without my top-master fellows Xiaoran Li and Alina Veligura. We had great times together, I am really proud of both of you, you did a fantastic job during your PhD and you deserve all the best. Marianna Manca, you brought a lot of life into the last years of my stay in Groningen, with all the sweet or bitter moments that entailed. I guess that's what makes a real friend. I am really happy you will be by my side on the "big day", but hope that this will continue to be the case for more important moments in the years to come.

Last but definitely not least, I hope the cornerstones of all my efforts, my family, my friends who still stand me and the one present at the diming of the day, know how much I appreciate their support and understanding.

For making these six years in Groningen a memory I will hold dearly, I thank you all.

Mainz, February 2013
Ilias